ABSTRACT

Title of Dissertation: NEUROMODULATION IN THE OLFACTORY BULB

Richard Scott Smith, Doctor of Philosophy, 2015

Dissertation directed by: Associate Professor, Ricardo C. Araneda, Department of Biology

State-dependent cholinergic modulation of brain circuits is critical for several high-level cognitive functions, including attention and memory. Here, we provide new evidence that cholinergic modulation differentially regulates two parallel circuits that process chemosensory information, the accessory and main olfactory bulb (AOB and MOB, respectively). These circuits consist of remarkably similar synaptic arrangement and neuronal types, yet cholinergic regulation produced strikingly opposing effects in output and intrinsic neurons. Despite these differences, the chemogenetic reduction of cholinergic activity in freely behaving animals disrupted odor discrimination of simple odors, and the investigation of social odors associated with behaviors signaled by the Vomeronasal system.

NEUROMODULATION IN THE OLFACTORY BULB

By

Richard Scott Smith

Dissertation submitted to the Faculty of the Graduate School of the
University of Maryland, College Park, in partial fulfillment
of the requirements for the degree of
Doctorate of Biology
2015

Dissertation Commette
Dr. Ricardo Araneda, Chair
Dr. Matthew Roche, Deans Representative
Dr. Alain Marty, Cotutelle Director
Dr. Hey-Kyoung Lee
Dr. Mark Stopfer
Dr. Daniel Butts
Dr. Pierre Vincent

Université Pierre et Marie Curie

Université de cotutelle

ED3C

UMR 8118 Laboratorie de Physiologie Cerebrale

Neuromodulation in the Olfactory Bulb

Richard SMITH

Cerveau, Cognition, Comportement

Dirigée par [Alain MARTY, Ricardo ARANEDA]

Présentée et soutenue publiquement le [8 Julliet 2015]

Devant un jury composé de :

LEE, Hey-Kyoung, Professor, Johns Hopkins Université USA, Rapporteur

STOPFER, Mark, Investigator, National Institutes of Health USA, Rapporteur

MARTY Alain, Research Directeur, Paris V, Directeur

ARANEDA Ricardo, Professor, Université of Maryland, Directeur

VINCENT Pierre, Research Directeur, Paris VI, Member

ROESCH Matthew, Professor, Université of Maryland, Member

BUTTS Daniel, Professor, Université of Maryland, Member

Acknowledgements

My Family, Friends, Labmates, Mentors and my Advisor.

Summary

Neuromodulation of olfactory circuits by acetylcholine (ACh) plays an important role in odor discrimination and learning. Early processing of chemosensory signals occurs in two functionally and anatomically distinct regions, the main and accessory olfactory bulbs (MOB and AOB), which receive significant cholinergic input from the basal forebrain. Here we explore the regulation of AOB and MOB circuits by ACh, and how this modulation influences olfactory mediated behaviors. Surprisingly, despite the presence of a conserved circuit, activation of muscarinic ACh receptors revealed marked differences in cholinergic modulation of output neurons: excitation in the AOB and inhibition in the MOB. Granule cells (GCs), the most abundant intrinsic neuron in the OB, also exhibited a complex muscarinic response. While GCs in the AOB were excited, MOB GCs exhibited a dual muscarinic action, a hyperpolarization and an increase in excitability uncovered by cell depolarization. Furthermore, ACh had a different effect on the input/output relationship of MCs in the AOB and MOB, showing a net effect on gain in MCs of the MOB, but not in the AOB. Interestingly, despite the striking differences in neuromodulatory actions on output neurons, chemogenetic inhibition of ACh release produced similar perturbations in olfactory behaviors mediated by these two regions. Decreasing ACh in the OB disrupted the natural discrimination of molecularly related odors and the natural investigation of odors associated with social behaviors. Thus, the distinct neuromodulation by ACh in these circuits could underlie different solutions to the processing of general odors and semiochemicals, and the diverse olfactory behaviors they trigger.

Résumé en Français

La neuromodulation de circuits olfactifs par l'acétylcholine (ACh) joue un rôle important dans la discrimination et l'apprentissage d'odeur. Le traitement précoce des signaux chimiosensoriels se produit dans deux régions fonctionnellement et anatomiquement distinctes, les principaux et accessoires bulbes olfactifs (MOB et AOB), qui reçoivent entrée cholinergique significative du cerveau antérieur basal. Ici, nous explorons la régulation des circuits de l'AOB et la MOB par ACh, et comment cette modulation influence le comportement à médiation olfactifs. De manière surprenante, malgré la présence d'un circuit conservé, l'activation des récepteurs muscariniques de l'ACh révèle des différences marquées dans la modulation cholinergique des neurones de sortie: l'excitation de l'AOB et l'inhibition de la MOB. Les cellules granulaires (GCs), le neurone intrinsèque le plus abondant dans l'OB, présentaient également une réponse muscarinique complexe. Alors que les GCs de l'AOB ont été excitées, les GCs de la MOB présentaient une action muscarinique double, une hyperpolarisation et une augmentation de l'excitabilité non couvert par la dépolarisation cellulaire. Par ailleurs, l'ACh a eu un effet différent sur la relation d'entrée / sortie des MCs dans l'AOB et la MOB, montrant un effet net sur le gain en les MCs de la MOB, mais pas dans l'AOB. Fait intéressant, malgré les différences frappantes dans les actions neuromodulateurs sur les neurones de sortie, l'inhibition de la libération d'ACh chemogenetic produit des perturbations similaires dans les comportements olfactifs médiés par ces deux régions. La diminution de l'ACh dans l'OB a perturbé la discrimination naturelle des odeurs liées moléculairement et l'enquête naturelle des odeurs associées à des comportements sociaux. Ainsi, la neuromodulation distincte par l'ACh dans ces circuits pourrait déclencher

des solutions différentes générales pour le traitement des odeurs et les médiateurs chimiques, ainsi que les comportements olfactifs diverses qu'ils déclenchent.

Preface

Organization of sensory processing circuits in the brain is complex and heterogeneous, with each sensory modality comprising of unique cell types and synaptic organization, as well as patterns of short and long-range brain connectivity. The goal of sensory physiology research is straightforward, identify and investigate components of sensory circuits, and determine their contributions to transforming sensory signals into meaningful information. In the past decade, modern genetic approaches have accelerated the precise dissection of sensory neural circuits to test and validate components roles in sensory processing. To this end, the present work seeks to evaluate the role of one component, top-down neuromodulation, within the olfactory sensory processing circuit: the olfactory bulb.

TABLE OF CONTENTS

LIST OF FIGURES

LIST OF ABBREVIATIONS

ACh acetylcholine
AChR acetylcholine receptor
ARs adrenergic receptors
α_1-ARs Alpha 1 adrenergic receptor
ACA anterior cortical amygdala
AON anterior olfactory nucleus
AMPA 2-amino-3-(3-hydroxy-5-methyl-isoxazol-4-yl) propanoic acid
AOB Accessory olfactory bulb
AOS Accessory olfactory system
AON accessory olfactory nucleus
C6 ethyl hexanoate
C7 ethyl heptanoate
C8 ethyl octanoate
ChAT choline acetyl transferase
ChR channelrhodopsin
CNO clozapine-N-oxide
DAG diacyl glycerol
DDI dendrodendritic inhibition
DDS dendrodendritic synapse
d.p.i. days post injection
DREADD Designed Receptors Exclusively Activated by a Designed Drug
dSAC deep short axon cell
dorsal raphe nucleus (DRN)
E/I excitation/inhibition
eIPSC evoked inhibitory postsynaptic current
EPL external plexiform layer
EPSC excitatory postsynaptic current
GABA gamma-aminobutyric acid
GAD glutamic acid decarboxylase
GC granule cell
GCL granule cell layer
GFP green fluorescent protein
GL glomerular layer
GLU glutamate
HDB horizontal limb of the diagonal band of Brocca
h.p.i. hours post injection
iGluR ionotropic Glutamate Receptor
IPL internal plexiform layer
IPSC inhibitory postsynaptic current
IP3 inositol 1,4,5-trisphosphate
I_{CAN} Calcium activated non-selective cationic current
Light optogenetic stimulation
LOT lateral olfactory tract
LC locus coeruleus
LTP Long Term Potentiation
LEC lateral entorhinal cortex
MTC mitral cell
MCL mitral cell layer
MCPO magnocellular preoptic area
MeA medial amygdala
mGLUR metabotropic glutamatergic receptor

mIPSC miniature inhibitory postsynaptic current
MHC Major histocompatibility complex
MOE Main olfactory epithelium
MOS Main olfactory system
MOT Medial olfactory tract
MUP Major urinary protein
MOB main olfactory bulb
NA noradrenaline
NMDA N-methyl-D-aspartate
NLO nucleus of the lateral olfactory tract
OB olfactory bulb
ONL olfactory nerve layer
OSN olfactory sensory neurons
ORs Olfactory receptor
OT olfactory tubercle
PFA paraformaldehyde
PCA posterolateral cortical amygdala
PGC periglomerular cell
PC piriform cortex
PLC Phospholipase C
PKC protein kinase C
pPC posterior Periform cortex
PN days post-natal
RMS rostral migratory stream
sIPSC spontaneous inhibitory postsynaptic current
5-HT Serotonin
STDP spike timing dependent plasticity
SVZ subventricular zone
ETC external tufted cell
TMT trimethlytoluine
VNO Vomeronasal organ
VNL Vomeronasal Nerve Layer
VNS Vomeronasal system
VR Vomeronasal receptor protein
w.p.i. weeks post injection

Olfactory System Overview

The detection and processing of environmental and social chemical stimuli by the olfactory system (OS) is essential for the survival of most mammalian species. The OS consists of two parallel pathways that include the Vomeronasal system (VNS) and the main olfactory system (MOS). Together, they analyze the broad array of chemosensory signals that range from small volatiles of simple chemical structure, to complex proteins. These odor signals in turn trigger a host of survival behaviors, including food consumption, aggression, mating, maternal functions, detection of conspecifics, and predator detection. Odors bind to chemosensory receptors located on olfactory sensory neurons (OSNs), specialized cells found in peripheral structures, which transmit odor signals to the brain. The olfactory bulb (OB) is the first brain region where processing of odor signals occurs before odor information is relayed to cortical and subcortical areas. The OB consists of two anatomically distinct regions, the main olfactory bulb (MOB), which is part of the MOS and detects mostly volatile odors, and the accessory olfactory bulb (AOB), which is part of the VNS. In addition to small molecules, the VNS relies information about non-volatiles signals including proteins, collectively known as pheromones, which trigger behaviors such as mating and aggression. Unlike other sensory modalities, projections from the OB reach cortical layers directly, bypassing the thalamus. However, similar to the thalamus, the OB neural circuit is highly regulated by top down neuromodulatory systems and cortical inputs. Among these regulatory inputs, state dependent activation of two neuromodulatory systems, the cholinergic and noradrenergic systems, play an important role in odor processing and olfactory behaviors. To this end, the olfactory system provides an attractive

model to study neuromodulation of a sensory system at a cellular, circuit, and behavioral level.

Olfactory Sensory Neurons and Chemoreception

Chemical odorants enter the nostrils and bind one of five families of chemosensory G-protein coupled receptors (GPCRs) (Buck and Axel, 1991; Kaupp, 2010). Olfactory receptors (ORs) consist of the largest family of GPCRs (~1100 genes depending on species), generating diverse physiochemical binding properties to detect millions of volatile odors in the olfactory epithelium (OE) (Zhang and Firestein, 2002). Two vomeronasal GPCRs types exist (V1R and V2R, VRs herein), which detect odor molecules within the liquid milieu in the vomeronasal organ (VNO), located ventral to the nasal cavity entrance in most mammals (See Fig 1.1, (Tirindelli et al., 2009). Generally, OSNs follow the "one neuron, one receptor rule", whereby OSNs express a single type of OR (or VR) on their cilia and these receptors show a specific odor ligand binding profile (Buck and Axel, 1991; Kaupp, 2010). ORs have different chemical receptive ranges; some ORs are classified as "generalists" and respond to many odors, while other ORs "specialists" display a narrow odor range (Araneda et al., 2000, 2004). Ultimately, the detection of odors occurs through a combinatorial strategy, whereby activation of several ORs types combine to generate olfactory odor representations (Mori and Sakano, 2011). In the MOS each OSN expressing one of ~1,000 ORs are distributed across the OE in a scattered manner, however a very coarse spatial organization may exist (Ressler et al., 1993; Miyamichi et al., 2005; Imai et al., 2010). Conversely, V1R and V2Rs are spatially separated in the apical and basal aspects of the VNO (Jia and

Halpern, 1996). Odor binding to ORs and VRs produces a GPCR-led activation of OSNs for electrical amplification and transmission of sensory signals via axonal segments to the OB (Shepherd and Greer, 1998). OSN generated electrical signals arrive to the olfactory nerve layer (ONL) where OSN axon terminals form glutamatergic synapses with projection neurons,

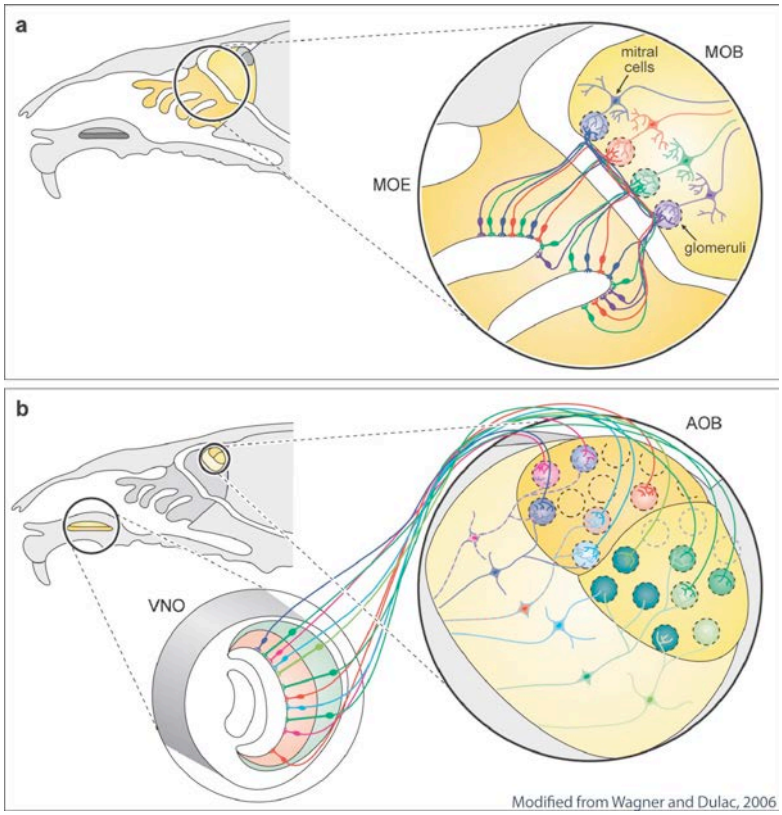

Fig 1.1 Synaptic connectivity in the olfactory bulb. Sensory projections from the Vomeronasal organ (VNO) and olfactory epithelium (MOE) into the accessory and main olfactory bulb (AOB and MOB, respectively). A. MOB mitral cells project a single apical dendrite to a glomerulus that is, in turn, innervated by sensory neurons expressing the same OR (color coded in this diagram). B. VRs in the sensory epithelium of the VNO are segregated into apical and basal zones, which project to multiple glomeruli along an antero-posterior axis. AOB mitral cells project several apical dendrites to multiple glomeruli.

Mitral and Tufted cells (MTC herein) in the glomerulus, a glial ensheathed bundle of synapses located on the superficial surface of the OB (Shepherd and Greer, 1998). Generally, in the mouse MOS, OSNs expressing the same OR converge within two of approx ~1,800 OB glomeruli (Fig 1.1A) (Royet et al., 1988; Mombaerts et al., 1996). In the VNS, OSNs expressing the same

VRs converge to 10-30 small glomeruli, giving the VNS a lower ratio of OSNs to glomeruli (Fig 1.1B) (Rodriguez et al., 1999). These glomerular structures provide the first location where the initial processing of odors signals occur in the OB (Shao et al., 2009; Gire et al., 2012).

The Olfactory Bulb, AOB and MOB Circuits

The OB is the initial site of odor processing, generating the first odor representations in the olfactory pathway (Mori et al., 1999; Takahashi et al., 2004). In the OB, the most salient physiological mechanism in olfactory processing is the precisely regulated excitability of the output neurons (MTCs) by the more numerous inhibitory interneurons (Shepherd and Greer, 1998). The most characterized among these inhibitory neurorns are the granule cells (GCs), the largest in number, and the periglomerular cells (PGCs) (Fig 1.2). These interneurons produce a robust inhibition of MTCs through lateral, feedforward, and recurrent inhibition at dendrodendritic synapses (DDS, Fig. 1.2) (Schoppa and Urban, 2003; Arevian et al., 2008). DDS have been extensively studied in the MOB, and are thought to function in a similar fashion in the AOB (Rall and Shepherd, 1968; Price and Powell, 1970a; Shpak et al., 2014). Briefly, the DDS reciprocal synapse consist of excitatory glutamatergic input from MTCs to GCs and PGCs, which induces the release of γ-aminobutyric acid (GABA) from the dendrites of GCs (or PGCs), in turn, inhibiting the MTC (See Fig 1.2) (Isaacson and Strowbridge, 1998; Schoppa and Urban, 2003). Through DDS inhibition, these interneurons effectively shape MTC spatial odor patterns which continue to evolve during the odor response (Spors and Grinvald, 2002; Niessing and Friedrich, 2010). During odor investigation, MTCs are spontaneously active and typically show spike

locking with respiration cycle (Rinberg et al., 2006; Cury and Uchida, 2010). Several layers of MTC processing exists, including latency of response and spike temporal phase modifications (Margrie and Schaefer, 2003; Cury and Uchida, 2010; Dhawale et al., 2010; Smear et al., 2011; Haddad et al., 2013), decreases in spiking (Rinberg et al., 2006; Davison and Katz, 2007) and modifications to MC synchronization (Kay and Stopfer, 2006). These provide a powerful mechanism for the transformation of olfactory signals within the OB and major targets for top-down modulation. In addition, MTC spatiotemporal patterns can be modulated by learning, as modifications of odor valance or providing an associative reward in the presence of an odor can produce changes in MTC firing patterns (Freeman and Schneider, 1982; Kay and Laurent, 1999; Doucette et al., 2011).

Additionally, the glomerular synaptic network is important for processing incoming odor signals, in particular, the rich GABAergic architecture primarily contributes to, among others, gain control and contrast enhancement of the incoming sensory signals (Olsen and Wilson, 2008; Shao et al., 2009; Gire et al., 2012; Carey et al., 2015). It is notable that DDS inhibition onto MTCs occurs at two different sites, from PGCs at the level of the input, while inhibition from GCs occurs at lateral dendrites mostly. These synaptic interactions have been shown to be the targets of several afferent neuromodulatory systems (Schoppa and Urban, 2003; Ennis et al., 2007).

Last, the OB's anatomical isolation provides a unique opportunity to study sensory transformations with minimal interference comparably to the dense inter-connectivity between the thalamus and cortex of other sensory systems. Moreover, the multilayered structure of the OB with feedback loops and

centrifugal input lend support to the role of the OBs as more than a relay synapse, but an active participant in the precisely timed activity of neurons in modifying odor transformations.

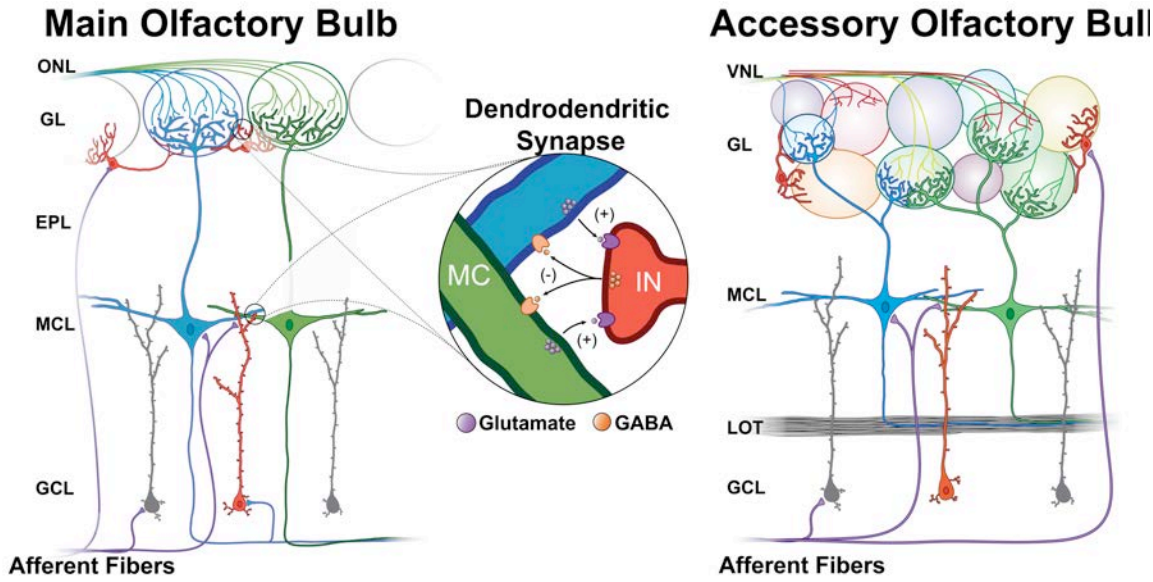

Figure 1.2 Synaptic organization of the main olfactory and accessory olfactory bulb Left. OSNs in the main olfactory system expressing a single odorant receptor project to the same glomerulus in the OB and shown are two representative populations of OSNs (blue, green). MCs of the MOB have a single apical dendrite projecting to a single glomerulus and several lateral dendrites that contact GC dendrites. Right, in the VNS, OSNs expressing the same VRs project to multiple small glomeruli (various colors). MCs of the AOB (blue, green) have several apical dendrites projecting to multiple glomeruli. In both regions, PGCs and GCs inhibit MTC activity through dendrodendritic synapses (DDS). Centre circle, schematic diagram of a MTC-GC DDS in the MOB. Glutamate released from MTCs acts on glutamate receptors to induce recurrent and lateral release of GABA from GCs. *OSN, Olfactory Sensory Neurons; ONL, Olfactory Nerve Layer; VNL, Vomeronasal Nerve Layer; GL, Glomerular Layer; MCL, Mitral Cell Layer; GCL, Granule Cell Layer; Lateral Olfactory Tract (LOT)*

Output of the Olfactory Bulb

The MOS and VNS both process chemosensory cues, which are represented in different brain areas and elicit distinct behavioral effects. Long range MTCs axonal projections synapse within several cortical and subcortical target structures, including a prominent connection by the VNS MTCs within limbic structures. MOB MTCs primarily target the olfactory cortex (OC) and

several olfactory recipient areas, which include the anterior olfactory nucleus (AON), the piriform cortex (PC), the tenia tecta, the olfactory tubercle (OT), the cortical amygdala, and the entorhinal cortex (EC) (Haberly, 2001; Mori and Sakano, 2011). Neuroanatomical and physiological studies reveal that MOB MTCs axons synapse broadly across the PC, with no obvious spatial orientation, including those MTCs receiving input from the same glomerulus (Ghosh et al., 2011; Sosulski et al., 2011; Igarashi et al., 2012). The anterior PC is thought to function in pattern recognition, whereby coincident MTC inputs onto pyramidal neurons provides long term potentiation (LTP), a mechanism for associating odor features that represent an odor (Stettler and Axel, 2009; Davison and Ehlers, 2011). The connectivity in the posterior PC (pPC) suggests it functions as a higher-order association cortex, performing multimodal associations (Haberly, 1985). The lack of an organized spatial odor map in PC, as determined by anatomical methods, is further confounded by the absence of “spike timing” based coding or odor-specific spatial patterns of activation, as those observed in the OB. These observations suggest that a robust transformation of information occurs from the OB to PC, and that odor signals may change from “timing” based to “firing rate” based representations in the PC (Uchida et al., 2000; Illig and Haberly, 2003). More recent studies, following two-point activation across specific glomeruli using optogenetics, have suggested that PC can read out gross relative timing differences at PC pyramidal cells (Haddad et al., 2013).

Within the VNS, MTCs primarily target subcortical areas of the limbic system, including the medial amygdala (MA), posteromedial cortical amygdala (PCA),

accessory olfactory nucleus, and the bed nucleus of the stria terminalis (Scalia and Winans, 1975; von Campenhausen and Mori, 2000). While V1Rs and V2Rs show anterior-posterior anatomical separation in their AOB MTC targeting, MTC axonal projections do not reflect this spatial patterning within amygdaloid target structures (Fig 1.3) (Salazar and Brennan, 2001; Mohedano-Moriano et al., 2007, 2008). Interestingly, a crude spatial organization may exist in the hypothalamus where MTC activation of neurohormonal responses can modulate sexual behaviors, maternal care, and fear responses (Brennan and Peele, 2003).

Crosstalk between AOB and MOB MTC upstream targets does exist, as AOB projections overlap within classically described MOB target areas, including the nucleus of the lateral olfactory tract (NLO), anterior cortical amygdaloid nucleus. MOB projections also overlap with AOB target structures, such as ventral anterior amygdala, the bed nucleus of the accessory olfactory tract (BST), and the anteroventral medial amygdaloid nucleus (Licht and Meredith, 1987; Pro-Sistiaga et al., 2007). The medial amygdala (MeA) also integrates cues from both the VNS and MOS and plays a vital role in social recognition (Brennan and Keverne, 2015). While it is clear that concurrent transmission of sensory signals to upstream olfactory associated areas occurs, it remains to be shown how combinatorial signals generate olfactory representations.

Figure 1.3 Schematic of MOB and AOB MTC axonal projections in the brain. Horizontal brain section stained with Westeria Flurobundia (WFA). Projections originating in the AOB and MOB are shown as arrows that target cortical and subcortical structures. For example, MTCs of the MOB project to cortical areas mostly AON, anterior olfactory nucleus; OT, olfactory tubercle; PC, piriform cortex; NLO, nucleus of the lateral olfactory tract; ACo, anterior cortical amygdala; PMCo, posterolateral cortical amygdala; MeA, medial amygdala; LEC, lateral entorhinal cortex; PCa, posteromedial cortical amygdala; BST, bed nucleus of the stria terminalis (Mori and Sakano, 2011)

Afferent input to the Olfactory bulb

Unlike the other sensory modalities, the OS operates without a thalamic relay and thus the OB is important area for top down regulation. Afferent input arising from several cortical and subcortical structures, including MTC recipient areas, are a critical component of olfactory processing. Analysis of PC **->** OB axonal targets reveals a disseminated projection that lacks a topographic organization, paralleling the lack of organization in OB**->**PC projections (Boyd et al., 2015). Cortical pyramidal neurons send glutamatergic axons to the OB, primarily synapsing onto GCs, and activate GABA release to inhibit MTC odor responses (von BAUMGARTEN et al., 1962; Price and Powell, 1970b; Mori and Takagi, 1978; Halasz and Shepherd, 1983). These cortical glutamatergic projections can activate NMDA receptors for short and long-term plasticity (de Olmos et al., 1978; Shipley and Adamek, 1984; Dietz and Murthy, 2005; Balu et al., 2007) providing a plasticity mechanism for signals in the OB (Wilson, 1995; McNamara et al., 2008; Gao and Strowbridge, 2009). Interestingly, amygdaloid structures also project glutamatergic afferents to AOB GCs, although little is known of their functional role (Fan and Luo, 2009). Additionally, feedback projections from olfactory associated areas to the MOB have been shown to be important for odor reward associations and modulate interneurons (Kiselycznyk et al., 2006; Mouret et al., 2009a). In addition to glutamatergic OB innervation, GABAergic nuclei located in the HDB/MCPO project afferent fibers to the MOB and AOB, and disruption of this top-down inhibitory input can interfere with odor discrimination (Nunez-Parra et al., 2013). The BST also sends GABAergic fibers to AOB, however little is known of the functional purpose for this afferent GABAergic input to the AOB (Fan and Luo, 2009).

Activation of neuromodulatory systems occurs on a state dependent basis, adapting the tone of neuromodulatory release to the demands of the behavioral task and animals environmental input (Marder, 2012). Several neuromodulatory centers project afferent axons to the OBs, including the cholinergic system from nucleus of the diagonal band of Broca (HDB) (Ichikawa and Hirata, 1986), the noradrenergic system from the locus coeruleus (LC) (McLean et al., 1989), and the serotonergic system from the raphe nuclei (RN) (McLean et al., 1989; Fletcher and Chen, 2010). Changes in MTC spike timing and synchronizations evoked by neuromodulators can affect several aspects of OB processing, including generating contrasting odor representations, variations in the signal to noise ratio, and short- and long-term plasticity mechanisms (Devore and Linster, 2012). For example, noradrenergic modulation of MTC synchrony has been shown during an odor reward task (Doucette et al., 2011). Noradrenergic activation in the AOB and MOB triggers robust inhibition of MTCs via activation of α_1-adrenergic receptors (ARs) located on GCs (Smith et al., 2009; Zimnik et al., 2013).

Noradrenaline (NA) acting on the AOB circuitry is thought to promote the structural and functional synaptic plasticity underlying VNS mediated behaviors that require learning (Brennan and Keverne, 1997; Matsuoka et al., 2004). Specifically, noradrenergic modulation of AOB circuitry underlies the formation of memory in the “Bruce effect” in mice, as well as a role in association between the conditioned odor and a reward (Brennan et al., 1998; Brennan and Peele, 2003). In sheep, NA plays an important role in olfactory learning of offspring odor (Lévy et al., 1990). Serotonergic input targets the

OB GL, where serotonin (5-HT) acts on PGCs to increase the inhibitory tone on MCs (McLean and Shipley, 1987; Hardy et al., 2005; Petzold et al., 2009; Liu et al., 2012). 5-HT may also synchronize inhibitory inputs among nearby, but not distant pairs of MTCs, thus contributing to MC firing dynamics (Schmidt and Strowbridge, 2014). While, the role of 5-HT in social stress, anxiety, and aggression has been well documented, little is known how 5-HT contributes to olfactory mediated behaviors and under what context activation of 5-HT modulates these behaviors (Sachs et al., 2013; Huo et al., 2014). Importantly, the concurrent activation of neuromodulatory systems to varying degrees provides multiple and opposing roles on OB neurons transforming sensory signals en route to secondary structures.

Cholinergic System and the Olfactory Bulb

The OB receives a rich projection of cholinergic axons from nuclei residing in the horizontal limb of the diagonal band of Broca (HDB) in the basal forebrain (Wenk et al., 1980; Zaborszky et al., 1986). The majority of cholinergic neurons (>70%) in the HDB send axons to the OB, where ACh activates both nicotinic and muscarinic ACh receptors (nAChR and mAChR, receptively), located within the multiple layers of the OB (Macrides et al., 1981; Ojima et al., 1988; Kasa et al., 1995; Le Jeune et al., 1995). Cholinergic neurons in the HDB are regulated in a behavioral state dependent manner, displaying neuronal bursting during active states (e.g. attention) and synchronize with gamma and theta oscillations (Manns et al., 2000; Lee et al., 2005; Parikh and Sarter, 2008). Recent work suggests the activation of post synaptic

targets by ACh likely occurs by a volume transmission mechanism (bulk neurotransmitter release in space), instead of the classic “wired” model with direct neurotransmitter release at the synapse (Sarter et al., 2009). Thus, activation of cholinergic axons leads to global changes in ACh levels to activate target neurons, which results in prolonged duration of its activation (Descarries et al., 1997). Furthermore, cholinergic neurons modulate several functions critical for generating neural representations of visual, somatosensory, and auditory signals (Tremblay et al., 1990; Kilgard and Merzenich, 1998; Goard and Dan, 2009).

The mAChR family is divided into five metabotropic receptor subtypes, termed M1-M5 mAChRs, and upon activation mAChRs elicits distinct cellular effects (Lanzafame et al., 2003; Gotti et al., 2006). Among the five mAChR subtypes, two subfamilies exist, the “M1-like” mAChRs (M1, M3, M5) which couple to PLC and excite neurons, and the “M2-like” mAChRs (M2, M4), which inhibit adenlylate cyclase (AC) to inhibit neurons (Thiele, 2013). On the other hand, nAChRs are ligand-gated non-selective cationic ion channels composed of five subunits that, unlike the neuromuscular junction channel, exist in the brain as a combination of α2–α10 and β2–β4 subunits (Fucile, 2004). Different subunit compositions bestow unique activation kinetics and conductance properties to each receptor subtype (Fucile, 2004). In the OB, AChRs exhibit differential patterns of distribution across its neuronal layers, and nAChRs are predominantly found in the glomerular layer while mAChR in internal layers, raising the interesting possibility that activation of these receptors modulate different aspects of olfactory processing (Hill et al., 1993; Le Jeune et al., 1996; Keiger and Walker, 2000; Whiteaker et al., 2009).

Recently, the presence of a small population of local cholinergic interneurons in the MOB was described, which were identified by their expression of choline acetyl transferase (ChAT), an enzyme critical for the production of ACh. A functional role of these neurons to the OB circuit remains unknown (Krosnowski et al., 2012).

Cholinergic axons densely innervate the GABAergic interneuron population of the OB and therefore ACh modifies inhibition at the GC to MC DDS (Elaagouby et al., 1991; Kasa et al., 1995; Tsuno et al., 2008). ACh binds M1-mAChRs on GCs and activates a slow after depolarizing potential (sADP) following a stimulus-induced train of action potentials that enhances the depolarization produced by ACh and therefore it potentiates the strength of inhibition onto MTC (Pressler et al., 2007; Smith and Araneda, 2010). The activation of a sADP appears to be a conserved neuromodulatory target in GCs, as activation of metabotropic glutamate receptor type 1 (mGluR1), and α_{1A} ARs also elicits the sADP (Smith et al., 2009; Smith and Araneda, 2010). Characterization of the ionic mechanisms underlying the M1-mAChR, α_1 ARs, and mGluR1 induced sADP indicated that this is mediated by a nonselective cationic current (I_{CAN}), which as in other brain regions is thought to occur through activation of transient receptor potential (TRP) channels (Yan et al., 2009; Smith and Araneda, 2010). However, another study of cholinergic neuromodulation of AOB GCs indicated that the M1-mAChR mediated excitation originated through closure of KCNQ/Kv7 channels (Takahashi and Kaba, 2010). The reason for these discrepancies are not known, but, regardless of the mechanism, neuromodulation of the GC lateral inhibitory network is thought to be an important contributor to MTCs spiking dynamics

and decorrelation of odor representations (Linster and Cleland, 2002; Cleland and Linster, 2005; Lepousez and Lledo, 2013). In addition, the glomerular microcircuit has several properties that modify the processing distributed odor representations, particularly gain modulation, thresholding of responses and feedforward activation (Carey et al., 2015). ACh has been shown to modulate the MOB glomerular circuit, activation of nAChR produces a depolarization on apical dendrites of MTC, external tufted cells (ETC), and PGCs (Castillo et al., 1999; Pignatelli and Belluzzi, 2008; D'Souza and Vijayaraghavan, 2012; D'Souza et al., 2013). Interestingly, although still a not fully settled issue, external tufted cells (ETCs) seem to convey and modulate sensory input in a diffuse multistep mechanism onto MCs, which suggests ACh may contribute a larger role than thought for modulating glomerular processing (Shao et al., 2009; Gire et al., 2012).

Results from *in vivo* and *in vitro* studies revealed mixed results on cellular effects produced by activation of OB neurons by ACh. For example, electrical stimulation of HDB neurons inhibits GCs and increases the activity of MTCs by disinhibition (Kunze et al., 1991; Zhan et al., 2013). Conversely, a more selective stimulation using optogenetic of HDB ChAT nuclei, showed that the effect of ACh on MOB MCs is inhibitory (Ma and Luo, 2012; Rothermel et al., 2014). However, in the same study (Rothermel et al., 2014), when optogenetic stimulation occurred superficially in the MOB, thus activating glomerular circuitry preferentially to the deeper inhibitory network, MTC neurons were excited. The observed disinhibitory effect could be ascribed to nonselective stimulation of GABAerigic neurons which reside juxtaposed in

the HDB to ChAT neurons and thus GABA release could be mediating this effect at several layers (Nunez-Parra et al., 2013). It is noteworthy that a small subset of HDB neurons project to the PC and AON, albeit to a much lesser degree, and could potentially affect OB processing through feedback projections (Woolf et al., 1986; Markopoulos et al., 2012).

Interestingly, Alzheimer's disease (AD) and ageing related pathophysiology is highly correlated with cholinergic dysfunction (Durand et al., 1998). In fact, in several neurodogenerative diseases, including AD, olfactory symptoms are the earliest markers of disease. This highlights the importance of understanding synaptic and circuit levels of cholinergic modulation in the OB circuits.

Olfactory System and Behavior

Social interactions in many mammalian species rely on the concurrent detection and processing of chemosensory signals by the MOS and VNS. Classically, the MOS has been associated with learned responses to odors, whereas the VNS is thought to mediate innate odor responses. However, recent evidences demonstrating neuroanatomical overlap of AOB and MOB MTC axonal projections to central structures suggests that a combined olfactory representation is more likely to underlie the execution of behaviors (Mucignat-Caretta et al., 2012). As MOS and VNS simultaneously detect biologically relevant odors, both volatile and non-volatiles, deciphering the degree to which one system contributes to specific olfactory behaviors is challenging, if not impossible with current experimental approaches.

Following the advent of molecular biology approaches to ablate sensory system components, the VNS and MOS contributions to detecting biologically relevant odor still remains unclear. For example, transgenic knockout mice lacking the TRPC2 channel (TRPC2 -/-), the primary cationic channel conductance in VRs, leads to indiscriminate male courtship and mounting toward females, however, these male mice can successfully mate with females (Leypold et al., 2002; Stowers et al., 2002; Kimchi et al., 2007). Further, male mice with VNOs surgically removed (VNOx) mate successfully, but also display impaired sexual behaviors and individual recognition through nonvolatile odorants (Kimchi et al., 2007). Most intriguingly, the VNOx induced disruption of sexual behavior only exists in sexually naïve males, as sexually experienced males that receive VNOx exhibit normal copulatory behaviors (Pfeiffer and Johnston, 1994). Intriguingly, more recent evidence demonstrates TRPC2-expressing sensory neurons in the main olfactory epithelium of the mouse, suggesting TRPC2 may play a functional role in the MOS, and that behavioral phenotypes observed in the TRPC2 -/- are not entirely due to VNO disruption (Omura and Mombaerts, 2014). Further confounding the classic VNS role in sexual behaviors, disruption of the MOE, either using chemical wash or a transgenic knockout mouse for CNGA2 channel (CNGA2 -/-), the primary cationic conductance in MOE ORs, also caused male mice display a marked decrease (chemical wash) and completely abolished (CNGA2 -/-) mating behaviors (Mandiyan et al., 2005).

Several additional biologically relevant olfactory behaviors rely on overlapping MOS and VNS roles. For example, odors critical for reproductive behaviors, such as mate identification and neonatal care, are detected by both of these

systems (Keller et al., 2009). The MOS mediates response to the airborn mammary pheromone *2-methylbut-2*-enal (2MB2) in rabbits, the sex pheromone trimethyl amine in mice, and the predator odor signal trimethlytoluine (TMT) (Schaal et al., 2003; Staples et al., 2008). However in mice, major urinary proteins (MUPs) are exclusively detected by VNS V2Rs and mediate avoidance behaviors (Papes et al., 2010). In addition, the VNS mediates the response to the male mouse pheromone exocrine gland-secreting peptide 1 (ESP1) (Haga et al., 2010).

The MOS and VNS also seem to play a complementary role in aggression responses. In rodents, male to male territorial aggression is an innate social behavior triggered by urinary compounds (Chamero et al., 2007). This behavior is most commonly assessed with the resident intruder paradigm, in which a male intruding mouse is presented in the home cage of a resident male mouse, leading to an aggressive encounter, which can be quantified ((Koolhaas et al., 2013) described in methods). Male mice with disrupted function of the VNO, VNOx and TRPC2 (-/-) mice, and fail to display proper aggression (Clancy et al., 1984; Maruniak et al., 1986; Stowers et al., 2002; Kimchi et al., 2007). Surprisingly, male mice with disrupted function in the MOE via chemical ablation of OSNs, or in transgenic CNGA2 -/- mice, display decreased aggressive behaviors toward intruding male mice (Mandiyan et al., 2005; Keller et al., 2006). Recently it has been shown that MOB targets in the cortical amygdala function in innate odor driven responses (Root et al., 2014). Taken together, these studies support the hypothesis that both systems participate in the detection of aggression relevant odors and that parallel

contributions to chemosensory perception may underlie the triggering of these olfactory mediate behaviors.

All reproductive and social behaviors are regulated ultimately by precise neuromodulatory changes in physiological and neuroendocrine states (Brennan, 2009). For example, in mice, NA is important for innate and learned fear responses, as well as the formation of stud memory (Brennan and Keverne, 1997; Brennan and Peele, 2003; Luo et al., 2003; Matsuoka et al., 2004; Do Monte et al., 2008). Furthermore, in the MOB, NA triggers maternal recognition in ewes, highlighting the role of olfactory circuits and neuromodulators in biologically relevant behaviors (Lévy et al., 1990). Interestingly, despite the well-documented role of NA in the processing of pheromonal information, little is known about the role of other neurotransmitters, including ACh, in modulating cellular and behavioral effects.

Pharmacological modification of cholinergic activity can impair or enhance odor discrimination, modify olfactory perception and short-term olfactory memories, and these effects are thought to occur via changes in odor coding by MTCs (Roman et al., 1993; Ravel et al., 1994; Doty et al., 1999; Mandairon et al., 2006; Chaudhury et al., 2009). Moreover, local infusion of cholinergic antagonists in the PC can disrupt acquisition of olfactory pattern separation, suggesting cholinergic activation could play a functional role in the cortex to mediate different olfactory behaviors (Chapuis and Wilson, 2013).

To summarize, while it is well known ACh can modulate several MOS

mediated olfactory behaviors, controversy remains as to the cellular mechanisms ACh to produce these behavioral effects. This study sought to further clarify ACh cellular activation in AOB and MOB neurons as a comparative study of ACh effects in these circuits. Further, MOS behaviors have been well characterized, however, the role of ACh in social behaviors is yet to be studied. We therefore, studied the role of top-down cholinergic modulation during biologically relevant behaviors (aggression and mating) thought to signal through the VNS.

CHAPTER 2: Methods

Animals

All animal procedures were carried out in accordance to the guidelines of the Institutional Animal Care and Use Committee (IACUC) of the University of Maryland. Electrophysiological and behavioral experiments were performed on wild-type strains (C57/BL6, Jackson Labs; Cf1/129S, Charles River) or transgenic mice expressing proteins under the choline acetyltransferase (ChAT) promoter: the ChAT-Cre, ChAT-Tau-GFP, and ChAT-Channelrhodopsin2-YFP lines (ChAT-ChR). The presence of the yellow fluorescent protein (YFP) in the latter allows for direct fluorescence detection of ChR expressing neurons. The ChAT-Cre and ChAT-ChR were obtained from Jackson Labs, stock # 006410 and 014546 (Rossi et al., 2011; Zhao et al., 2011). The Chat-Tau-GFP line was generously provided by Dr. Sukumar Vijayaraghavan (Salcedo et al., 2011), and the M1 and M1/M3 −/− double knockout mouse were provided by Dr. Jurgen Wess, NIH (Gautam et al., 2004). The OMP-YPF mice was obtained from Jackson Labs, stock # 014173 (Shusterman et al., 2011). Experiments were conducted in mice ranging in age from postnatal day 20 (PD-20) through 6 months old. Animals were kept on a 12-h light/dark cycle with access to food and water *ad libitum*. Behavioral testing occurred within a 5 hour window after the start of the dark phase of the light cycle.

Slice preparation

Electrophysiological recordings were performed in OB slices using methods previously described (Smith et al., 2009). Briefly, after euthanasia, the brain

was quickly removed and placed in oxygenated ice-cold artificial cerebrospinal fluid (ACSF) containing low Ca^{2+} (1 mM) and high Mg^{2+} (6 mM). Sagittal and horizontal sections (250 µm) of the OB were obtained using a Leica microslicer (Redding, CA). Slices were then transferred to an incubation chamber containing normal ACSF (see below) and left to recuperate at 35°C for 30 min, and at room temperature thereafter. For all experiments, the extracellular solution was ACSF of the following composition (in mM): 125 NaCl, 25 $NaHCO_3$, 1.25 NaH_2PO_4, 3 KCl, 2 $CaCl_2$, 1 $MgCl_2$, 3 myo-inositol, 0.3 ascorbic acid, 2 Na-pyruvate, and 15 glucose, continuously oxygenated (95% O_2/5% CO_2). Experiments were performed at room temperature (~25°C).

Data acquisition and analysis

After incubation, the slices were transferred to a recording chamber mounted on the stage of an Olympus BX51 microscope. Recordings were performed using a dual EPC10 amplifier (HEKA, Union City, NY) in the current-clamp mode. Fluorescence labeled neurons were visualized using 10X and 40X LUMPlanFI/IR Olympus water immersion objectives. Fluorescent illumination was achieved using an OPTOLED (Cairn Research LTD, UK) with blue and white LEDs (blue exciter λ 488 nm, green exciter λ 594 nm, Chroma Technology, VT). Emitted light was collected using an ORCA-Flash4.0 V2 sCMOS camera (Hamamatsu, Japan). LED stimulations were commanded using the PatchMaster software (HEKA USA, Bellmore, NY) and imaging analysis was performed offline using the ImageJ, IgorPro software (Wavemetrics, OR) and MATLAB. Current simulations mimicking *in vivo* synaptic activity were generated with MATLAB software and modeled using

neuronal parameters previously described (Galan et al., 2008; Padmanabhan and Urban, 2010). These simulated currents were superimposed onto direct current stimuli of different intensity (-20 to 80 pA) that were randomly interleaved. For ChR light stimulations, the blue light (λ 488 nm) intensity after the 40x objective was placed over the OB was 5 mW. Recordings were performed using standard patch pipettes (3-8 MΩ resistance), with an internal solution of the following composition (in mM): 120 K-gluconate, 10 Na-Gluconate, 4 NaCl, 10 HEPES-K, 10 Na phosphocreatine, 2 Na-ATP, 4 Mg-ATP, and 0.3 GTP, adjusted to pH 7.3 with KOH. In voltage-clamp, the internal solution had the following composition (in mM): 125 Cs-gluconate, 4 NaCl, 2 $MgCl_2$, 2 $CaCl_2$, 2 EGTA, 10 HEPES, 2 Na-ATP, 4 Mg-ATP, and 0.3 GTP adjusted to pH 7.3 with CsOH. The fluorescent marker Alexa-Fluor 594 (10 μM, Life Technologies) was included in the pipette solution for reconstruction and post hoc analysis of cell morphology using confocal imaging. MCs lacking primary and/or lateral dendrites were not included in the analysis. For Ca-imaging experiments, slices from ChAT-Cre mice expressing hM_4D_i (see below), containing the HDB, were transferred to a Milicell culture dish (Millipore Corp, Billerica, MA) containing 5 mL of oxygenated ACSF with 5 μM of the calcium indicator Fluo-4 AM (Molecular Probes, Life Technologies). Slices were submerged in the dye for 20 min and then transferred to the recording chamber. Illumination was achieved using an OPTOLED blue LED (exciter 488 nm center wavelength, Chroma; Cairn Research LTD). The emitted light was collected using an ORCA-Flash4.0 camera (Hamamatsu), and images were recorded using the HCimage software (Hamamatsu). Optical recordings in Fig. 5B correspond to selected HDB neurons responding to clozapine N-oxide (CNO). The ratio of the

change in fluorescence with respect to baseline was expressed as $\Delta F/F_0$. Electrophysiology and imaging analysis was performed offline using the ImageJ and IgorPro (Wavemetrics) software. The afterhyperpolarization (AHP) was measured as the most negative value of membrane potential following the depolarizing stimulus, and its peak usually occurred within 100 ms after the end of the pulse. The sADP was measured as the most positive value of membrane potential after the end of the pulse and its peak generally occurred within 5–10 s of the end of stimulus. The baseline value of membrane potential prestimulus was subtracted from each of these values; therefore the reported values of sADP correspond to the ΔV. The size of the sADP reported here corresponds to averages of the largest sADP recorded in different cells in the presence of agonist or agonist plus antagonist. To quantify the increase in synaptic activity induced by mAChR activation, we calculated the frequency of spontaneous excitatory potentials before and after oxotremorine (Oxo) addition. The average dose-response curve (DRC) for nicotine (Nic) was obtained from cells where at least three different concentrations of nicotine were applied, including 30 μM, which was used to normalize the responses. The DRC for Oxo was obtained in each cell using a concentration range of 0.3–10 μM, and the responses were normalized to 10 μM. For Nic and Oxo, the DRC for each cell was fitted to the Hill equation using the IgorPro software. The current-voltage relation for Nic in MCs was obtained using a ramp protocol from –120 to +60 mV (300 mV/ms) and in the presence of Ni 100 μM, Cd 100 μM, d-2-amino-5-phosphonopentanoic acid (APV) 100 μM, 2,3-dihydroxy-6-nitro-7-sulfamoybenzo-(f)-quinoxaline (NBQX) 10 μM, BMI 10 μM, and TTX 1 μM. Data values are presented as the mean ± SEM and statistical significance (p values) for pairwise comparisons were

calculated using the Student's t test, and presented as follows (unless noted in Figure): *p < 0.05, **p < 0.02 and ***p < 0.01.

Confocal imaging and immunohistochemistry

Mice were perfused intracardially with 4% paraformaldehyde (PFA) and after dissection, the brains were post fixed overnight at 4 °C. Subsequently, the brains were placed in phosphate buffered saline (PBS) and sagittally sliced at 100 µm. Similarly, for MCs fluorescently labeled during electrophysiological recordings, at the end of the experiments, slices were placed in 4% PFA for 20 min at room temperature (RT) and then washed overnight in PBS. Cells were visualized using TO-PRO-3 (T3605, Life Technologies) or DAPI (F6057, Sigma-Aldrich). For double-labeling immunofluorescence, free-floating sections (100 µm) obtained in a Vibroslicer (Vibratome Series 1000) were washed twice in PBS and then incubated with 10% donkey serum (Sigma Aldrich) in 0.1% PBS-Triton X-100 (PBS-T) for 1 h at RT. Slices were incubated overnight with one or more of the following primary antibodies, diluted in PBS-T with 2.5% of donkey serum; goat anti-ChAT (1:500, ab144p, Millipore), rabbit anti-VAChT (1:150, ab68984, Abcam), mouse anti-AChE (1:100, ab2803, Abcam), rabbit anti GFP (1:1000, A11122, Life Technologies) and mouse anti-RFP (1:750, ab65856, Abcam). After incubation with the primary antibodies the samples were washed with PBS-T seven times (5 min each), and then incubated for 2 h at RT with the secondary antibody: donkey anti-rabbit Alexa-488 (A-21206, Life Technologies); donkey anti-mouse Alexa-594 (A-21207, Life Technologies) and donkey anti-goat Alexa-488 (A-11055, Life Technologies), all diluted at 1:750 in PBS-T with donkey serum (2.5%). The sections were then washed three times in PBS-T and then four times in

regular PBS (5 min each). To visualize immunofluorescence, slices were mounted with Vectashield (Vector Laboratories) and imaged with a Leica SP5x confocal microscope (Leica Microsystems). Confocal imaging reconstructions and analysis were performed using the Leica software and ImageJ. For analysis of the density of ChAT positive (ChAT+) fibers in the OB (Fig. 4.4), we used an anti-GFP antibody to enhance the signal. Reconstruction were produced from stacked confocal images (63x, 50 μm in the z plane) and fluorescence intensity profiles were generated along a randomly selected 10 μm wide ROI. Fluorescence intensity values were quantified for the glomerular layer (GL), mitral cell layer (MCL), and granule cell layer (GCL). For each slice the fluorescence intensity values were normalized to the background fluorescence (ΔF/F), and values were averaged across animals. Analysis of axonal fiber density in the OB was performed as previously described (Krosnowski et al., 2012). Briefly, the raw images are filtered (5px median filter) and normalized to the peak values for each image. We then determined the average fluorescence intensity (normalized pixel intensity) across each layer.

Stereotaxic viral injections

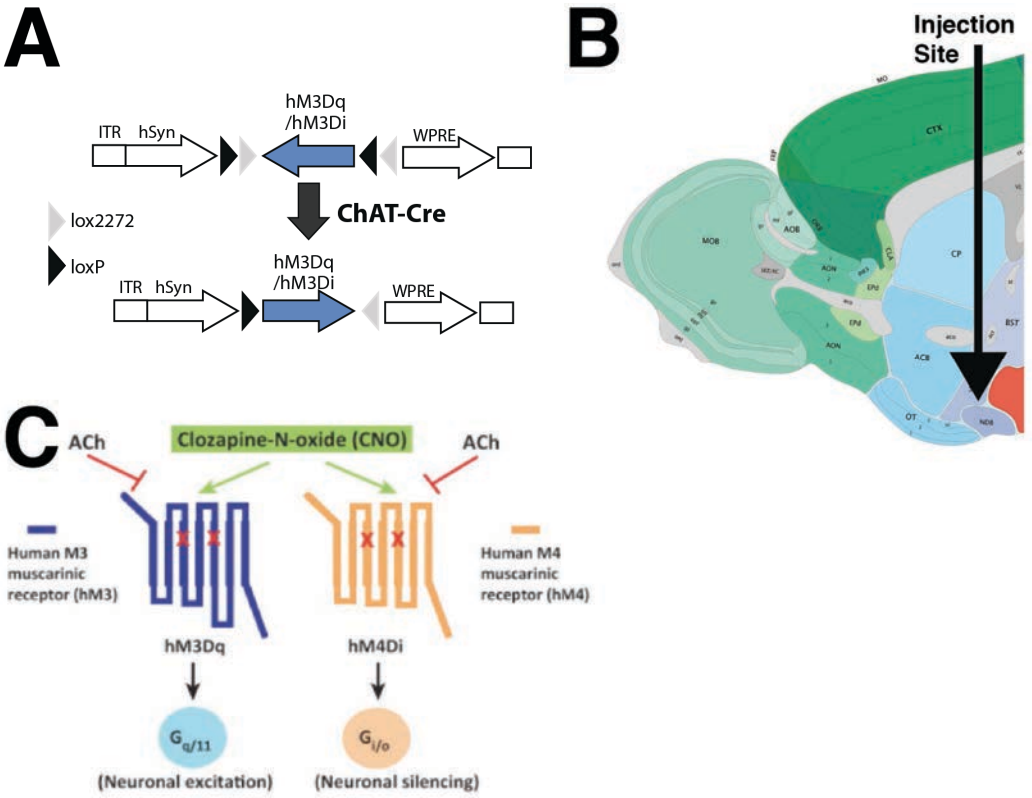

Figure 2.1 Chemogenetic control of HDB cholinergic neurons (ChAT) *in vivo*.

A. Stereotaxic targeting of a recombinant adeno-associated virus (AAV2) containing a doubly-floxed inverted open reading frame encoding $hM3D_q$ (AAV8-hSyn-DIO-hM3D(Gq)-mCherry) or $hM4D_i$ (AAV8-hSyn-DIO-hM4D(Gi)-mCherry) into the HDB of *ChAT-cre* transgenic mice, in which Cre-recombinase is highly and specifically expressed in acetylcholine producing neurons **(B).** These AAV vectors facilitate the expression of mCherry in $hM3D_q$ or $hM4D_i$ exclusively in Cre-expressing cells. **C.** DREADDs are mutant muscarinic receptors, $hM3D_q$ and $hM4D_i$. CNO activation of $hM3D_q$ couples with Gq to activate PLC-B to stimulate PIP2 hydrolysis into inositol-trisphosphate (IP3) and diacylglycerol (DAG), then DAG activates PKC, and IP3 activates the IP3 receptor (IP3R) to cause calcium release from the ER, and leads to cellular excitation. CNO activation of $hM4D_i$ couples to Gi-GPCRs opens GIRK to activate a hyperpolarizing current (Also see Figure 5.6). Figure C modified from J Wess Review, 2013.

Expression of the hM_4D_i and hM_3D_q Designer Receptors Exclusively activated by Designer Drugs (DREADDS) in ChAT-Cre mice was achieved by stereotaxic targeted injections (1 µL) of the adenovirus AAV8-hSyn-DIO-

hM3D(Gq)-mCherry or AAV8-hSyn-DIO-hM4D(Gi)-mCherry (University of North Carolina vector core) bilaterally into the HDB**.** Anesthetized mice (1.5% Isoflurane) were head-fixed (Model 900, Kopf Instruments) and a 33-gauge needle (5 µL syringe, Hamilton Company) was inserted through a 1 mm craniotomy window. The speed of virus injection (100 nL/min) was achieved by using a syringe pump (Micro4 Microsyringe pump, World Precision Instruments). Injections in the HDB was targeted using the following coordinates, in relation to bregma (in mm); Dorsal-Ventral axis -5.4, Medial-Lateral -1.625, Anterior-Posterior +0.14. Virus injections occurred at PD-30 and behavioral experiments were conducted beginning 6 weeks after the virus injection. We note that at 6 weeks post injection, the presence of the DREADDs can be readily detected using antibodies, however the red fluorescence (mCherry) in live tissue is very low, making the targeted patch recordings difficult.

Behavioral tests for natural odor discrimination

Odor discrimination was tested using the habituation/dishabituation paradigm as previously described (Nunez-Parra et al., 2013). Briefly, ChAT-Cre mice virally transfected with hM_4D_i or hM_3D_q received an intraperitoneal (i.p.) injection of PBS (control) or the biologically inert ligand clozapine N-oxide (CNO, 0.5mg/1 mL/100g, treated). Activation of DREADDS with CNO allows for modulation of HDB cholinergic neurons at physiological levels, with optimal behavioral effects observed 2 hours post CNO injection (Sternson and Roth, 2014). Ninety minutes post injection, mice were placed in a clean

cage (20 cm x 40 cm) in the presence of an unscented wooden block for 30 minutes.

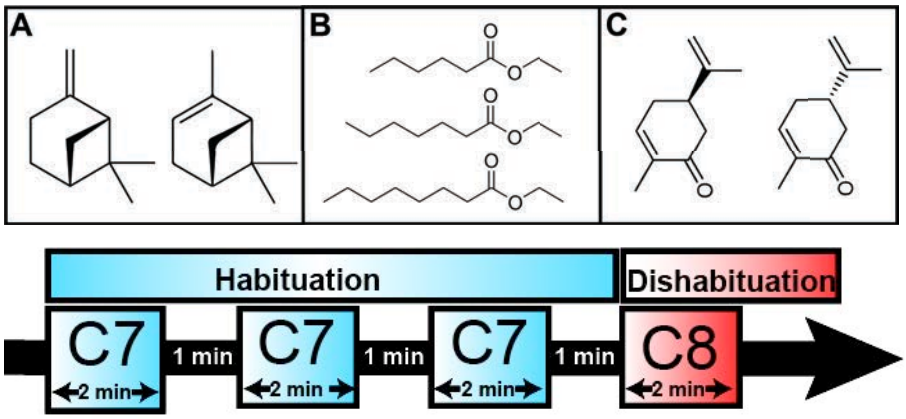

Figure 2.2 Odor Discrimination Test paradigm.
Top, Chemical structure of odors tested in habituation/dishabituation paradigm **A.** L- and D-Carvone, **B.** ethyl hexanoate (C6), ethyl heptanoate (C7), ethyl octanoate(C8). **C.** α–β pinene. *Bottom,* Graphic depicts timeline for odor presentations during habitiaiton/dishabaituaiton paradigm.

Following this familiarization period, both groups were tested for their ability to discriminate between the following odor pairs; ethyl heptanoate (C7)/ ethyl octanoate (C8), ethyl hexanoate (C6)/ ethyl octanoate (C8), L-carvone /D-carvone and α-pinene /β-pinene. During the habituation phase, each mouse was exposed during three consecutive trials to a wooden block scented with 100 µL of the first odor (1:1,000 dilution). The fourth exposure consisted of the test odor (dishabituation); each exposure lasted 2 min, with a 1 min inter trial interval. Each trial was videotaped for off-line quantification of the time the mouse spent investigating the block. The investigation time was defined as the total time when the mouse's nose was within a 2 cm radius of the wooden block. For assessment of odor threshold in the ChAT-hM_4D_i and

hM_3D_q mice, C7 was tested at increasing odor concentrations (1:60,000; 1:40,000; 1:30,000; 1:20,000) following three presentations of a block "scented" with distilled water. Odor discrimination was considered successful when mice showed a significant increase in investigation during the presentation of the test odor (C7).

Behavioral tests for natural investigation of male and female odors

Assessment of aggression-induced avoidance of conspecific odors in males was conducted using a modified resident-intruder paradigm (Koolhaas et al., 2013). Sexually naïve ChAT- hM_4D_i mice (intruders) and background matched CF1/129S mice (residents) were housed in isolation for two weeks prior to the experiments. Following the isolation period, experiments were performed in a neutral environment (20 cm x 40 cm cage) and soiled bedding from a conspecific was presented in a petri dish (100 x 15 mm) for 15 min. Ninety minutes post injection of PBS, or CNO, the ChAT-hM_4D_i intruder mice were presented again with soiled bedding from a resident male. Next, ChAT-hM_4D_i intruder mice undergo an aggressive encounter with the resident in which the ChAT- hM_4D_i intruder is defeated. Following the aggressive encounter, the ChAT- hM_4D_i intruder is returned to the neutral test arena and presented again with the soiled bedding from the resident mouse. To assess male preference for female bedding, male ChAT-hM_4D_i mice were first placed in the test arena in the presence of male soiled bedding as a control. Next, they were presented with female soiled bedding (15 min each). Female soiled bedding was obtained from group housed, sexually *naïve*, age/background matched mice (CF1/129S). All experiments were filmed using a camera with IR sensitivity for offline analysis (Full Spectrum 1080p IR Camera, Cleveland

Paranormal Supply Co, OH). Mice trajectories were analyzed using a custom MATLAB tracking software. Data shown in Fig. 4.6 are presented as a ratio from Trial 2 to Trial 1 (Trial 2 / Trial 1) of the average distance from the dish the intruder spent during the trial. Larger absolute values for the ratio indicate preference or avoidance for the soiled bedding. Quantifications of stereotypic social behaviors were performed by a blind observer and quantified as the total duration (s) within the 15 min investigation trial. The behaviors quantified included; investigating, (mouse nose in downward position on/in the petri dish), exploring (traversing cage, digging, climbing on walls, nondescript movement), grooming, and freezing.

Behavioral test for novel object recognition

The two samples, one environment, version of the novel object recognition (NOR) task was used following the protocol (Bevins and Besheer, 2006). The training objects used were two blue marbles, and the novel object used was a yellow wooden cube of approximately similar size. Prior to the NOR task, ChAT-hM_4D_i mice were familiarized to the testing arena for 10 minutes during two consecutive days. For NOR, the training period was 10 minutes, followed by a 45 minute interval before a 5 minute testing period. CNO injections were administered 2 hours before the start of training. The familiarization, training, and testing periods, were filmed and analyzed in custom MATLAB software to quantify investigation times and motor behavior in general.

Solutions and pharmacological agents

The following drugs were bath applied: *N,N,N*-trimethyl-4-(2-oxo-1-pyrolidinyl)-2-butyn-1-ammonium iodide (oxo), 6-imino-3-(4-methoxyphenyl)-1(6H)-pyridazinebutanoic acid hydrobromide (GABAzine), 6-cyano-7-nitroquinoxaline-2,3-dione disodium (CNQX), DL-2-Amino-5-phosphonopentanoic acid (APV), 11-[[2-[(Diethylamino)methyl]-1-piperidinyl]acetyl]-5,11-dihydro-6*H*-pyrido[2,3-*b*][1,4]benzodiazepin-6-one (AFDX-116), [*S*-(*R**,*R**)]-[3-[[1-(3,4-Dichlorophenyl)ethyl]amino]-2-hydroxypropyl](cyclohexylmethyl) phosphinic acid (CGP-54626), (−)-nicotine ditartrate (Nic), tetrodotoxin (TTX), 4-[[[(3-chlorophenyl)amino]carbonyl]oxy]-*N,N,N*-trimethyl-2-butyn-1-aminium chloride (MCN-A-343), 1,1-dimethyl-4-diphenylacetoxypiperidinium iodide (4-DAMP), (−)-cytisine (Cys), mecamylamine hydrochloride (MM), dihydro-β-erythroidine hydrobromide (DHBE), methyllycaconitine citrate (MLA), LY367385, and *N*-methyl-d-glucamine (NMDG).

For electrophysiology recordings the speed of perfusion permitted for full solution exchange of the recording chamber in < 30 s. However, the reported values of "time to peak" are an overestimate, as we do not subtract the dead volume in the perfusion line, which also adds to the total time it takes the agonist to reach the recorded neuron. Therefore, in a few experiments we conducted experiments using local perfusion of drugs (AutoMate Scientific, CA). Antagonists were applied for at least 10 min before the application of the agonist. All drugs were purchased from Tocris Cookson (UK) unless otherwise indicated. CNO, (Enzo Life Science) was prepared fresh daily in PBS at 0.5mg/mL, and injected at 0.5mg/100g. All odors used for behavior experiments were purchased from Sigma-Aldrich (St. Louis, MO).

Chapter 3 Cholinergic modulation of neuronal excitability in the accessory olfactory bulb

Citation

Smith RS, Weitz CJ & Araneda RC (2009). Excitatory actions of noradrenaline and metabotropic glutamate receptor activation in granule cells of the accessory olfactory bulb. J Neurophysiol 102, 1103–1114

Abstract

The accessory olfactory bulb (AOB), the first relay of chemosensory information in the Vomeronasal system, receives extensive cholinergic innervation from the basal forebrain. Cholinergic modulation of neuronal activity in the olfactory bulb has been hypothesized to play an important role in olfactory processing; however, little is known about the cellular actions of acetylcholine (ACh) within the AOB. Here using in vitro slice preparation, we show that muscarinic acetylcholine receptor (mAChR) activation increases neuronal excitability of granule and mitral/tufted cells (GCs and MCs) in the AOB. Activation of mAChRs increased excitability of GCs by three distinct mechanisms: induction of a long-lasting depolarization, activation of a slow afterdepolarization (sADP), and an increase in excitatory glutamatergic input due to MC depolarization. The depolarization and sADP were elicited by the selective agonist 4-[[[(3-chlorophenyl)amino]carbonyl]oxy]-*N,N,N*-trimethyl-2-butyn-1-aminium chloride (100 μM) and blocked by low concentrations of pirenzepine (300 nM), indicating that they result from activation of M1-like mAChRs. In contrast, cholinergic stimulation increased the excitability of MCs via recruitment of nicotinic AChRs (nAChRs) and M1-like mAChRs. Submaximal activation of these receptors, however, decreased the excitability of MCs. Surprisingly, we found that unlike GCs in the main olfactory bulb, GCs in the AOB are excited by mAChR activation in young postnatal neurons, suggesting marked differences in cholinergic regulation of development between these two regions of the olfactory bulb.

Introduction

The olfactory bulb (OB) is the site of initial information processing in the olfactory pathway. The most abundant neurons within the main and accessory OB (MOB and AOB, respectively) are the inhibitory granule cells (GCs). The GCs regulate the excitability of the principal projection neurons, the mitral and tufted cells (MCs) through GABAergic inhibition at reciprocal dendrodendritic synapses (Shepherd and Greer 1998). The processing of sensory information in the OB, and the relay of this information to higher centers by the MCs is crucial for the survival of most mammals (e.g., feeding and mating). The inhibitory synapses from GCs to MCs play an important role in olfactory processing and are the target of several afferent neuromodulatory systems to the OB (Ennis et al. 2007; Schoppa and Urban 2003).

The OB receives a rich cholinergic innervation from the nucleus of the horizontal limb of the diagonal band of Broca (HDB), located in the basal forebrain, which has divergent projections that innervate all layers of the OB (Kasa et al. 1995; Le Jeune and Jourdan 1991; Le Jeune et al. 1995; Nickell and Shipley 1988; Ojima et al. 1988; Zaborszky et al. 1986). Two types of cholinergic receptors, nicotinic and muscarinic receptors, mediate the actions of acetylcholine (ACh) throughout the brain (nAChRs and mAChRs, respectively). ACh receptors are further divided into subtypes that elicit distinct cellular effects on activation, thereby providing a diverse array of mechanisms to regulate neuronal activity (Lanzafame et al., 2003; Gotti et al., 2006). Both nAChRs and mAChRs are found in the OB, albeit with a differential pattern of distribution, suggesting that selective activation of these receptors could modulate different aspects of olfactory processing (Hill et al.,

1993; Le Jeune et al., 1996; Keiger and Walker, 2000; Whiteaker et al., 2009).

In the MOB, the cellular and behavioral consequences of cholinergic neuromodulation have been extensively studied. For example, blocking the cholinergic input to the MOB has a profoundly deleterious effect on odor discrimination, while enhancing cholinergic activity improves discrimination between chemically similar odorants (Ravel et al., 1994; Linster et al., 2001; Mandairon et al., 2006). In addition, in vitro studies have indicated that MCs and GCs are differentially modulated by the cholinergic system. Both inhibitory and excitatory muscarinic effects have been described in GCs while excitatory nicotinic and muscarinic effects have been described in MCs (Castillo et al., 1999; Pressler et al., 2007; Pignatelli and Belluzzi, 2008). Furthermore, recent studies in the MOB have suggested that neuromodulation by the cholinergic system is developmentally regulated (Ghatpande et al., 2006; Gelperin and Ghatpande, 2009). Thus in early postnatal development (<10 days), cholinergic neuromodulation exists only in MCs, while later in development, GCs begin to exhibit a cholinergic excitatory effect (Ghatpande and Gelperin 2009). This developmental shift in cholinergic neuromodulation may have an important implication for the functioning of developing GCs and/or their role in perinatal olfactory mediated behaviors (Brennan and Keverne 1997).

Despite the crucial role of the AOB in the processing of pheromonal information by the Vomeronasal system (Halpern and Martinez-Marcos 2003), the targets and cellular effects of the cholinergic system in this region remain insufficiently understood. Neuromodulation of the AOB circuitry by afferent

input is thought to promote the structural and functional synaptic plasticity underlying AOB mediated behaviors that require learning (Brennan and Keverne 1997). Specifically, extensive studies have shown that modulation of AOB circuitry by the noradrenergic system underlies the formation of memory in the Bruce effect in mice (Brennan and Peele 2003). Here we characterize the cellular actions of cholinergic modulation in the AOB using whole cell recordings of GCs and MCs. Using selective pharmacological agents, we show that activation of an M1-like mAChR produces a long-lasting excitation in both GCs and MCs. However, the mAChR-mediated excitation differed between these cells. In GCs but not MCs, M1-like mAChR activation also elicited the appearance of a stimulus-driven slow afterdepolarization. In addition, cholinergic stimulation in MCs also involves the recruitment of ionotropic nAChRs. Surprisingly, we find that unlike the developmental shift in excitatory muscarinic response observed in the MOB, the M1-like excitatory action in GCs is present in the AOB from early postnatal ages throughout adulthood in the AOB. Together, these results indicate that GCs are directly excited by muscarinic receptor activation, resulting in an increase in the inhibitory input onto MCs, thereby decreasing MC activity. Concomitantly, stimulation of either nicotinic or muscarinic receptors would increase MC activity, resulting in an opposite effect on bulbar output. However, under submaximal cholinergic stimulation, only the inhibitory effect onto MCs prevails. Further, our study also provides evidence for developmental differences in the function of cholinergic modulation controlling neuronal components of the AOB compared with the MOB.

Results

M1-like muscarinic acetylcholine receptor activation excites granule cells

At least five different muscarinic receptor types have been identified all of which can be activated by the nonselective agonist Oxo. Application of Oxo (30 μM, 2–3 min) produced a long-lasting depolarization of GCs (14.8 ± 1.0 mV; *n* = 45, Fig. 3.1*A*, *left trace*). The depolarization had a slow onset (>45 s) and typically persisted several minutes (>10 min) after washout. In addition, Oxo induced the appearance of a sADP following a stimulus-evoked train of action potentials (5–50 pA; 500 ms, Fig. 3.1*A*, *right*). In control, a depolarizing current stimulus elicited several nonaccommodating spikes, which were followed by a small AHP at the end of the stimulus pulse (Fig. 3.1*A*, *middle*, ↓, –1.7 ± 0.3 mV, *n* = 4). Following this AHP (~2 s), the membrane potential was not significantly different from baseline (baseline, −66.4 ± 2.0 mV; after stimulus, −66.5 ± 2.0 mV, *n* = 4. In the presence of Oxo, the stimulus pulse produced an increase in the number of evoked action potentials and the AHP was now overridden by a sADP (5.0 ± 0.3 mV, *n* = 20, Fig. 3.1*A*, *right*). The depolarization and the sADP were significantly reduced by pirenzepine (Pir, 300 nM), which at low concentrations selectively blocks M1 muscarinic acetylcholine receptors (M1-mAChR; Fig. 3.1*B*, *left trace*). In the presence of pirenzepine (300 nM), the depolarization was reduced by ~88% (control, 14.0 ± 0.9 mV; in Pir, 1.6 ± 0.7 mV; $P < 0.0005$; *n* = 7, Fig. 3.1*D*, *top*) while the sADP was reduced by ~92% (control, 5.7 ± 0.4 mV; in Pir, 0.5 ± 0.3 mV; $P < 0.0002$; *n* = 6, Fig. 3.1*D*, *bottom*). Furthermore, application of the selective M1-

mAChR agonist MCN-A-343 (100 μM) mimicked the depolarization and sADP produced by Oxo (depolarization, 10.9 ± 1.6 mV; sADP, 4.4 ± 0.5 mV; *n* = 11, Fig. 3.1*C*, *right* and *middle traces*, and *D*). Activation of M1 and M3 mAChRs produce similar effects in various neuronal types (Lanzafame et al. 2003); however, the selective M3-mAChR antagonist 4-DAMP (300 nM) did not affect the depolarization induced by Oxo (depolarization; 15.3 ± 1.3 mV; sADP 4.5 ± 0.3 mV, *n* = 4; data not shown). Like Oxo, application of a high concentration of nicotine (300 μM) depolarized and increased excitatory synaptic activity in GCs (21.2 ± 0.6 mV, *n* = 5; Fig. 3.2*A*). However, these excitatory responses were drastically reduced in the presence of blockers of glutamatergic synaptic transmission (2.0 ± 0.6 mV; in 10 μM CNQX, 100 μM APV, and 100 μM LY367385; $P < 0.002$; Fig. 3.2*C*), indicating that this depolarization does not result from a direct nicotinic effect on GCs (see also following text).

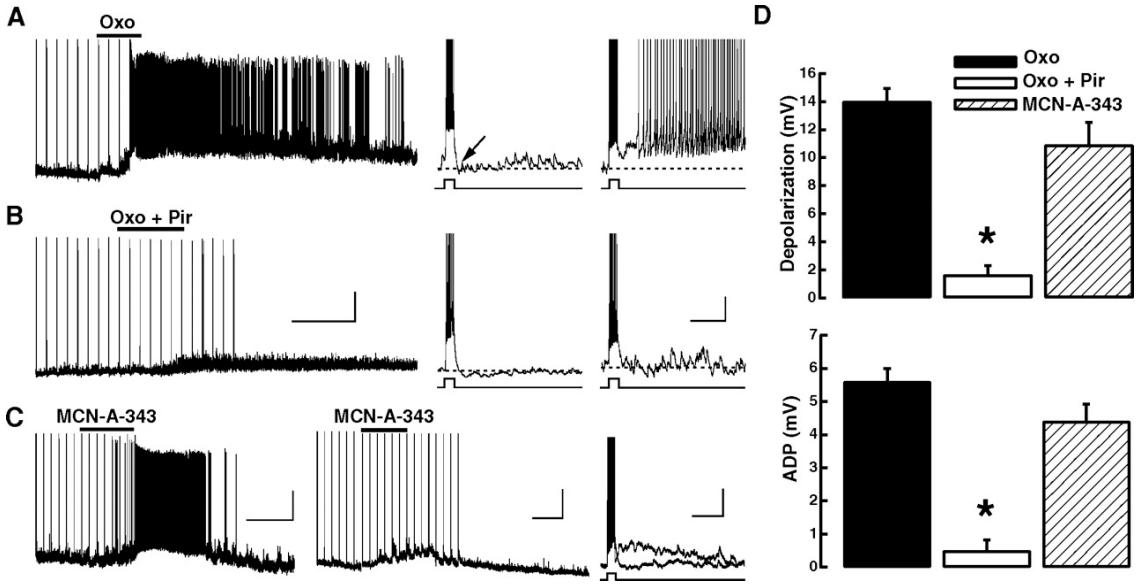

Figure 3.1 Muscarinic acetylcholine receptor (mAChR) agonists excite granule cells (GCs). *A, left*: bath application of the nonselective muscarinic agonist oxotremorine (Oxo, 30 μM, 2 min) produced a robust membrane depolarization and sustained firing of action potentials. *Right*: in addition to membrane depolarization, Oxo (30 μM, 3 min) induced the appearance of a slow afterdepolarization (sADP) following a stimulus-induced train of action potentials (20 pA, 500 ms, *right trace*). In control the action potentials are followed by a small AHP (↓, see text). *B, left trace*: low concentration of the M1 mAChR antagonist pirenzepine (Pir, 300 nM) greatly reduced the Oxo-induced depolarization and sADP (*right traces*). Responses in *A* and *B* are from the same cell, the calibration bar is 20 mV and 3 min (traces on the *left*) and 10 mV and 2 s (traces on the *right*). The resting membrane potential (RMP) is –65 mV. *C*: the M1 mAChR agonist 4-[[[(3-chlorophenyl)amino]carbonyl]oxy]-*N*,*N*,*N*-trimethyl-2-butyn-1-aminium chloride (MCN-A-343; 100 μM, 3 min) mimics the Oxo-induced depolarization and sADP. *Right*: superimposed traces showing the stimulus-induced sADP obtained in control and MCN-A-343 from the cell in the *middle panel*. The calibration bar is 20 mV and 3 min (*left traces*) and 10 mV and 2 s (*right traces*); the RMP is –61 mV (*left*) and –64 mV (*right*). *D*: summary of the pharmacological profile of the excitatory muscarinic response in GCs. Pir (□) significantly reduced the Oxo-induced depolarization (■) and sADP (depolarization, *top*, $*P < 0.0005$; sADP, *bottom*, $*P < 0.0002$). Both excitatory effects were mimicked by MCN-A-343 (▨).

Application of Oxo (30 μM) also produced an increase in synaptic activity in GCs most likely due to an increase in glutamatergic excitation at dendrodendritic synapses. This excitatory response results from activation of muscarinic receptors in MCs (see following text); accordingly, application of Oxo increased the frequency of excitatory postsynaptic potentials (EPSPs) by fourfold (baseline, 2.4 ± 0.6 Hz; Oxo, 9.4 ± 2 Hz; $n = 4$), and this effect was greatly reduced in the presence of ionotropic glutamate receptor blockers (NBQX and APV, 10 and 100 μM, respectively; Oxo plus blockers; 3.0 ± 0.8 Hz, $P < 0.02$; $n = 4$). Nevertheless, in the presence of the fast synaptic transmission blockers, the M1-like mAChR-induced depolarization of GCs was reduced only slightly (Oxo control, 16.0 ± 1.2 mV; Oxo plus blockers, 14.2 ± 1.7 mV; $P < 0.3$; $n = 5$). These results indicate the increase in the excitatory synaptic drive onto GCs only partially contributes to the M1-like mAChR-induced depolarization in GCs. Furthermore, we have previously shown that activation of metabotropic glutamate receptor type 1 (mGluR1) and α_1 adrenergic receptors produce an excitatory response and activation of a sADP in GCs. In these studies, the α_1 excitatory response was reduced by blockers of mGluR1 receptors, suggesting that α_1 adrenergic receptor activation potentiates a basal mGluR1 activity (Smith et al. 2009). We wondered if activation of muscarinic receptors in GCs could act through a similar mechanism. Therefore we recorded GC responses to carbachol (30 μM) in the presence of a mixture of glutamate receptors blockers that included 100 μM LY367385; 10 μM CNQX, and 100 μM APV. As shown in Fig. 3.2*A*, in the presence of these blockers carbachol still produced a robust depolarization

and the stimulus-induced sADP (depolarization: 15.3 ± 2.0 mV; sADP, 4.8 ± 0.5 mV; *n* = 4, Fig. 3.2*C*).

Similarly, the depolarization and sADP produced by Oxo were not affected by 100 μM LY367385 (depolarization, 17.3 ± 1.2 mV; sADP, 5.8 ± 0.1 mV; *n* = 9, not shown). These results further indicate that the muscarinic response results from a direct action in GCs and that this excitatory response is not dependent on activation of mGluR1.

The muscarinic-induced depolarization and sADP are qualitatively similar to those previously described in the GCs of the MOB as well as in olfactory cortex (Constanti et al., 1993; Libri et al., 1994; Pressler et al., 2007). Interestingly, we have shown that activation of α_1-adrenergic receptors also produces a similar excitatory effect in the GCs of the AOB (Smith et al. 2009). Further, the physiological and pharmacological properties of the excitation produced by Oxo and α_1-adrenergic receptor agonists on GCs have indicated that activation of these receptors results in the recruitment of a nonselective cationic current, I_{CAN} (Pressler et al. 2007; Smith et al. 2009). Accordingly, reducing the driving force for sodium ions by lowering the extracellular concentration to 10 mM by replacing the external Na ions with *N*-methyl-glucamine (NMGM), and in the presence of TTX (0.5 μM), greatly reduced the depolarization (control, 14.0 ± 3.5 mV; NMGM, 3.3 ± 0.3 mV; $P < 0.05$; *n* = 3, Fig. 3.3*B*) and sADP (control, 4.7 ± 0.6 mV; NMGM, 0.7 ± 0.1 mV; $P < 0.02$; *n* = 3, *B*) induced by M1-like mAChR activation.

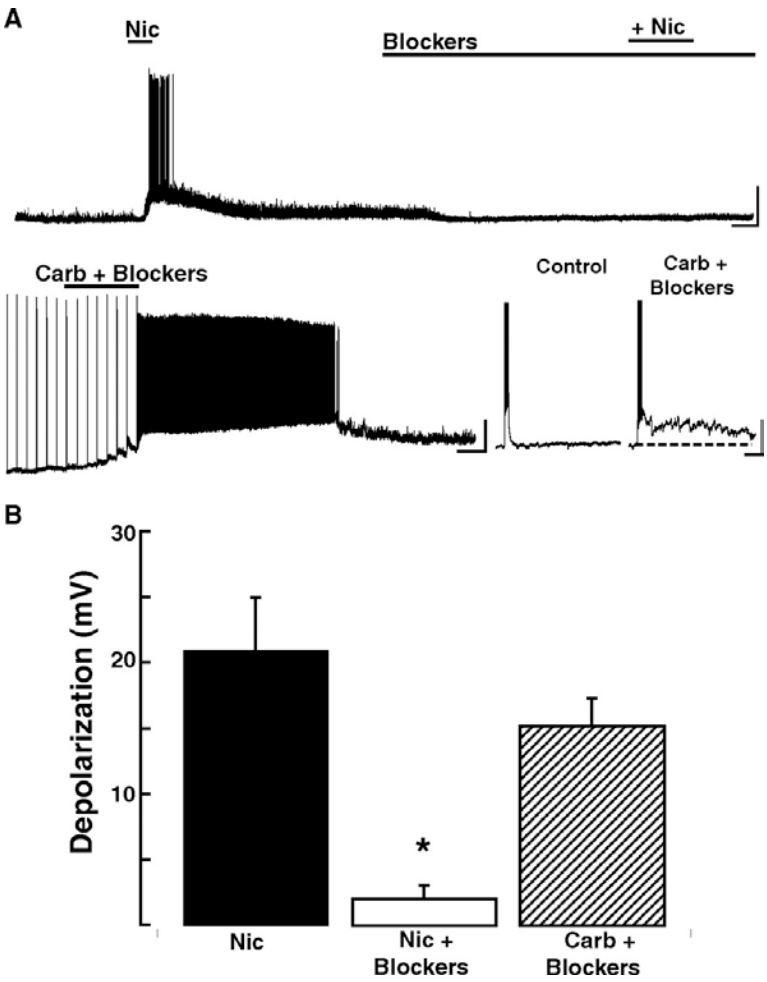

Figure 3.2 Muscarinic but not nicotinic acetylcholine receptor activation directly excites GCs. *A, top*: bath application of nicotine (Nic, 300 μM, 1 min) produced a robust depolarization that elicited firing of action potentials and increase in excitatory synaptic activity. Application of a mixture of glutamate receptor (GluR) blockers including 100 μM LY367385, 10 μM 6-cyano-7-nitroquinoxaline-2,3-dione disodium (CNQX), and 100 μM d-2-amino-5-phosphonopentanoic acid (APV) produced a decrease in the excitatory synaptic activity and greatly reduced the response to nicotine. The calibration bar is 20 mV and 1 min. *Bottom*: in the presence of the same mixture of GluR blockers, application of carbachol (30 μM, 3 min) produced a robust depolarization and the appearance of a sADP following a stimulus-induced train of action potentials (20 pA, 500 ms, *right trace*). The calibration bar is 20 mV and 1 min for the *left trace* and 10 mV and 2 s for the *right-hand traces*. The RMP is –60 mV (*top*) and –61 mV (*bottom*). *B*: graph bar summarizing the effects of GluR blockers on the excitatory responses to carbachol (30 μM) and nicotine (300 μM). The nicotinic excitatory response (■) is significantly reduced in the presence of the blockers (□, * $P < 0.002$), while the response to carbachol is not affected (▨; see text).

We note that extracellular Na substitution did not significantly reduce the AHP that follows the stimulus-induced action potentials in GCs (control, −1.8 ± 0.1 mV; NMGM, −1.5 ± 0.5 mV; *n* = 4, Fig. 3.3*A*, AHP indicated by ↓), indicating that the equilibrium potential for K ions was not perturbed under these conditions. A recent study in the AOB indicated that the increase in GABA mIPSC frequency recorded in MCs is sensitive to blockers of the M-current (Takahashi and Kaba 2010). However, we found that the selective blocker of the KCNQ K-channel, XE-991 (50 μM), failed to reduce the depolarization produced by Oxo (10 μM) (Oxo plus XE-991, 16.5 ± 1.5 mV; *n* = 3, data not shown). Together this suggests that the excitatory action produced by M1-like mAChR activation in GCs in the AOB is due to the activation of I_{CAN}.

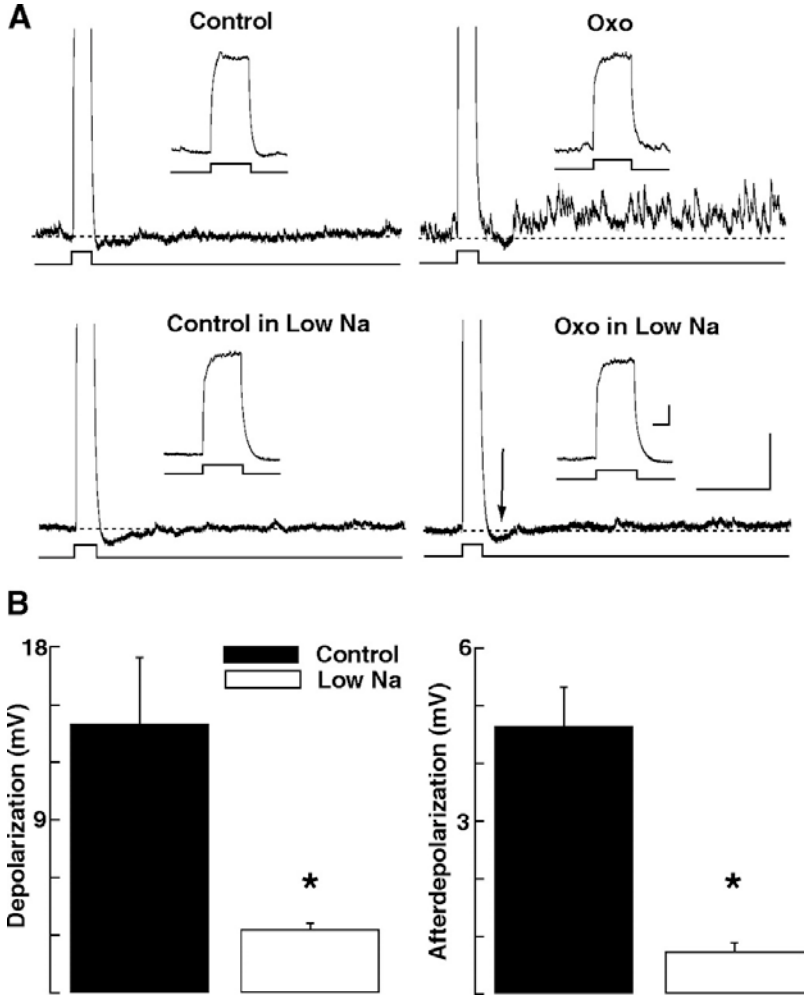

Figure 3.3 The sADP an d depolarization is dependent on extracellular Na. *A, top*: in the presence of fast synaptic transmission blockers and TTX (1 μM, NBQX 10 μM, and APV 100 μM, see text), Oxo (30 μM) depolarized GCs (not shown) and induced the appearance of sADP (*right trace;* 5.1 mV in this cell) following a current stimulus (25 pA, 500 ms). *Bottom traces*: the extracellular Na concentration was reduced to 10 mM with iso-osmolar replacement with NMDG. In low Na, the Oxo-induced sADP following current stimulus (50 pA, 500 ms) and a depolarization (not shown) were almost completely abolished. The dotted line indicates the membrane potential before the depolarizing stimulus, control –64 mV, low Na –67 mV. ↓, the AHP following the current stimulus is not reduced in the low-Na solution (*bottom right trace*, see text). The calibration bar is 2 s and 10 mV, and 200 ms and 10 mV for the *inset*. *B*: graph bar summarizing the effects of low extracellular Na concentration (□) on the depolarization and sADP elicited by Oxo (30 μM); both the depolarization and sADP are significantly reduced in low Na (* $P < 0.05$, see text).

M1-like induced depolarization has a young age onset in granule cells

Recent studies have indicated that the muscarinic-induced excitation of GCs is developmentally regulated in the MOB (Ghatpande and Gelperin 2009; Ghatpande et al. 2006). Thus GCs at postnatal day 10 (P10) or younger do not exhibit a direct M1-mAChR excitatory response in the MOB (Ghatpande and Gelperin 2009). Surprisingly, in the AOB the M1-like mAChR mediated excitation of GCs was present at postnatal age younger than P10. As shown in Fig. 3.4*A*, the effect of Oxo (30 μM) was qualitatively similar at early postnatal days (P6, Fig. 4*A*, *top left*) to that of the adult (P60, 4*A, top right*), and both the depolarization and sADP were present (depolarization 16 ± 1 mV; sADP, 5.1 ± 0.3 mV; n = 9, Fig. 3.4*A*, *inset*). Additionally, Oxo increased the frequency of spontaneous EPSPs by about fourfold in these young postnatal GCs, consistent with activation of mAChRs in MCs (see following text, baseline, 0.5 ± 0.1 Hz; Oxo, 2.2 ± 0.5 Hz; n = 4). Furthermore, when we grouped the responses by age, we found no significant differences between cells at $P < 10$ days, onward (Fig. 4*B*). Additionally, the excitatory effect of Oxo at P6 was abolished by Pir (300 nM), which at nanomolar concentrations blocks M1 mAChRs (control: 13.3 ± 1.2 mV; in Pir, 0.9 ± 0.3 mV; $P < 0.01$, n = 3, Fig. 3.4*C*). More importantly, at P6, blockers of ionotropic glutamatergic receptors (10 μM NBQX and 100 μM APV) did not significantly reduce the Oxo induced excitatory response, suggesting a direct effect of Oxo on GCs (control, 16.6 ± 2.2 mV; Oxo plus blockers, 11.5 ± 1.3 mV, n = 5, $P < 0.06$, Fig. 3.4*C*). Thus GCs in the AOB do not exhibit a developmentally triggered switch on the site of action of M1-mAChR-mediated excitation as it has been shown in GCs of the MOB (Ghatpande and Gelperin 2009).

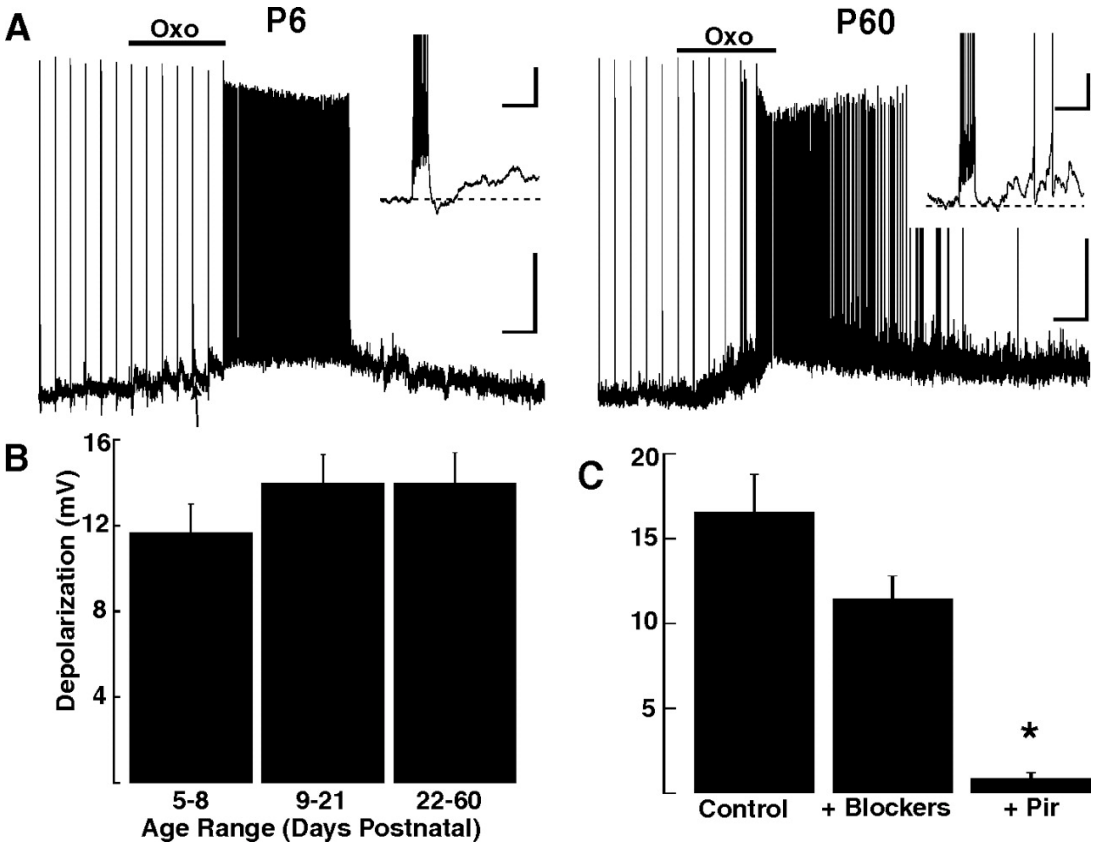

Figure 3.4. Excitatory muscarinic responses in GCs are present from early postnatal days. *A*: GCs recorded in slices from postnatal day 6 (P-6, *left trace*) exhibit a robust depolarization and stimulus-induced sADP (*inset*) in the presence of Oxo (30 μM). This response is qualitatively similar to the excitatory muscarinic response in adult mice (P-60, *right trace*). The RMP of both cells is –67 mV; calibration bar is 20 mV and 1 min and 10 mV and 1 s for the *inset*. *B*: bar graph showing the average depolarization in postnatal, age-grouped, cells. No significant difference is observed in the degree of depolarization induced by Oxo (30 μM) in these different groups. *C*: the muscarinic depolarization response in the young mice is insensitive to blockers of excitatory fast synaptic transmission (10 μM NBQX, and 100 μM APV, $P < 0.06$), but it was greatly reduced by the selective M1 mAChR antagonist Pir (300 nM, $P < 0.01$).

Nicotinic and M1 muscarinic acetylcholine receptor activation excites mitral cells

Cholinergic projections are found throughout the layers of the OB suggesting the potential regulation of different neuronal populations by this neuromodulatory system (Le Jeune and Jourdan 1991; Le Jeune et al. 1995; Ojima et al. 1988). To this end, application of the nonselective muscarinic agonist Oxo (30 μM, 2–3 min) also depolarized MCs in the AOB (12.8 ± 1.0 mV; *n* = 25, Fig. 3.5*A*). This depolarization was greatly reduced in the presence of Pir (300 nM; control, 13.0 ± 0.8 mV; in Pir, 1.3 ± 0.7 mV; $P < 0.0001$; *n* = 6, Fig. 3.5, *B, right*, and *D*) and mimicked by MCN-A-343 (100 μM; 9.5 ± 0.6 mV; *n* = 4, Fig. 3.5*B*, *left*). These results suggest that the muscarinic-induced depolarization in MCs is due to the activation of M1-like mAChRs. Surprisingly, activation of mAChRs was not accompanied by a stimulus-induced sADP in MCs. Thus at 5 s poststimulus (see methods), the membrane potential was similar in the absence and presence of Oxo (Fig. 3.5*A*, *right*). On the other hand, we observed an increase in the size of the AHP triggered by the stimulus, consistent with the depolarization of the membrane potential by Oxo (control, −2.1 ± 0.2 mV; Oxo, −4.9 ± 0.5 mV; $P < 0.02$; *n* = 3, data not shown). One possibility is that the sADP in MCs is relatively small and was therefore masked by recurrent inhibition from GCs triggered by our stimulus protocol. To test this possibility, we applied Oxo in the presence of blockers of glutamate (100 μM APV and 10 μM NBQX) and GABA ionotropic receptors (5 μM, GABAzine, Fig. 3.5*C*). In the presence of these blockers, the current-stimulus still failed to induce a sADP (baseline before stimulus, −56.0 ± 1 mV; after stimulus, −55.9 ± 0.9 mV; *n* = 3, Fig. 3.5*C*, *bottom*), while the

depolarization produced by Oxo was not significantly different (control, 15.0 ± 2.7 mV; plus blockers, 16.4 ± 3.5 mV; *n* = 7, data not shown). These results suggest that the M1-mAChR depolarization in MCs is mechanistically different in MCs versus GCs.

The cholinomimetic carbachol (CCh, 30 μM; 2–3 min) also depolarized MCs; however, under our recording conditions, the onset of this response was faster than in the Oxo response (CCh, 37.5 ± 3.2 s; Oxo, 104.1 ± 9.0 s; $P < 0.005$; $n = 4$, data not shown). In addition, application of Pir (300 nM) only partially reduced the depolarization produced by CCh (control, 12.0 ± 1.3 mV; in Pir, 8.75 ± 1.1 mV; $P < 0.004$; $n = 4$) while the onset of the response was unchanged (CCh control, 37.5 ± 3.2 s; in Pir, 37.2 ± 3.0 s; $n = 4$). The faster onset and partial sensitivity to Pir suggests that the depolarizing response produced by CCh is due to activation of mAChR and nicotinic AChRs (nAChR). Accordingly, application of the selective nAChR agonist Nic (30 μM) resulted in depolarization of MCs that in most cells resulted in robust firing (Fig. 3.6*A*, $n = 7$).

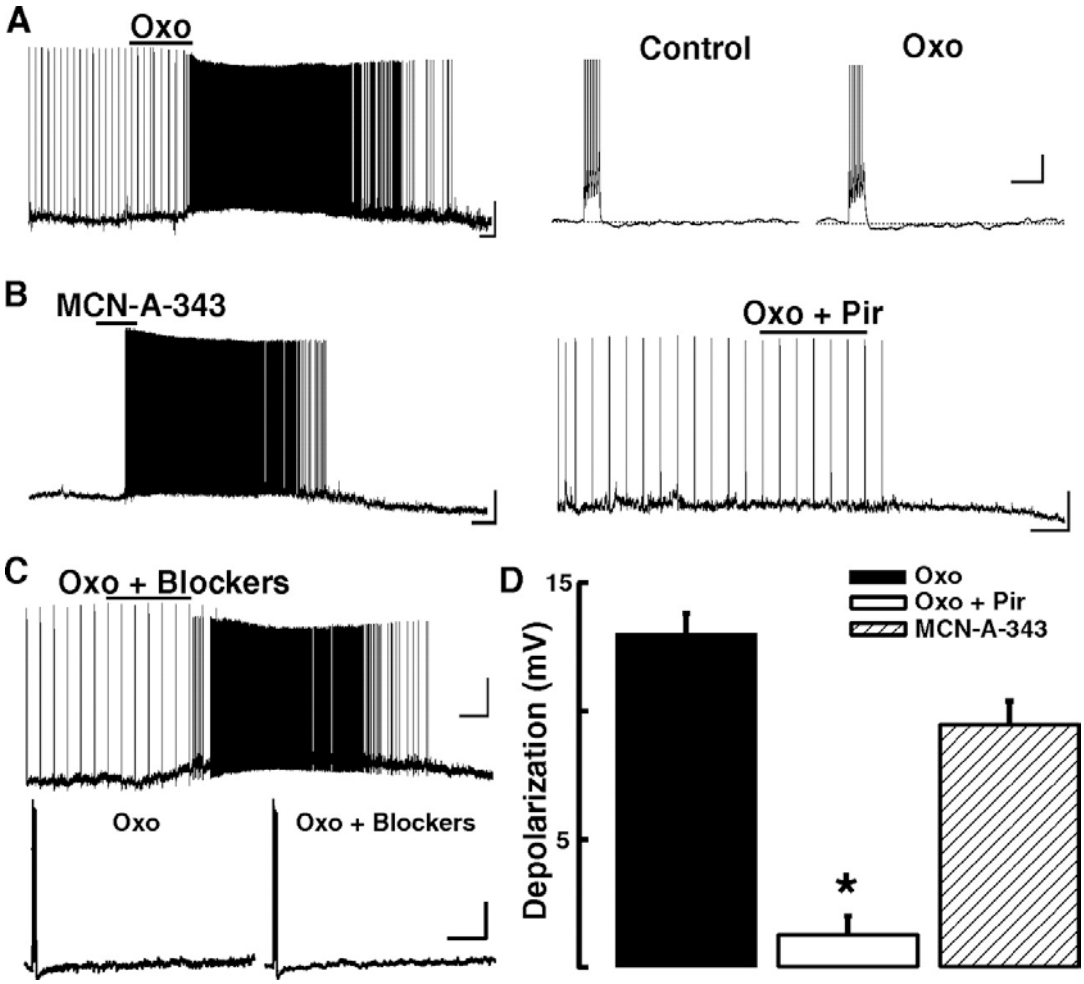

Figure 3.5. M1-mAChR activation produces an excitatory response in mitral and tufted cells (MCs). *A*: MCs are depolarized by Oxo (30 μM; 3 min, *left*), but a train of stimulus-induced action potentials is not followed by a sADP (stimulus: 75 pA, 500 ms, *right traces*). Compared with GCs, the depolarization elicited by Oxo in MCs has a faster onset (<45 s), but it similarly lasted several minutes (>10 min, see Fig. 1). The RMP in this cell is –62 mV; the calibration bar is 20 mV and 1 min (*left*) and 10 mV and 1 s (*right*). *B*: the excitatory effect of Oxo is mimicked by the selective M1 mAChR agonist MCN-A-343 (100 μM, 2 min, *left*) and greatly reduced by Pir (300 nM, *right*). The RMP in these cells is –62 and –66 mV, respectively. *C*: Oxo (30 μM) still produced a robust depolarization in the presence of blockers of fast excitatory and inhibitory synaptic transmission (100 μM APV, 10 μM CNQX, 5 μM GABAzine). In the presence of blockers, the sADP was still present. *D*: bar graph summarizing the effects of selective mAChR agonist and antagonists in MCs. The depolarizing response of Oxo (30 μM, ■) was significantly decreased in the presence of Pir (300 nM, □, $P < 0.02$) and mimicked by MCN-A-343 (100 μM, ▨).

Several receptor subunit composition and properties distinguish neuronal nAChR, including sensitivity to agonists and propensity to desensitization (Hogg et al., 2003). To further characterize the nicotinic response in MCs, we conducted voltage-clamp experiments. At −60 mV, bath application of Nic (1–300 μM; 30 s) produced a fast onset (<20 s) inward current (Fig. 3.6*B*, Nic 30 μM; −347 ± 27 pA; *n* = 36). In the presence of inhibitors of fast synaptic transmission (20 μM BMI, 10 μM NBQX, 100 μM APV) and TTX (1 μM), the response to Nic (30 μM) was only partially reduced (−267 ± 76 pA control; Nic + Blockers, −143 ± 20 pA, *P* < 0.01, *n* = 4, Fig. 3.6*C*), suggesting that a direct action of Nic on MCs contributed to the depolarization. The nicotinic response was nondesensitizing, as consecutive applications of Nic (within 10 min) resulted in responses that were similar in amplitude (1st application, −312 ± 53 vs. 2nd −337 ± 74 pA; *n* = 7) and exhibited dose dependency, with an EC_{50} of 42 ± 2 μM (*n* = 5, not shown). Additionally, the voltage dependency of the inward current produced by Nic (30 μM) exhibited the characteristically strong inward rectification of neuronal nAChRs. Figure 3.6*D* shows the voltage-dependency of the normalized inward current induced by Nic at −60 mV. The current at −40 mV was −84 ± 34 pA while at +30 mV was −18 ± 7 pA (*n* = 3). We further characterized the properties of the nAChR in the AOB by using various pharmacological agents that distinguish between receptors with distinct subunit compositions. The nonselective neuronal nAChR agonist cytisine (Cyt) produced a greater effect than nicotine at the same concentrations (10 μM, Nic, −152 ± 54 pA vs. Cyt −295 ± 63 pA, *P* < 0.02, *n* = 3). Application of choline (100–1,000 μM) failed to depolarize MCs (Fig. 3.6*B*)

while acetylcholine, like nicotine, produced a fast inward current (not shown). The nonselective nicotinic antagonist MM (30 μM; *n* = 4) completely blocked the response to Nic (30 μM; Fig. 3.6*B*, *bottom*; control, −275 ± 45 pA; in MM, −5 ± 5 pA, *P* < 0.02), while in the presence of the α4-containing nAChR antagonist DHBE (3 μM) the response to Nic was reduced to 39 ± 27% of control (*P* < 0.02, *n* = 3). The selective α7-containing nAChR antagonist MLA (10–30 nM) had no effect on the nicotinic response (Fig. 3.6*B*, *top*; control, −123 ± 47 pA; in MLA 10 nM, −130 ± 47 pA, *n* = 4). These results suggest that the nicotinic responses in MC are due to activation of α4β2* -like nAChRs. In addition, we found that like the M1-like mAChR response in GCs, MCs exhibited both nicotinic and M1-like muscarinic responses early in postnatal development (control, 12.6 ± 1.6 mV; in 300 nM Pir, 1.0 ± 0.97 mV; *P* < 0.02; *n* = 3, data not shown), suggesting that the receptor subtypes and their distribution among neuronal components of the AOB is established early in postnatal development.

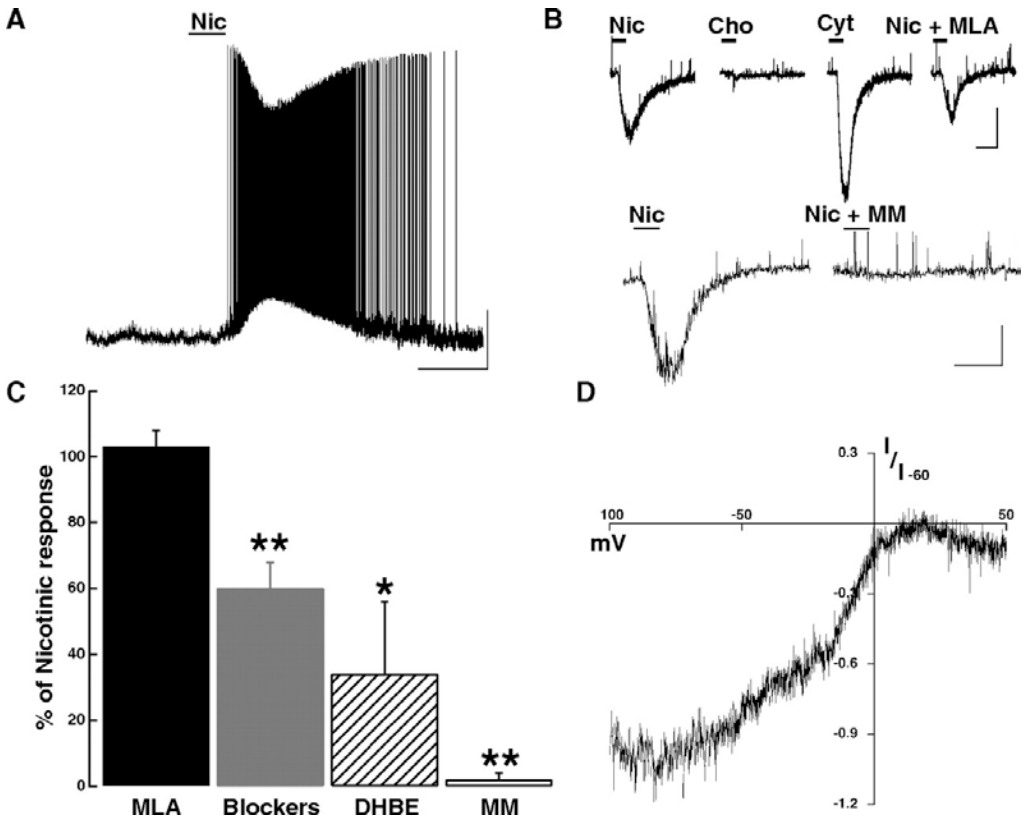

Figure 3.6. Nicotinic AChR activation excites MCs. *A*: bath application of Nic (30 μM, 1 min) produced a fast-onset depolarization in MCs (<20 s). The membrane potential in this cell is –66 mV. Calibration bar is 20 mV and 2 min. *B, top*: voltage-clamp recordings showing nAChR activated inward currents in presence of selective agonists and antagonists in the same cell. Nic (10 μM) produced a fast onset inward current (–153 pA), Cho (100 μM) failed to produce an inward current, while Cyt (10 μM) produced a larger response than Nic (–292 pA). The response to Nic was not significantly reduced in the presence of the a7-containing nAChR antagonist MLA (10 nM, –108 pA). *Bottom trace*: in a different cell, the response to Nic (30 μM, –231 pA) was completely abolished in the presence of MM (30 μM). For both cells, the calibration bar is 100 pA and 1 min. *C*: sensitivity of the nicotinic response to selective antagonists; the response to Nic was 103 ± 5% in MLA 10 nM, in Blockers (NBQX, APV, BMI and TTX) 60 ± 8%, 34 ± 22% in dihydro-β-erythroidine hydrobromide (DHBE) and 2 ± 2% in mecamylamine hydrochloride (MM, see text, $*P < 0.05$, $** P < 0.02$). *D*: the inward current produced by Nic (30 μM) showed a strong inward rectification; *I-V* graph shows the average normalized current at –60 mV in 3 cells. In all cells, the holding potential is –60 mV.

Submaximal activation of nicotinic and muscarinic receptors decreases the output from MCs

Our results demonstrate that the main cholinergic effect on GCs is excitation mediated by M1-like mAChRs, which would result in an increase in inhibitory GABAergic input onto MCs. Concomitantly, the main cholinergic effect on MCs is excitation by both nicotinic and muscarinic receptors, which would result in lowering the threshold for excitatory sensory input and increasing the output from MCs. To ask which neuromodulatory action predominates on MCs (i.e., excitation or inhibition), we selectively activated nicotinic or muscarinic receptors with low agonist concentrations to elicit a submaximal excitatory effect on MCs while driving action potentials with current injection (3–8 Hz). To determine the submaximal dose for these experiments, we constructed dose-response curves for Oxo in the 0.3–10 μM concentration range. The EC_{50} was 3.11 ± 0.22 μM in GCs (*n* = 7) and 0.79 ± 0.02 μM in MCs (*n* = 4; not shown). In these experiments, the membrane potential was maintained at a steady value by manually injecting current. Surprisingly, we found that in the presence of either Nic (3 μM) or Oxo (3 μM), the frequency of stimulus-elicited action potentials in MCs was significantly depressed (Fig. 3.7*A*). In the presence of Nic, the firing frequency was decreased by 53 ± 12% ($P < 0.002$, *n* = 7, Fig. 3.7*B*), while in the presence of Oxo, it was reduced by 45 ± 11% ($P < 0.002$, *n* = 7, Fig. 3.7*B*), suggesting that under these conditions, the influence of increased inhibitory input from GCs overrides the excitation of MC. Accordingly, when the actions of these agonists were tested in the presence of GABAzine (5 μM) to block the inhibitory input from interneurons, only the

excitatory effect prevailed and there was a slight increase in the frequency of firing (Nic, 10 ± 7%; Oxo, 15 ± 15%, Fig. 3.7*B*). Lowering the concentration of Oxo to 1 μM resulted in a smaller yet significant reduction in the frequency of MC firing (18 ± 3%; $P < 0.003$; $n = 13$, not shown), while in the presence of GABAzine the increase in frequency was also observed (15 ± 3%; $P < 0.02$; $n = 10$, not shown). Thus submaximal concentrations of Oxo decrease the firing rate in MCs.

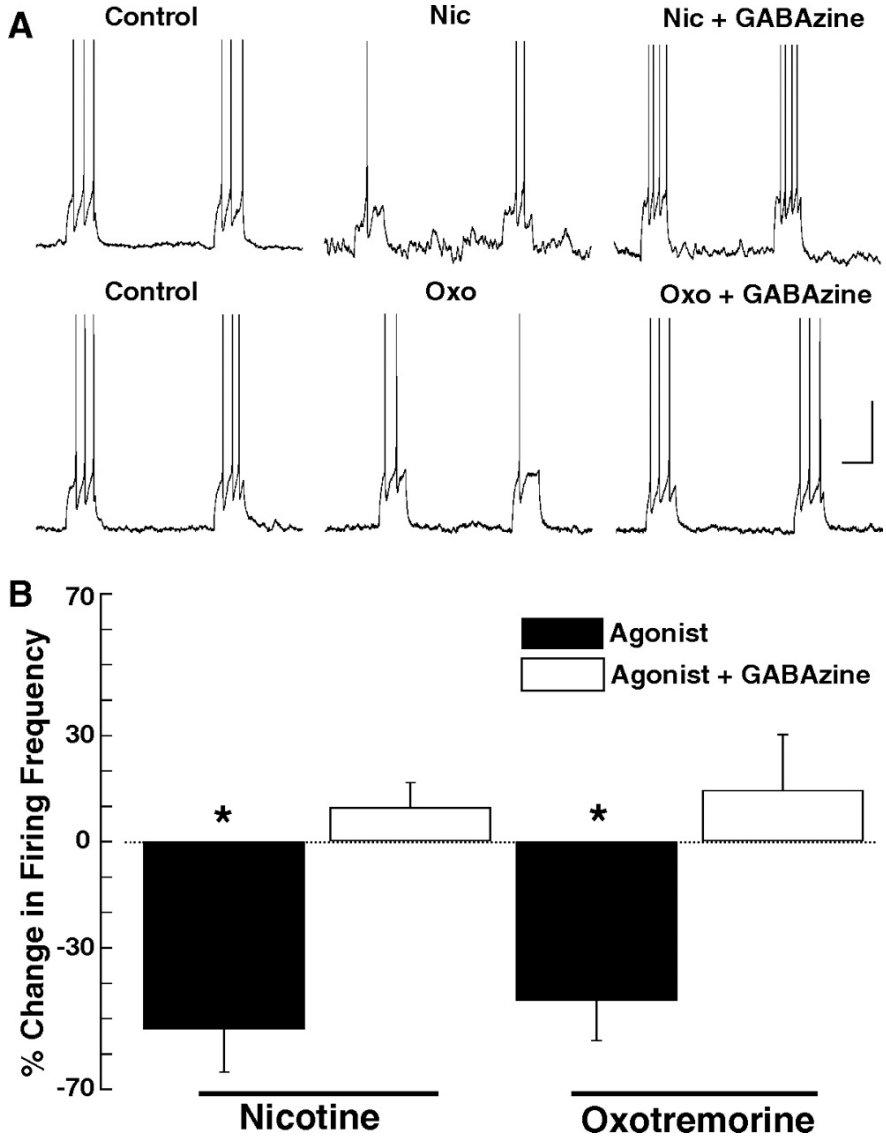

Figure 3.7. Submaximal activation of nicotinic and muscarinic receptors decreases the output from MCs. *A, top*: a low concentration of Nic (3 μM) reduced the firing rate in this MC. In the same cell, the GABA receptor antagonist GABAzine (5 μM) blocked the inhibitory response produced by Nic and only a slight excitatory remained. *Bottom traces*: low concentrations of Oxo (3 μM) decreased the firing rate in this MC and GABAzine (5 μM) also reduced this inhibitory effect. Cells were manually clamped at –60 mV; the calibration bar in is 0.5 s and 20 mV. *B*: graph bar summarizing the effects of submaximal concentrations of Oxo (3 μM) and Nic (3 μM) in the firing frequency of MCs (see text, ■, $*P < 0.002$). Both Nic and Oxo significantly reduced the frequency of firing. In the presence of GABAzine (5 μM, □), the inhibitory effects of these agonists were greatly diminished leaving a slight excitatory effect.

DISCUSSION

Modulation of neuronal circuits in the OB by cholinergic and noradrenergic afferent systems plays a crucial role in the proper execution of several survival-dependent behaviors (Brennan 2004; Brennan and Keverne 1997; Wilson et al. 2004). Yet the mechanisms by which these afferent systems regulate neuronal excitability in the OB remain poorly understood. Here we provide evidence that the excitability of both GCs and MCs is enhanced by AChR activation in the AOB, a region involved in control of mating and aggressive behaviors, suggesting that the cholinergic system may play a role in regulating the neuronal processing required for these behaviors. Activation of M1-like mAChRs depolarized GCs and induced the appearance of a sADP following a stimulus-induced train of action potentials. In addition, MCs were also excited through activation of M1-like mAChRs and nAChRs, suggesting that cholinergic modulation may enhance excitability in the AOB and increase sensitivity of MCs to sensory input. However, our results demonstrate that under submaximal activation of these receptors, the main effect is inhibition of MC excitability. These results suggest that under physiological conditions, the cholinergic system may act to increase the overall inhibitory tone of MCs instead. Intriguingly, in the AOB the cholinergic excitatory action on GCs and MCs is present from early postnatal days, suggesting that unlike in the MOB, excitatory muscarinic responses do not exhibit a developmental switch, suggesting that neuromodulation of GCs in the AOB may play an important physiological role in early postnatal ages.

Modulation of neuronal excitability by acetylcholine, as in other sensory systems, plays an important role in olfactory processing. Cholinergic

projections to the OB from the basal nuclei of the forebrain, in particular the HDB, are found throughout the different cellular layers of the OB, suggesting this system can modulate several neuronal components in the OB (Kasa et al. 1995; Le Jeune et al. 1996; Nickell and Shipley 1988; Ojima et al. 1988; Zaborszky et al. 1986). Studies in vivo have indicated that in the MOB acetylcholine enhances discrimination of similar odors and promotes odor learning (Chaudhury et al. 2009; Levy et al. 1997; Linster and Cleland 2002; Mandairon et al. 2006; Ravel et al. 1994; Roman et al. 1993). Field potential recordings in the olfactory bulb have reported conflicting results in response to cholinergic agents or stimulation in the HDB with some reporting decreased GC-MC inhibition (Elaagouby et al., 1991; Kunze et al., 1991; Elaagouby and Gervais, 1992; Tsuno et al., 2008) and others, in agreement with our findings, reporting inhibition of MC (Nickell and Shipley 1988). It should be noted that the HDB projections include both GABAergic and cholinergic neurons that may underlie these discrepancies (Zaborszky et al. 1986). In contrast, only a few studies have addressed the cellular effects of the cholinergic system in the OB. Noticeably, most of these studies have been confined to the MOB where both inhibitory and excitatory cholinergic effects have been described (Castillo et al. 1999; Ghatpande and Gelperin 2009; Ghatpande et al. 2006; Pignatelli and Belluzzi 2008; Pressler et al. 2007). For example, cholinergic stimulation inhibited GC firing in cell-attached recordings and increased the frequency of GABA inhibitory postsynaptic currents (IPSCs) in whole cell recordings from MCs (Castillo et al. 1999). The increase in IPSC frequency was attributed to activation of presynaptic mAChRs at dendrodendritic synapses (Castillo et al. 1999; Ghatpande et al. 2006). These finding are consistent with the abundant expression of M1 receptor in the external plexiform layer of the OB, where

most dendrodendritic synapses occur (Spencer et al., 1986; Buckley et al., 1988). We now provide evidence that activation of M1-like muscarinic receptors in GCs of the AOB produces a depolarization and a sADP following a stimulus-induced train of action potentials that increases the release of GABA onto MCs. Our results are in agreement with previous studies in the MOB (Pressler et al. 2007), showing that GCs exhibit an M1 muscarinic receptor excitation and an ADP. Characterization of the ionic mechanisms underlying the mAChR induced ADP indicated that this is due to the activation of a nonselective cationic current (I_{CAN}), which occur through activation of transient receptor potential (TRP) channels (Yan et al. 2009). These data suggest that GCs in the AOB and MOB exhibit similar cellular mechanism of modulation by the cholinergic system and are in agreement with M1 excitatory effects found in other brain regions (Haj-Dahmane and Andrade, 1999; Egorov et al., 2006). Only one other study to date has examined cholinergic neuromodulation in the AOB (Takahashi and Kaba 2010). In agreement with the robust M1-like mAChR-induced depolarization of GCs described here, this study reported that M1 receptor activation increased the frequency of GABA IPSCs in MCs. However, our data are consistent with previous work in the MOB indicating that muscarinic depolarization in GCs results from recruitment of a nonselective cationic current (I_{CAN}) rather than the closure of K channels (M-current) as proposed by (Takahashi and Kaba, 2010). Further studies are necessary to determine the reason for this discrepancy; however, the use of different mice strains may be a contributing factor.

Muscarinic activation of nonselective cationic currents have been described in various regions of the brain where they promote long-lasting depolarization, providing an interesting mechanism for cholinergic-induced neuronal plasticity

(Krnjevic et al., 1971; Schwindt et al., 1988; Constanti et al., 1993; HajDahmane and Andrade, 1996; Haj-Dahmane and Andrade, 1999; Egorov et al., 2006). In general, GCs exhibit a hyperpolarized resting membrane potential, so coincident excitatory input can enhance the cholinergic excitatory effect. Glutamatergic inputs onto GCs occur mainly through dendrodendritic synapses and synapses from afferent fibers originating in the olfactory cortex. Basal dendrites and the soma of GCs receive synapses from centrifugal fibers and axon collaterals from MCs (Mouret et al., 2009b). It has been suggested that this segregated pattern of connectivity is likely to have an important physiological role in GC function (Whitman and Greer, 2007). Thus coincident excitatory activity at any of these sites could selectively potentiate the cholinergic depolarization of GCs, leading to an increased release of GABA to induce inhibition of MCs. In this regard, we hypothesize that the dual muscarinic and nicotinic excitation of MCs that leads to increased glutamatergic input at dendrodendritic synapses can also significantly contribute to the excitation of GCs. Interestingly, we recently showed that α-1 adrenergic and metabotropic glutamate receptor activation also depolarizes GCs and induces the appearance of an ADP (Smith et al. 2009). These results suggest that neuromodulation by these distinct afferent systems could use a convergent mechanism to increase the excitability of GCs. In addition, increased inhibition at dendrodendritic synapses may play an important role in the discrimination of sexual cues by the AOB, including those involved in the Bruce effect, emphasizing the important neuromodulatory role of these systems at dendrodendritic synapses (Hendrickson et al., 2008).

Cholinergic agonists also excited MCs; however, unlike GCs, this excitation recruited both muscarinic and nicotinic receptors, similar to the responses of

MCs in the MOB. Diversity in subunit composition gives rise to a great number of homomeric and heteromeric nAChRs subtypes, each with unique physiological and pharmacological properties (Luetje and Patrick, 1991; Gotti et al., 2007). The pharmacological profile of the nicotinic excitation we describe here suggests that the response in MCs is mediated by nAChRs of the α4β2* type (Albuquerque et al., 2009). Accordingly, we found that the nicotinic response was sensitive to DHBE but not to MLA. The α4β2* type nAChR exhibits a lesser degree of desensitization, as reported here, suggesting that nicotinic activation could tonically excite MCs. These results are in agreement with other studies that show that in the OB the most abundant nAChRs are the α7-type and α4β2*type (Hogg et al. 2003). In addition, we found that M1-like mAChR activation excited MCs; however, unlike GCs, the sADP was not present. One possibility is that M1 activation couples to different targets in MCs and/or that the ADP does not contribute substantially to the depolarization in MCs; we are currently addressing this question.

Intriguingly, in sharp contrast with the MOB, the excitatory cholinergic responses in MCs and GCs were present from early postnatal days (Ghatpande and Gelperin 2009; Ghatpande et al. 2006). Recordings from MCs in the MOB indicated that early postnatal M1 mAChR activation occurs on MCs, which then indirectly excite GCs through glutamate receptors, and only at around P10 do GCs become sensitive to direct mAChR activation. It's possible that this difference is due to the heterogeneity of GCs within the OB or differences in the species used (rat vs. mice). Nonetheless, the presence of M1 responses in GCs at early postnatal days suggests that cholinergic modulation could play an important role in the maturation of the AOB circuitry,

which happens during the first week of postnatal development (Salazar et al., 2006; Mouret et al., 2009b). Afferent neuromodulatory systems play an important role in olfactory learning both in the AOB and MOB (Brennan and Keverne 1997), thus it is tempting to speculate that neuromodulation by cholinergic system in the AOB may also play an important role in perinatal behaviors.

Although several studies have shown the presence of cholinergic fibers in the vicinity of MCs, the precise cellular distribution of muscarinic and nicotinic receptors in MCs is not known. We postulate that activation of somatic excitatory receptors could produce a more pronounced effect on MC output, while activation of receptors located on lateral dendrites could have a stronger effect on recurrent and lateral inhibition (i.e., local processing). Further studies are necessary to determine the contribution of either receptor type to the output and local processing of MCs. Nevertheless, we find that activation of either receptor with low concentrations of cholinergic agonists tends to promote overall inhibition in MCs; that is, the inhibitory drive from GCs, and to a lesser extent from PGs, dominates. Under these conditions, lateral and recurrent inhibition of MCs could be enhanced by cholinergic neuromodulation. Interestingly, ACh can also increase the inhibitory drive in other brain regions where it modulates the balance between excitation and inhibition (Lucas-Meunier et al., 2009). On the other hand, under decreased inhibitory activity from the interneurons (GC and PGs), the excitatory effect of muscarinic and nicotinic receptors on MCs predominates. Thus different levels of activity of afferent cholinergic fibers or stimulation of selective compartments within the MC could lead to different neuromodulatory effects on OB output. It is possible that in vivo several other factors may influence the neuromodulatory action of

ACh at the network level. For example, ACh could produce differential activation of metabotropic and ionotropic cholinergic receptors or spatial and temporal constraints could bias these responses to distinct neuronal components (i.e., GCs vs. MCs). Nevertheless, our studies provide further insight on the cellular mechanism by which the cholinergic system modulates excitability in the bulb. Further in vivo studies are necessary to determine how these cellular mechanisms convene to functionally modify odor processing and output of the bulb.

Chapter 4: Differential Muscarinic Modulation in the Olfactory Bulb

Citation

R.S. Smith, R. Hu, W. Chan, A. Desouza, K. Krahe, R.C. Araneda, "Cholinergic Modulation in the Olfactory Bulb" Journal of Neuroscience (Accepted)

Abstract

Neuromodulation of olfactory circuits by acetylcholine (ACh) plays an important role in odor discrimination and learning. Early processing of chemosensory signals occurs in two functionally and anatomically distinct regions, the main and accessory olfactory bulbs (MOB and AOB), which receive significant cholinergic input from the basal forebrain. Here we explore the regulation of AOB and MOB circuits by ACh, and how cholinergic modulation influences olfactory-mediated behaviors in mice. Surprisingly, despite the presence of a conserved circuit, activation of muscarinic ACh receptors revealed marked differences in cholinergic modulation of output neurons: excitation in the AOB and inhibition in the MOB. Granule cells (GCs), the most abundant intrinsic neuron in the OB, also exhibited a complex muscarinic response. While GCs in the AOB were excited, MOB GCs exhibited a dual muscarinic action, a hyperpolarization and an increase in excitability uncovered by cell depolarization. Furthermore, ACh had a different effect on the input/output relationship of MCs in the AOB and MOB, showing a net effect on gain in MCs of the MOB, but not in the AOB. Interestingly, despite the striking differences in neuromodulatory actions on output neurons, chemogenetic inhibition of cholinergic neurons produced similar perturbations in olfactory behaviors mediated by these two regions. Decreasing ACh in the OB disrupted the natural discrimination of molecularly related odors and the natural investigation of odors associated with social behaviors. Thus, the distinct neuromodulation by ACh in these circuits could underlie different solutions to the processing of general odors and semiochemicals, and the diverse olfactory behaviors they trigger.

Introduction

Throughout the brain, ACh produces a state-dependent regulation of sensory circuits, shaping cognition and behavior (Fournier et al., 2004; Marder, 2012). Cholinergic neurons in the horizontal limb of the diagonal band of Broca (HDB) provide a rich innervation to the olfactory bulb (OB) and upstream olfactory areas, where ACh regulates odor processing (Doty et al., 1999; Linster and Cleland, 2002; Wilson et al., 2004; Hellier et al., 2012; Zaborszkyy et al., 2012; Chapuis and Wilson, 2013). Odor cues orchestrate a host of behaviors, including foraging, prey detection, aggression, and sexual bonding. Upon detection by sensory neurons, odors signal through two parallel pathways that synapse onto principal neurons, the mitral and tufted cells (MCs herein) in the main and accessory OB (MOB and AOB, respectively). Unlike other sensory modalities, MCs project directly to higher odor processing areas, bypassing the thalamus, which highlights the importance of top-down cholinergic regulation of OB circuits (Kay and Sherman, 2007; Gire et al., 2013).

While the role of ACh in enhancing odor discrimination by the MOB is well established (D'Souza and Vijayaraghavan, 2014), the contribution of neuromodulation of AOB neurons by ACh to behaviors mediated by the Vomeronasal system (VNS) is poorly understood. Furthermore, at the cellular and circuit level, the mechanism of cholinergic modulation, at least in the MOB, remains controversial and activation of both muscarinic and nicotinic ACh receptors (mAChR and nAChR, respectively) has been shown to either enhance or decrease inhibition in the MOB (Castillo et al., 1999; Ghatpande et al., 2006; Pressler et al., 2007; Zhan et al., 2013). ACh also enhances the

excitability of output and intrinsic neurons in the AOB (Smith and Araneda, 2010; Shpak et al., 2014), supporting a functional role for cholinergic inputs in the AOB. At the circuit level, the AOB and MOB appear remarkably similar, both characterized by the presence of ubiquitous reciprocal synapses between MCs and a extensive network of local inhibitory neurons, the granule cells (GCs) (Shepherd and Greer, 1998; Larriva-Sahd, 2008), suggesting that neuromodulators regulate these circuits by similar mechanisms. However, anatomical and functional evidence shows important differences in the connectivity at the level of the sensory input, suggesting that the AOB and MOB analyze chemosensory information differently (Mucignat-Caretta et al., 2012), therefore, neuromodulation by ACh could serve different functions in these related systems.

Here, we show that cholinergic modulation produces distinct and opposite effects on the excitability of neurons in the AOB and MOB. In the AOB, activation of M1-mAChRs directly excites MCs, while in the MOB, M2 activation inhibits MCs. Similarly, while in the AOB M1 activation depolarized GCs, the response of GCs to ACh in the MOB involved both M1 and M2 mAChRs. Moreover, chemogenetic activation of HDB cholinergic neurons improved the natural discrimination of volatile odors, while silencing them disrupted odor discrimination. Importantly, silencing cholinergic neurons also disrupted the investigation of social odors signaled by the AOB. Thus, despite the differences in modulation at a network level, decreased ACh affected odor-mediated behaviors signaled though both MOB and AOB, suggesting that neuromodulatory control is dependent on the nature of the chemical signals processed by these regions.

Results

Muscarinic cholinergic activation produces opposite effects of output neurons of the AOB and MOB

To determine the neuromodulatory effects of ACh on OB output neurons, we examined the actions of selective mAChRs on MCs of the AOB and MOB (Fig. 1). In agreement with our previous work (Smith and Araneda, 2010), application of the non-selective mAChR agonist oxotremorine (oxo, 10 μM) produced a robust depolarization in AOB MCs, which usually elicited firing (Fig. 4.1B, ΔVm, 15.4 ± 2.7 mV, n = 28, $p < 0.01$). Surprisingly, in the MOB, the same agonist treatment produced a significant inhibition of MCs (*top*, ΔVm, −2.2 ± 0.5 mV, n = 17, $p < 0.01$). The time course of these muscarinic responses in the MOB and AOB MCs exhibited slow kinetics (time to peak, MOB, 41.6 ± 6.8 s, n = 17, AOB, 71.4 ± 8.8 s, n = 28, $p < 0.01$). However, these values are an overestimate (see methods); thus, in a few experiments we applied oxo (30 μM) in the vicinity of the recorded cell, using a fast perfusion system. Under these conditions the time to peak was 31.1 ± 5.7 s in the MOB and 21.3 ± 4.5 s in the AOB (n = 5).

To rule out the possibility that the inhibitory response in the MOB was disynaptic in origin, we examined the effects of oxo in the presence of blockers of fast excitatory and inhibitory synaptic transmission (APV 100 μM, CNQX 10 μM and GABAzine, GZ, 5 μM). As previously shown for the excitatory response in the AOB (Smith and Araneda, 2010), the muscarinic inhibition in the MOB was not affected by the presence of the ionotropic receptor blockers, indicating a direct effect on MCs (ΔVm, oxo, −2.4 ± 0.6 mV, oxo + blockers, −2.1 ± 0.4 mV, n = 8, $p = 0.68$). Furthermore, in the presence of the ionotropic

blockers, the time to peak of the responses remained unchanged (MOB, oxo 40.8 ± 8.3 s, oxo + blockers 45.1 ± 6.6 s, n = 8, p = 0.7). Similarly, the $GABA_B$ receptor antagonist (CGP-54626, 5 μM) did not block the hyperpolarization in MCs of the MOB (ΔVm, oxo −2.7 ± 0.5 mV, oxo + CGP −2.4 ± 0.2 mV, n = 5, p = 0.52). In addition, as previously reported, nicotine (Nic, 10 μM) produced a fast depolarization in both MOB and AOB MCs (time to peak, MOB, 24.4 ± 4.7 s; AOB, 30.1 ± 6.3 s) (Smith and Araneda, 2010; D'Souza and Vijayaraghavan, 2012). Like the muscarinic effect, the nicotinic depolarization was not affected by blockers of fast synaptic transmission (ΔVm, AOB, Nic 11.1 ± 0.9, Nic + Blockers 12.6 ± 1.3, n = 12, p = 0.77; ΔVm, MOB, Nic, 9.3 ± 2.0, Nic + blockers, 11.3 ± 2.5, n = 11, p = 0.68), indicating the direct activation of nAChRs on MCs. Last, the oxo (10 μM) induced depolarization in the AOB and the hyperpolarization in the MOB were not affected by the non-selective nicotinic antagonist, mecamylamine (MM, 30 μM) (ΔVm oxo + MM, AOB, 15.9 ± 3.2 mV, n = 3; MOB, −3.2 ± 0.4 mV, n = 3).

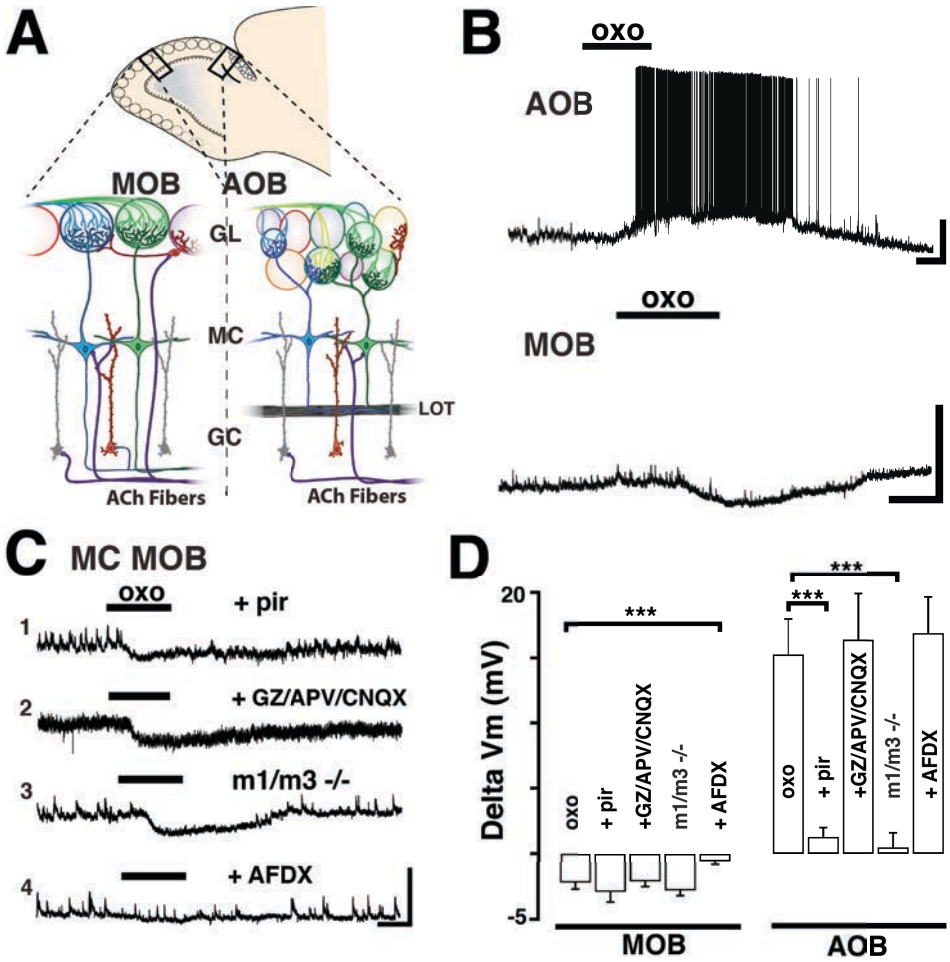

Figure 4.1. Muscarinic receptor activation produces opposite effects on mitral cells of the AOB and MOB.

A. Diagram of a sagittal view through the OB. The magnified sections enclosed by the black rectangles are shown below. *Left*; main olfactory bulb (MOB); *right*, accessory olfactory bulb (AOB). In the glomerular layer (GL), sensory axons (green and blue) relay information to output neurons residing in the mitral cell layer (MC, blue and green). Granule cells (GC, red and grey) are the most abundant cells in the MOB and AOB and form dendrodendritic synapses with MCs, influencing bulbar output through GABAergic inhibition. Cholinergic fibers arising in the basal forebrain (ACh fibers, purple) innervate both the MOB and AOB (LOT, lateral olfactory tract). **B**. Current clamp recordings from MCs shows opposite effects of the muscarinic ACh receptor (mAChR) agonist oxotremorine (oxo,10 μM, here and in all figures); a depolarization in the AOB (top) and hyperpolarization in the MOB (bottom); the resting membrane potential in these MCs is −57 and −59 mV respectively (top scale bar; 20 mV and 1 min; bottom; 10 mV and 1 min). **C**. Examples of responses to oxo in MOB MCs under different conditions. **C1**, the hyperpolarizing response to oxo is unchanged in the presence of M1-mAChR antagonist pirenzepine (Pir, 300 nM, Vm is −59 mV) or in the presence of ionotropic glutamate receptor (iGluR) blockers and GABA antagonist (**C2**, APV 100 μM, CNQX 10 μM and GABAzine 5 μM, Vm is −55 mV). **C3**, the hyperpolarization persisted in MOB MCs from M1/M3−/− K.O mice (Vm is −58 mV). However, the oxo-induced hyperpolarization is abolished in the presence of an M2-mAChR antagonist AFDX-116 (**C4**, 300 nM, Vm is −57). For all traces, the scale bar is 10 mV and 1 min). **D**. Summary of the effects produced by oxo on MC excitability in the MOB and AOB. The muscarinic hyperpolarization in MOB MCs is sensitive to AFDX-116.

We have previously shown that the muscarinic depolarization in AOB MCs results from M1-mAChR activation (Smith and Araneda, 2010). However, a low concentration of pirenzepine (Pir, 300 nM), which selectively blocks M1-mAChRs, was ineffective in reducing the inhibitory response in MOB MCs (Fig. 4.1C, ΔVm, oxo + Pir, −2.9 ± 0.8 mV, n = 5). To further corroborate these findings, we examined MC responses in the M1 knockout mice (M1−/− K.O. mice). Unexpectedly, the inhibitory responses in MOB MCs but also the excitatory response in AOB MCs still persisted in the M1−/− K.O. mice. Pharmacological characterization indicated that the depolarization in AOB MCs was sensitive to M3-mAChRs blockers, suggesting an up-regulation of these receptors in the OB of M1−/− K.O. mice (data not shown). Therefore, we next conducted experiments in the M1/M3 double K.O. mice (M1/M3 −/−). As shown in Fig. 4.1C, oxo still elicited a hyperpolarization in MOB MCs (ΔVm, −2.8 ± 0.6 mV, n = 5, p = 0.82), while the oxo induced excitation in AOB MCs was completely absent in the M1/M3 −/− mice (ΔVm, −0.2 ± 0.1 mV, n = 4, $p < 0.01$, data not shown). Additional pharmacological experiments revealed that the hyperpolarization in MOB MCs results from activation of M2-mAChRs. Accordingly, the inhibitory response to oxo was significantly reduced (8 of 9 cells) in the presence of a submicromolar concentration (300 nM) of AFDX-116 (Fig. 4.1C, ΔVm, control, −3.1 ± 0.4 mV, oxo + AFDX-116, −0.6 ± 0.2 mV, n = 8, $p < 0.01$). In summary, M1-mAChR activation in AOB MCs produces a depolarization. In contrast, M2-mAChR activation in MOB MCs produces an opposite effect (i.e. hyperpolarization). In both MOB and AOB, MCs also exhibit a nAChR-mediated excitation; however, we focus the scope of this work on muscarinic mediated effects.

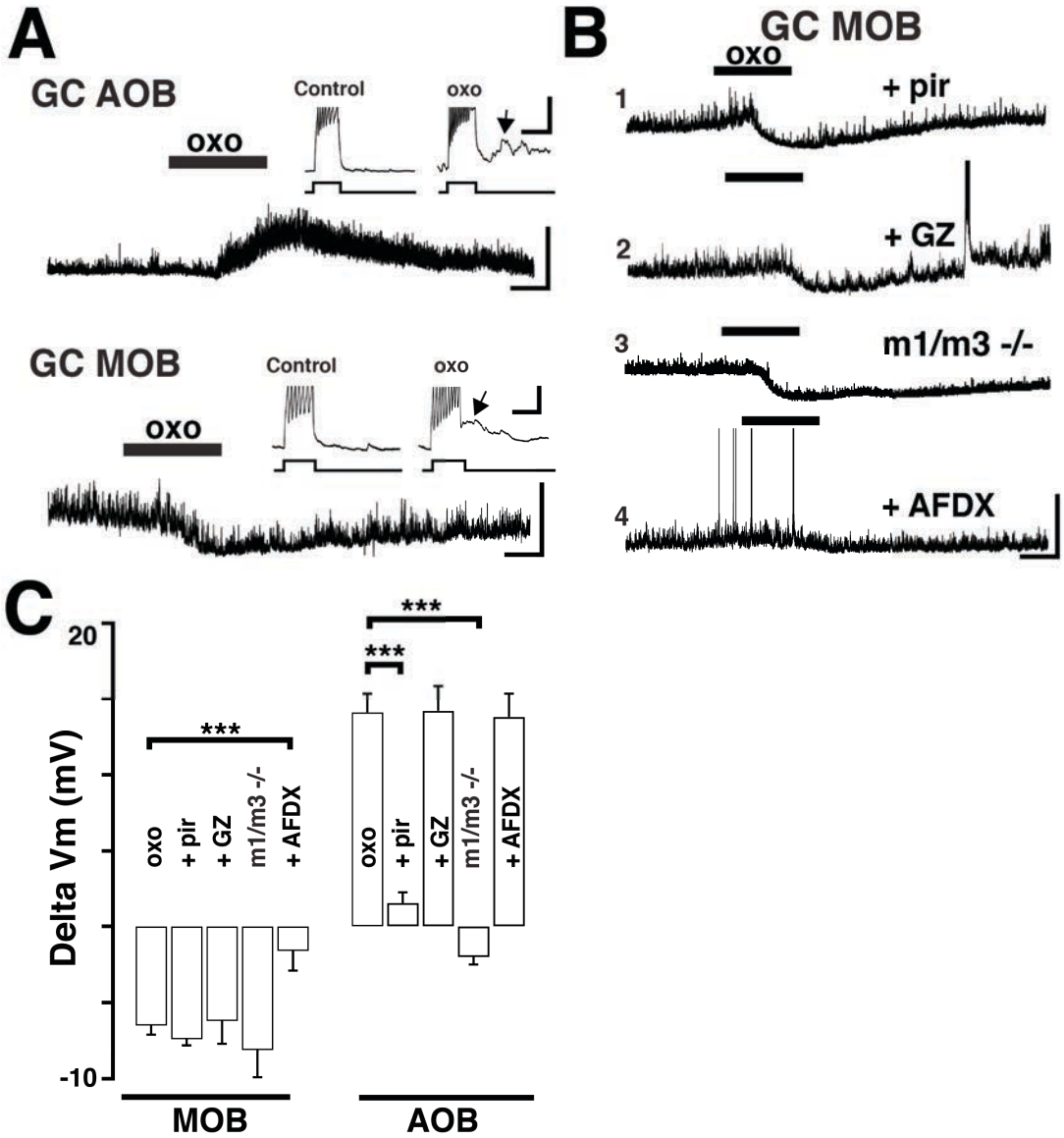

Figure 4.2. Activation of M2 muscarinic receptors hyperpolarizes MOB GCs.

A. Current clamp recordings from GCs showing opposite muscarinic effects in the AOB and MOB. In the AOB (top) oxo produces a depolarization while in the MOB (bottom) a hyperpolarization. The Vm is −62 mV (top) and −61 mV (bottom) (scale bar; 20 mV and 1 min). *Insert*, 25 pA current injections reveal an increase in excitability and the appearance of a sADP (arrows, scale bar; 5 mV and 0.5 s). **B**. Examples of responses to oxo in MOB GCs under different conditions. **B1**, the hyperpolarization was not affected by Pir (300 nM, Vm is −61 mV) or by the GABA antagonist GABAzine (**B2**, GZ, 5 µM, Vm is −62 mV). **B3**, oxo still produced a robust hyperpolarization in M1/M3−/− K.O mice (Vm is −60 mV). However, the hyperpolarization was abolished in the presence of the M2-mAChR antagonist AFDX-116 (**B4**, 300 nM, Vm is −61 mV). For all traces, the scale bar is 20 mV and 1 min. **C**. Summary of the properties of muscarinic response of GCs in the MOB and AOB. The muscarinic hyperpolarization in MOB GCs is sensitive to AFDX-116.

We wondered whether the opposite effects in muscarinic modulation extended also to the regulation of GCs, the most abundant intrinsic neuron in the OB. In agreement with our previous work (Smith and Araneda, 2010), activation of M1 mAChRs produced an increase in excitability of GCs in the AOB, consisting of a depolarization and the appearance of a slow after-depolarizing current (sADP) following a stimulus-induced train of action potentials (Fig. 4.2A, ΔVm, 14.1 ± 1.3 mV; sADP, 5.8 ± 0.4 mV, n = 9). In contrast, in MOB GCs oxo (10 μM) produced a hyperpolarization (Fig. 4.2A, ΔVm −6.5 ± 0.6 mV, n = 8). This hyperpolarization persisted in the presence of GZ (5 μM), ruling out the involvement of a $GABA_A$ mediated inhibition (Fig. 4.2B, ΔVm, −6.2 ± 1.5 mV, n = 3, p = 0.83). Additionally, the hyperpolarization in MOB GCs was not reduced by application of a low concentration of Pir (300 nM; Fig 4.2B, ΔVm, −7.4 ± 0.4 mV, n = 4, p = 0.41). However, application of AFDX-116 (300 nM) produced a significant decrease in the hyperpolarization elicited by oxo (Fig 4.2B, ΔVm, −1.5 ± 1.3 mV, n = 5, p < 0.01). Furthermore, like the inhibitory response in MOB MCs, the hyperpolarization in GCs was still present in the M1/M3 −/− mice (Fig 2B, ΔVm, −8.1 ± 2.0 mV, n = 5, p = 0.36). A previous report indicated the activation of sADP in MOB GCs, which like the response in AOB GCs, is dependent on activation of M1 mAChRs (Pressler et al, 2007). To examine this possibility, we elicited a train of action potentials with a depolarizing current while using a constant current injection to maintain the membrane potential at approximately −60 mV, thus counteracting the M2-mediated inhibition. In the presence of oxo, a stimulus-induced train of spikes was followed by a sADP in 5 out of 7 cells (Fig. 4.2A, inset, ΔVm, 10.6 ± 1.2 mV, n = 5). Importantly, in all GCs, the number of action potentials (APs)

induced by a stimulus increased during the application of oxo (Fig. 4.2A insert, APs Hz, 15.6 ± 1.2 to 26.2 ± 1.8 Hz, n = 7, $p < 0.01$). These data suggest that muscarinic activation of MOB GCs produced two opposing effects, an M2-mediated hyperpolarization and an M1-mediated increase in excitability. In contrast, as shown previously, activation of M1-mAChRs alone produces a large increase in GCs excitability in the AOB (Smith and Araneda, 2010).

Optogenetic activation of HDB cholinergic projections reveals opposing actions of acetylcholine on output neurons of the AOB and MOB.

HDB cholinergic neurons are regulated in a behavioral state-dependent manner, displaying neuronal bursting during active states and synchronize with gamma and theta oscillations (Manns et al., 2000; Lee et al., 2005; Parikh and Sarter, 2008). To examine the mechanisms by which endogenous release of ACh regulates the activity of output neurons, we used a transgenic line that co-expresses ChR and YFP in cholinergic neurons of the HDB. Immunostaining ChR-YFP positive neurons (ChR-YFP+) with a ChAT primary antibody showed that ~99% of ChR-YFP+ neurons (93 ± 12 cells/mm^2, n = 6) co-labeled for ChAT (92 ± 9 cells/mm^2, n = 6), indicating a robust ChR expression in HDB cholinergic neurons. Moreover, the distribution pattern of ChR-YFP+ fibers in the OB (not shown) closely resembled the distribution pattern of fibers in another transgenic mice, the ChAT-Tau-GFP (see Fig. 4.4A). As shown in Fig. 4.3A, prolonged blue light stimulation over the OB (λ 488 nm, 5 mW, 10 Hz, 50 ms pulses, 30 s) reliably elicited action potentials in ChAT-YFP-ChR+ neurons in the HDB (95 ± 2.1% success, Fig. 4.3A). We next recorded from MCs while eliciting release of endogenous ACh with blue light (10 Hz, 50 ms duration, 15 s); a similar stimulation protocol was

previously shown to elicit evoked cholinergic responses in the OB (Ma and Luo, 2012; Rothermel et al., 2014). As shown in Fig. 4.3B, endogenous ACh elicited a small, but consistent hyperpolarization in MOB MCs (ΔVm, −0.7 ± 0.3 mV, n = 7, $p < 0.05$), while the same light stimulation protocol produced a depolarization in AOB MCs (ΔVm, 4.3 ± 0.5 mV, n = 7, $p < 0.01$). Importantly, in agreement with the pharmacological studies Pir (300 nM), completely abolished the light induced excitation in AOB neurons (ΔVm AOB, Light, 3.4 ± 0.4 mV, Light + Pir 0.31 ± 0.54 mV, n = 6, $p < 0.01$, Fig 4.3B). Similarly, AFDX (300 nM), reduced the light-induced hyperpolarization in MOB MCs (ΔVm MOB, Light, −0.5 ± 0.14 mV, Light + AFDX 0.08 ± 0.09 mV, n = 5, $p < 0.05$). Together these results indicate that the optogenetic-induced responses in MCs were mediated by muscarinic receptors.

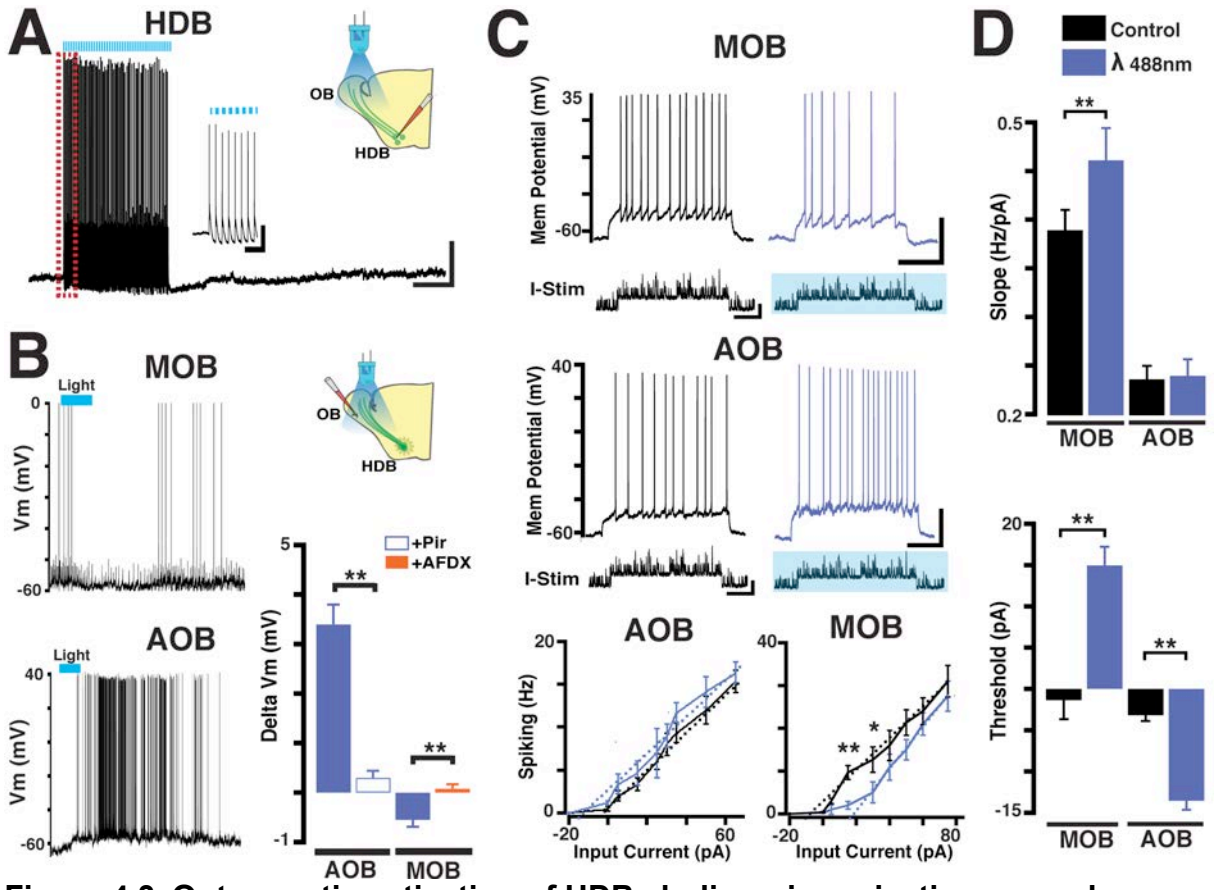

Figure 4.3. Optogenetic activation of HDB cholinergic projections reveals opposing actions of acetylcholine on output neurons of the AOB and MOB.
A. Current-clamp recording in a ChAT-ChR-YFP+ neuron in the HDB; consecutive stimulation pulses with blue light (λ 488 nm, blue bar, 10 Hz, 50 ms, 30 s) reliably excited this neuron (scale bar; 20 mV and 1 min). *Left inset,* expanded time scale showing the light evoked action potentials during the time highlighted by the red rectangle; all light pulses induced an action potential in this cell (scale bar; 20 mV and 400 ms, Vm is −60 mV). **B**. *Top*, current-clamp recording from a MC in the MOB; optogenetic stimulation (10 Hz, 50 ms duration, 15 s) of ChAT-ChR fibers revealed a small hyperpolarization (Vm is −59 mV). *Bottom*, recording from a MC in the AOB; optogenetic stimulation produced a depolarization of this MC (Vm is −62 mV). The bar graph shows a summary of the pharmacology of the optogenetically-elicited responses in MCs. The depolarization in the AOB is abolished by Pir (300 nM), while the hyperpolarization on the MOB is sensitive to AFDX. In **A** and **B** the diagrams on the right show the recording configuration indicating the position of the light stimulus in relation of to the recorded cell (i.e. HDB vs. OB). **C**. Current-clamp recording of a MC in the MOB (top) and in the AOB (bottom); neuronal spiking was elicited by injection of modeled excitatory synaptic currents overlying square current pulses (I-Stim, see methods), in control (black traces) and in the presence of light stimulation (blue traces). The stimulus duration is 2 s and the amplitude is 25 pA in the MOB and 15 pA in the AOB (Vm is −58 and −60 mV in the MOB and AOB, respectively). *Bottom*, average firing frequency of MCs in response to increasing current stimuli in the AOB (Left) and MOB (Right). The dotted lines (black, control; blue, light stim) correspond to the best fit to the rising phase of the current-voltage curves. **D**. *Top*, quantification of the gain, measured by the slope (Hz/pA) of the curves shown in (**C)**. Bottom, quantification of MC spiking threshold obtained from the x-intercept (pA) of the regression fit to the slope of the relationships shown in **(C).**

Cholinergic modulation has an important role in gating of visual, auditory, and somatosensory information (Niell and Stryker, 2010; Marguet and Harris, 2011; Petersen, 2014). The opposite changes in output neuron excitability elicited by ACh suggested that cholinergic modulation could have a different role in sensory gating in the MOB and AOB. To examine this possibility, we recorded responses of MCs to modeled excitatory potentials that occur in MCs during odor sniffing (see methods) in the presence of endogenous ACh release. Simulated synaptic currents were superimposed on current stimuli of different intensity while concurrently stimulating with light (Fig. 4.3C, I-stim, −20 pA to +80 pA). In the MOB, the effect of light stimulation was dependent on the intensity of current used to depolarize MCs. At low current intensities (pA < 30), light stimulation produced a significant decrease in MC firing (−71 ± 26 %, n = 6, $p < 0.01$) but at higher current intensities (pA > 50) there was no effect on MC firing (−5 ± 19 %, n = 6, $p = 0.85$). In contrast, the firing frequency of MCs in the AOB was consistently higher across the range of current stimuli tested, albeit due to variability in the analyzed sample it did not reach significance (pA < 30, 15 ± 7%; $p = 0.07$; pA > 50, 5.5 ± 12 %, $p = 0.65$, n = 5).

We next determined neuronal gain by measuring the slope of linear regression fit to the rising phase of the input/output curves (Chance et al., 2002). As shown in Fig. 4.3C, endogenous ACh produced a significant shift in the slope (Hz/pA) in the MOB (Hz/pA, control, 0.36 ± 0.02, blue light, 0.46 ± 0.03, n = 6, $p < 0.02$), but not in the AOB (Hz/pA, control, 0.24 ± 0.01, blue light, 0.24 ±

0.02, n = 5, p = 0.86). Furthermore, in the presence of endogenous ACh, the x-intercept (pA) of lines fitted to the input output is shifted towards larger (more positive) input values in the MOB, but require less input (more negative) current the AOB (MOB control, −0.3 ± 2.3 pA, blue light, 14.9 ± 2.3 pA, n = 6, p<0.01; AOB control, −3.2 ± 0.7 pA, blue light, −13.5 ± 1.1 pA, n = 5, p < 0.01). Together, these results indicate that cholinergic neuromodulation produces a non-linear inhibitory effect on output neurons in the MOB, but a linear increase in excitation in AOB MC, suggesting that neuronal gain is modulated in the MOB but not in the AOB.

Cholinergic afferent fibers are absent in the glomerular layer of the AOB. The above results revealed significant differences in cholinergic modulation in the MOB and AOB, specifically in regards to the contribution of M1 and M2 mAChRs to the regulation of these circuits. Surprisingly, confocal analysis of a transgenic line expressing the Tau-GFP fusion protein under the ChAT promoter (ChAT-Tau-GFP mouse) revealed a divergence in the distribution pattern of cholinergic fibers between the MOB and AOB. In agreement with previous findings (Salcedo et al., 2011; Krosnowski et al., 2012), confocal analysis revealed the presence of ChAT-GFP positive (ChAT-GFP+) fibers across all layers of the MOB, albeit with different degree of intensity (Fig. 4.4A). Similarly in the AOB the distribution of fibers exhibited various degrees of intensity; however, there was a significant absence of cholinergic fibers in the glomerular layer (GL, Fig. 4.4A). To quantify the distribution pattern of cholinergic fibers across the distinct layers of the MOB and AOB, we analyzed fluorescence intensity (ChAT fibers) across the complete dataset (see methods). As shown in Fig. 4.4B, the intensity was lowest in the GL of the

AOB, but there was abundant fluorescence in the GL of the MOB. The average intensity in the GL was significantly different between the AOB and MOB (AOB, 0.08 ± 0.04; n = 6; MOB, 0.77 ± 0.09; n = 6; $p < 0.01$). This differential pattern of labeling was also observed when we used additional cholinergic markers, the vesicular acetylcholine transporter (VAChT, AOB vs. MOB, 0.17 ± 0.06 vs. 0.65 ± 0.11; n = 4; $p < 0.01$, Fig 4.4C) and acetylcholinesterase (AChE, AOB vs. MOB, 0.15 ± 0.08 vs. 0.73 ± 0.16; n = 4; $p < 0.01$, Fig 4.4C). In contrast, as shown in Fig 4.4A, the fluorescence intensity in the AOB GL was high, when we used an anti-GFP antibody in slices from an OMP-YFP mouse, suggesting that the glomerular neuropil in the AOB was accessible to the antibodies. The differential distribution of cholinergic fibers at the level of the GL, where MCs form synapses with incoming sensory fibers, suggests ACh may play a lesser direct role in regulating synaptic processes in the glomeruli of the AOB.

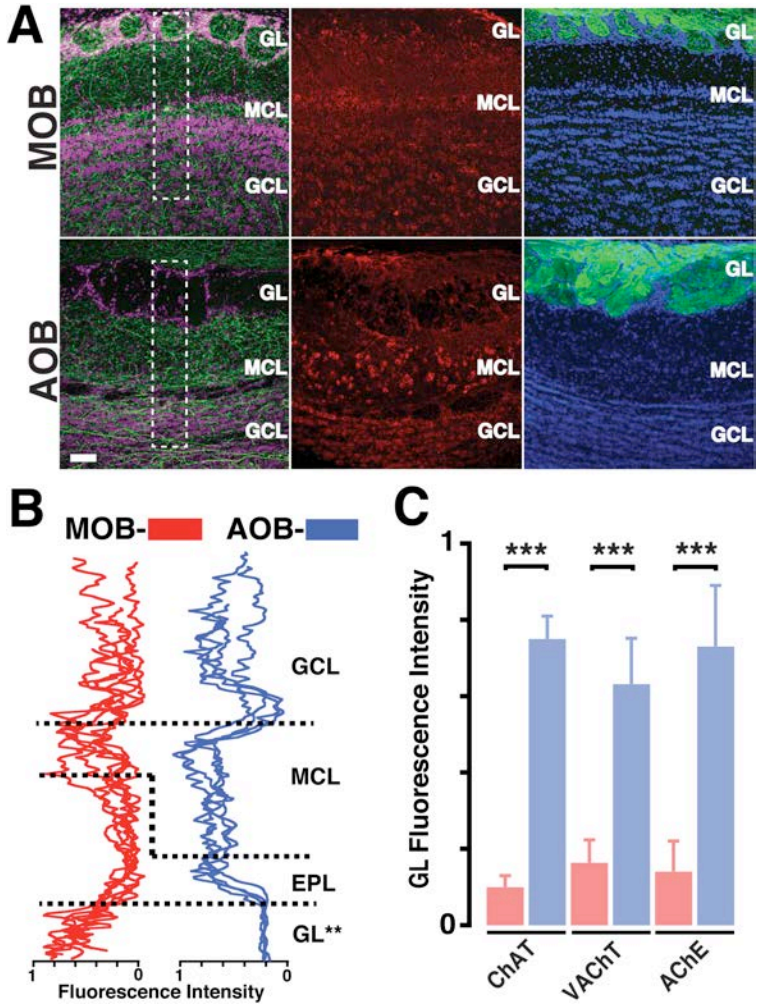

Figure 4.4: Cholinergic afferent fiber density is differentially distributed in the AOB and MOB.

A. High magnification confocal images of the MOB (top) and AOB (bottom) sections stained for different markers. *Left*, sections from a ChAT-Tau-GFP mouse brain, stained with anti-GFP (green) and nuclear stain TOPRO (pink). The ChAT-GFP fibers are found in all layers of the MOB but are absent in the GL of the AOB. *Middle*, sections from a wild type mouse brain stained with anti-VAChT (red). The VAChT staining is prominent in the MOB GL but not in the AOB. *Right*, sections from an OMP-YFP mouse, stained with anti-GFP (green) and DAPI (blue). There is abundant labeling in the glomerular layers of the MOB and AOB (Scale bar: 50 μm). **B**. Fluorescence intensity line plots from the regions outlined in A (white dotted rectangles, see methods) for the MOB (red) and AOB (blue). Each line represents sections obtained from different animals. In all sections, the intensity is lowest in the GL of the AOB. **C**. Bar Graph, normalized fluorescence intensity in the GL of MOB (red) and AOB (blue) for different cholinergic markers. All the markers show low intensity in the AOB (see text). ChAT, Choline acetyltransferase; VAChT, vesicular acetylcholine transporter; AChE, acetylcholinesterase.

Modification of HDB cholinergic neuron activity affects natural discrimination of odors.

At the network level, our findings suggest a differential effect of ACh in the MOB and AOB, thus, we wondered whether cholinergic modulation has a different role in odor-mediated behaviors signaled by these parallel chemosensory circuits. To modify the cholinergic tone in the OB of awake behaving animals, we utilized a chemogenetic approach, using Designer Receptors Exclusively Activated by Designer Drugs (DREADDs). This allows for site-specific expression of genetically modified GPCRs (hM3Dq and hM4Di), which activate distinct cellular mechanisms to excite and inhibit neurons in the presence of clozapine N-oxide (CNO), a biologically inert compound that binds DREADD receptors (Armbruster et al., 2007). As shown in Fig. 4.5A, 6 weeks post-virus injection hM3Dq and hM4Di DREADDs show robust expression in the HDB (Fig. 4.5A). Double immunostaining against ChAT (green) and the DREADDs (mCherry) indicated that 59% ± 9 of the ChAT positive (ChAT+) neurons also expressed hM4Di (n = 4), while 70% ± 11 of ChAT+ neurons expressed hM3Dq (n = 4). As shown in Fig. 4.5B, two weeks post injection, HDB cholinergic neurons expressing hM4Di were inhibited in the presence of CNO (5 μM) (baseline; 1.1 ± 0.3 Hz; CNO, 0.4 ± 0.4 Hz, n=3, $p < 0.02$). Additionally, 4 weeks post-injection, we conducted Ca-imaging recordings in HDB neurons expressing hM3Dq. As shown in Fig. 4.5B, CNO produce increases in calcium signals in these neurons ($\Delta F/F_0$, 11.6 ± 0.55 %, n = 6, $p < 0.01$).

To validate our chemogenetic approach, we evaluated the natural discrimination of structurally similar odors using a habituation/dishabituation. This odor discrimination task has traditionally assessed the contribution of ACh to MOB processing (Mandairon et al., 2006; Chaudhury et al., 2009). As shown in Fig. 4.5C, ChAT-hM4Di mice injected with saline habituated to three consecutive presentations of ethyl heptanoate (C7) as shown by a decrease in investigation time (first trial 10.01 ± 0.42 s vs. third trial, 2.14 ± 0.38 s; n = 4, $p < 0.01$). Presentation of the novel odor, ethyl octanoate (C8), resulted in a significant increase in investigation time or dishabituation (Fig. 4.5C, C7 2.14 ± 0.38 vs. C8 8.82 ± 0.49 s, n = 4, $p < 0.01$). ChAT-hM4Di mice injected with the CNO (0.5 mg/1 mL/100 g) displayed normal habituation to C7 (first trial 9.7 ± 1.0 s vs. third trial, 4.0 ± 0.4 s; n = 4, $p < 0.01$), but failed to dishabituate to the C8 ester (C7, 4.0 ± 0.4 s vs. C8, 3.7 ± 0.6 s, $p = 0.81$), indicating these mice did not discriminate these odors when the cholinergic activity is reduced. This disruption in odor discrimination was reversible and following the washout of CNO (~5 hours), ChAT-hM4Di mice showed normal habituation/dishabituation for the C7/C8 odor pair (C7, 3.8 ± 0.5 s vs. C8, 6.2 ± 0.4 s, $p < 0.02$). Furthermore, the disruption of discrimination was limited to closely related molecules, as chemogenetic silencing of cholinergic neurons did not affect discrimination of less similar odor pairs. Thus, ChAT-hM4Di mice injected with CNO displayed normal habituation/dishabituation for ethyl esters that differ by two carbons (Fig. 4.5C, C6, 3.5 ± 0.5 s vs. C8, 7.8 ± 1.0 s, $p < 0.02$). Importantly, odor detection threshold for esters was not different between control and CNO treated hM4Di mice (investigation time C7, 1:30,000, control 4.3 ± 0.5 s, CNO 3.7 ± 0.8 s; 1:40,000, control 0.6 ± 0.5 s, CNO 0.1 ± 0.8 s, see methods). Together, these results indicate that

transiently inhibiting HDB cholinergic neurons does not disrupt odor detection threshold, but impairs discrimination of structurally similar odors.

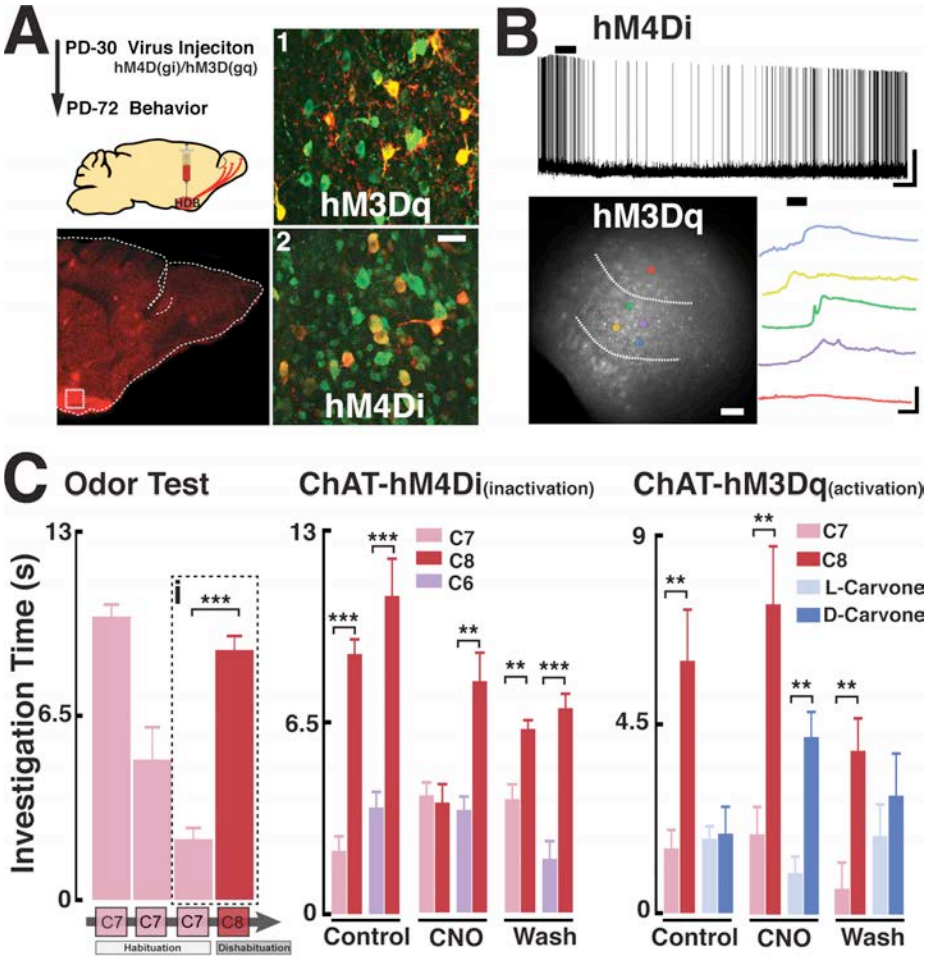

Figure 4.5 Invivo modification of HDB cholinergic neurons activity affects natural odor discrimination **A**. *Top Left*, schematic diagram for the virus injection and behavioral testing schedule. *Bottom Left*, confocal image of a sagittal section of the OB from a ChAT-Cre mouse expressing hM4Di (red, mCherry) in the HDB, dotted box indicate the region shown on the right pictures (I and ii). **A1** and **A2**, magnified HDB sections immunostained for ChAT (green) and mCherry (red) showing co-localization (yellow) with hM3Dq (i) and hM4Di (ii) (scale bar 25 µm). **B**. *Top*, recording from an HDB neuron expressing the hM4Di DREADD in the presence of iGluR blockers (APV 100 µM, CNQX 10 µM) and GABAzine (5 µM). Application of CNO (5 µM) produced a hyperpolarization in this cell (Vm is −54 mV, scale bar is 20 mV and 1 min). *Bottom left*, image of HDB neurons expressing the hM3Dq DREADD, loaded with the calcium dye Fluo-4; the dotted lines outlines the HDB. Colored circles represent selected cells within the HDB (yellow, green, blue and purple) responding to CNO, the red circle corresponds to a cell outside the HDB. *Bottom right*, optical recording traces color-coded to the cells shown on the left; cells in the HDB show an increase in calcium signal in the presence of CNO (5 µM). The scale bar is 10% $\Delta F/F_0$ and 2 min. **C**. *Left*, habituation/dishabituation protocol used for test natural discrimination of odors. Mice presented with the same odor (i.e. ethyl heptanoate, C7, pink) three times show a decrease in investigation time (habituation). On the fourth trial, a novel odor (i.e. ethyl octanoate, C8, red) is presented and investigation time increases (dishabituation). The dotted box (i) highlights the quantification of habituation/dishabituation for this odor set (C7/C8), which is used to determine the discrimination of odors pairs in the middle and right graphs. *Middle*, ChAT-hM4Di mice were tested for natural discrimination of the C7/C8 (pink/red) and C6/C8 (purple/red) odor pairs (ethyl hexanoate, C6, purple). Odor discrimination was assessed pre-CNO injection (Control, saline injected), CNO injection (CNO), and 5 hours post CNO (Wash). *Right*, ChAT-hM3Dq mice were similarly tested for olfactory discrimination with the C7/C8 odor pair and carvone isomers (L- carvone, dark blue; D-carvone, light blue).

To determine whether chemogenetic enhancement of ACh produces the opposite effect in odor discrimination, we tested the ChAT-hM3Dq mice against odor pairs that these mice naturally fail to discriminate. Like wild-type mice (not shown), ChAT-hM3Dq mice injected with saline fail to discriminate the L- and D-carvone isomers (Fig. 4.5C, L, 2.4 ± 0.4 s; D, 2.5 ± 0.9 s, n = 4, p = 0.84), or the α- and β-pinene pair (α, 2.1 ± 0.6 vs. β, 1.8 ± 0.5 s, n = 4, p = 0.66, data not shown). Interestingly, following CNO injection, ChAT-hM3Dq mice were now able to discriminate the carvone isomers (Fig. 4.5C, L-, 1.3 ± 0.5 s vs. D-, 5.6 ± 0.8 s, p < 0.02). Similarly, the investigation time during dishabituation also increased for the α–β pinene pair, although within our limited sample this increase was not significant (α 2.4 ± 0.5 vs. β 4.3 ± 0.5, n = 4, p < 0.07, data not shown). As expected, ChAT-hM3Dq mice injected with CNO were still able to discriminate the C7/C8 pair (C7, 2.1 ± 0.7 vs. C8, 7.1 ± 0.8 s, n = 4, p < 0.02). Interestingly, similar to the hM4Di mice, odor detection threshold was not affected in hM3Dq mice after CNO (investigation time C7, 1:30,000, control 4.3 ± 0.5 s, CNO 3.9 ± 0.2 s; 1:40,000, control 0.6 ± 0.5 s, hM3Dq 0.8 ± 0.4 s). These results indicate that chemogenetic manipulation of cholinergic tone in the MOB produces a reliable and reversible outcome on the natural discrimination of odors. Surprisingly, however, odor detection threshold is not affected by these manipulations.

Chemogenetic silencing of HDB cholinergic neurons disrupts investigation of social odors.

The dense innervation of the AOB by HDB neurons and the neuromodulation of this circuit by ACh predicts an important regulation of behaviors signaled through the VNS by the cholinergic system, however at present this possibility

remains unknown. We therefore examined the natural investigation of semiochemicals in male ChAT-hM4Di mice in the context of aggressive and sexual behaviors, which are known to rely on VNS signaling (Chamero et al., 2007). Overall, the motor behavior, characterized by the total exploratory distance and speed, was not different between PBS and CNO injected ChAT-hM4Di mice (exploratory distance, PBS vs. CNO, 5,232 ± 532 vs. 4,451 ± 676 cm; speed, cm/s, 5.8 ± 0.6 vs. 5.0 ± 0.8, n = 4, p = 0.39). These results indicate that under experimental conditions, chemogenetic inhibition of HDB cholinergic neurons does not disrupt motor behavior.

Next, we assessed male avoidance to the odor of a dominant male following an aggressive encounter using the resident-intruder paradigm (Koolhaas et al., 2013)(see methods). Before the aggressive encounter, naïve ChAT-hM4Di intruder males injected with PBS (control) or CNO showed neither preference nor avoidance for the bedding soiled with odors of the resident (trial 1, 15 min), spending a similar average distance from the dish (D.D.) containing the bedding (Fig. 4.6A, D.D., PBS vs. CNO, 13.1 ± 1.5 vs. 13.0 ± 1.7 cm, n = 4, p = 0.9). However, following the aggressive encounter (in which the resident defeats the intruder) intruders injected with PBS exhibited strong avoidance towards the resident's soiled bedding (Fig. 4.6B, D.D., PBS trial 1 vs. trial 2, 13.1 ± 1.5 vs. 27.4 ± 0.7 cm, n = 4, p < 0.01; Ratio 2.1 ± 0.2). It should be noted that in this assay the avoidance behavior in the intruder is elicited only by the odor of the resident encountered during the fight. Thus, defeated mice presented with the soiled bedding of a different resident (unknown to the intruder) do not exhibit this avoidance behavior (D.D. trial 1 vs. trial 2, 14.3 ± 0.5 vs. 15.2 ± 0.7 cm, n = 4, p = 0.42), indicating that the avoidance does not

generalize to odor of other males nor that it results from an unspecific change in behavior post-fight. Importantly, intruders injected with CNO do not show avoidance for the resident's soiled bedding after the fight (Fig. 4.6A, D.D., CNO trial 1 vs. trial 2, 13.0 ± 1.7 vs. 14.2 ± 3.6 cm, n = 4, p = 0.67; Ratio 1.09 ± 0.03). Additionally, in contrast to PBS injected mice after the aggression encounter, the CNO injected group spent more time investigating the petri dish (Fig. 4.6B Right, investigation time, PBS 20.4 ± 8.1 vs. CNO 206 ± 31 s, n = 4, $p < 0.01$). However, the time spent displaying exploratory behaviors (see methods) was not different between the two groups after the fight (Fig 4.6B Right, exploration time, PBS, 232 ± 32 vs. CNO, 192 ± 26 s, n = 4, p = 0.50). We also observed a significant reduction in grooming and freezing in mice injected with CNO (grooming time, PBS vs. CNO, 351 ± 33 vs. 214 ± 22 s, $p < 0.02$; freezing time, 62.9 ± 18.1 vs. 13.3 ± 5.2 s, n = 4, $p < 0.04$), reflecting less anxiety-related behaviors post-fight in the defeated mice.

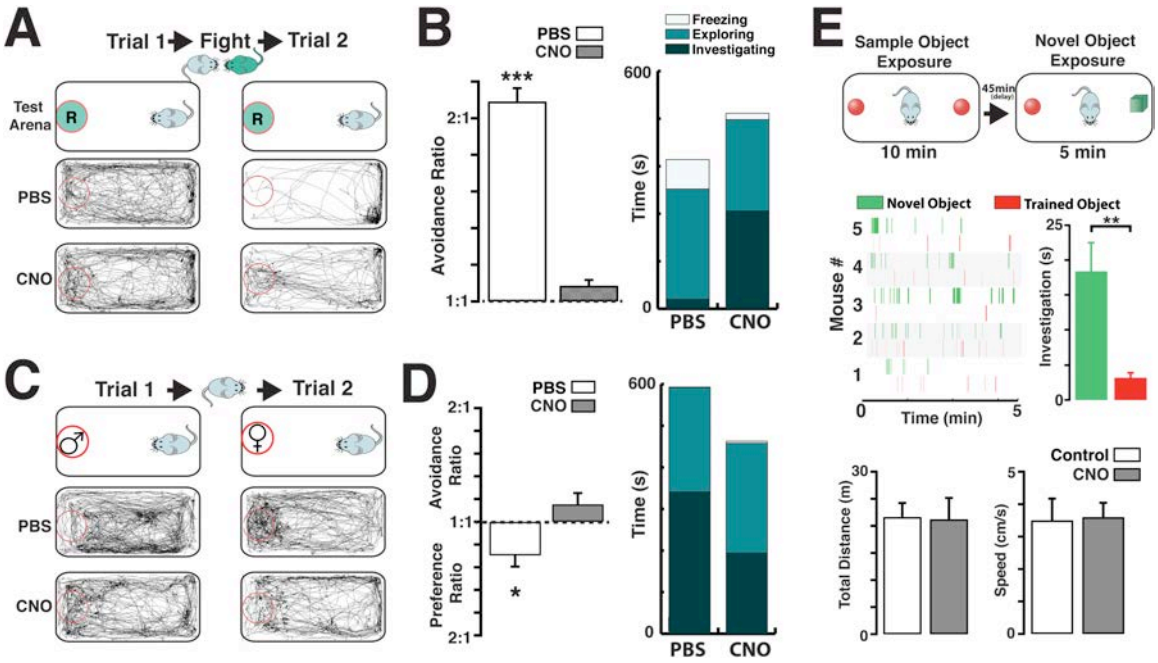

Figure 4.6. Chemogenetic silencing of cholinergic neurons disrupts investigation of social odors

A. *Top*, schematic illustration of the behavior paradigm used for the aggression induced olfactory avoidance (see methods). Before the aggressive encounter, a ChAT-hM4Di intruder (light blue) is placed in a neutral environment (trial 1, 15 min), containing a dish with the soiled bedding from a resident (green circle marked "R"). Following the aggressive encounter, in which the intruder losses the fight, the same odor presentation is repeated (trial 2, 15 min). *Bottom*, movement trajectories during trials 1 and 2, before the fight mice injected with PBS show no preference for a particular region of the neutral environment (left). After the fight, the mice spend most of the time avoiding the dish containing the resident's bedding (right). Following the fight, mice injected with CNO in the presence of the resident's bedding show no avoidance. **B** *Left*, the avoidance ratio is significantly larger for the PBS treated mice (white bar) compared to the CNO group (gray bar). *Right*, stacked bar graph showing the average freezing (white), exploration (light green), and investigating (dark green) times, post-fight (trial 2) for PBS and CNO group. **C**. *Top*, schematic illustration for the assessment of female odor preference (see methods). During the first trial (trial1, 15 min), a ChAT-hM4Di male mouse is presented with a dish containing male soiled bedding (red circle marked "♂"), while in the second trial (trial 2, 15 min), the mouse is presented with a dish containing a female's soiled bedding (red circle marked "♀"). *Bottom*, movement trajectories during trials 1 and 2; in the presence of male bedding, mice injected with PBS navigate throughout the neutral environment indiscriminately (left). In the presence of female bedding, males spend a significantly longer time investigating the dish. In mice injected with CNO the movement trajectories show decreased preference for female's bedding. **D.** *Left*, the preference ratio is significant in the PBS treated mice (white bar), while the CNO exhibits an avoidance ratio (gray). *Right*, stacked bar graph showing the average time spent by mice exhibiting freezing (white), exploration (light green), and investigation (dark green) behaviors during trial 2 for the PBS and CNO groups. **E.** *Top*, schematic illustration for the novel object recognition task. The trained object (red) consisted of a marble while the novel object was a cube (green, see methods). *Middle*, raster plots for the investigation events of the novel object in different ChAT-hM4Di mice injected with CNO. The mice spend a significant amount of time investigating the novel object. Bottom, the exploratory distance (left), and the average speed during the task is not affected by CNO.

In addition to aggressive behaviors, the VNS plays an important role in the detection and processing of semiochemicals that trigger sexual behaviors (Stowers et al., 2013). Therefore, we assessed the investigative behavior of naïve ChAT-hM4Di males towards bedding containing female odors. As shown in Fig. 4.6C, under control conditions males showed a significant preference for female soiled bedding compared to non-specific male soiled bedding (Fig. 4.6C, D.D., male vs. female soiled bedding, 17.5 ± 0.5 vs. 12.5 ± 1.7 cm, n = 4, $p < 0.03$; Ratio −1.29 ± 0.13). However, ChAT-hM4Di males injected with CNO no longer showed preference (or avoidance) for female soiled bedding compared to control males (D.D. CNO, 13.3 ± 1.1 vs. 14.6 ± 1.2 cm, n = 4, $p = 0.40$, Ratio 1.09 ± 0.09). Accordingly, we found that the CNO injected mice spent less time investigating the dish (investigation time PBS vs. CNO, 366 ± 36 vs. 194 ± 15 s, n = 4, $P < 0.01$). However, the overall exploring time, grooming and freezing was not different in the CNO injected ChAT-hM4Di males (Fig 4.6D Right, grooming time PBS vs. CNO, 11.9 ± 5.1 vs. 17.1 ± 11.9 s, $p = 0.65$; freezing time, 2.85 ± 0.12 vs. 4.67 ± 1.22 s, n = 4, $p = 0.3$; exploring time, 251 ± 6 vs. 264 ± 11 s, n = 4, $p = 0.43$). Additionally, CNO injection in ChAT-hM4Di males does not affect the investigation of other male's bedding (D.D., Pre CNO 17.5 ± 0.5 cm; Post CNO, 16.2 ± 1.5 cm, n = 4, $p = 0.44$). Together these results suggest that a reduction of cholinergic tone also disrupts the natural preference of male mice for female odors.

Last, we wondered whether inhibition of cholinergic function in the ChAT-hM4Di mice could also interfere with a non-olfactory task. To this extent we used a novel object-recognition task (Bevins and Besheer, 2006). As shown

Fig. 4.6E (bottom), ChAT-hM4Di mice injected with CNO do not show difference in exploratory distance (Control vs. CNO, 2,164 ± 259 vs. 2,123 ± 393 cm, $p = 0.93$, $n = 5$) or average speed (Control vs. CNO, 3.5 ± 0.67 vs. 3.6 ± 0.44 cm/s, $p = 0.95$, $n = 5$) during the task (see methods). Importantly, novel object recognition was not disrupted by the CNO injection (Fig. 4.6E, top). During the task, ChAT-hM4Di CNO treated mice spend more than 80% of the time investigating the new object (novel object, 18.6 ± 4.6 s vs. trained object 3.2 ± 0.7 s, $p < 0.01$, $n = 5$). Thus, under our experimental conditions, the behavioral deficits in CNO-treated ChAT-hM4Di mice are not widespread.

Discussion

The MOB and AOB have a remarkably similar neural circuit, including a prominent neuromodulatory regulation by ACh. Surprisingly, despite this conserved circuitry, we found striking differences in muscarinic cholinergic modulation between the MOB and AOB. Endogenous release of ACh elicited a consistent depolarization of MCs in the AOB, but elicited a hyperpolarization in MOB MCs. Similarly, the predominant muscarinic effect on GCs is hyperpolarization in the MOB, but depolarization in the AOB. The pharmacological profile of the inhibitory response in MOB MCs and GCs, together with its persistence in the M1/M3 −/− mice, indicated the participation of M2 mAChRs. Throughout the OB, M1-like (M1, M3 and M5) and M2-like (M2 and M4) receptors exhibit abundant expression (Le Jeune et al., 1996; Ennis et al, 2007), and these receptors produce different cellular effects (Wess et al., 2007). Thus, our studies are the first to show a physiological role for M2 receptors in the OB.

The M2-mediated inhibition in MOB MCs described here agrees with previous *in vivo* studies showing inhibitory effects in MCs by ACh (Bloom et al., 1964; Nickell and Shipley, 1988). In addition, in agreement with the M2-mediated inhibition of GCs, non-selective cholinergic agonists decreased the frequency of spontaneous action potentials in MOB GCs (Castillo et all, 1999). On the other hand, M1 mAChR activation increased the excitability in MOB and AOB GCs, including depolarization and the activation of an sAPD, leading to an increase of GABA release onto MCs (Smith and Araneda, 2010) (Pressler et al., 2007; Ghatpande & Gelperin, 2009). Together, our results provide the first evidence that neuronal components of the AOB and MOB are

regulated in opposing fashion by ACh, recruiting the activation of M2 and M1 mAChRs to produce inhibitory and excitatory effects, respectively.

GCs play an important role in lateral inhibition and network oscillations in the MOB (Shepherd et al., 2007). The inhibitory and excitatory components of muscarinic modulation in MOB GCs suggest that the overall inhibition of MCs in the presence of ACh will greatly depend on the level of activity in the circuit (Li and Cleland, 2013). We propose that at sub-threshold levels of activation in MOB GCs, the M2-mediated hyperpolarization is the predominant effect of ACh, reducing the inhibitory drive onto GC-MC synapses. However, in the presence of strong excitatory input onto GCs (i.e. from excited MCs), the M1-mediated activation of the sADP will prevail, prolonging the activation of GCs (Pressler et al., 2007). In turn, in the AOB activation of M1-mAChRs is always excitatory in GCs, suggesting GCs contribute differently to the overall response of MCs. One possibility is that ACh produces a more generalized increase in excitability in the AOB, not to enhance odor discrimination, but rather to facilitate the integration of pheromonal signals. In this case, a reduction in ACh levels will disrupt signal integration and thus behavior (see below).

It is noteworthy that MCs, but not GCs, also exhibit a nicotinic excitatory response in the AOB and MOB (Castillo et al., 1999; Smith and Araneda, 2010; D'Souza and Vijayaraghavan, 2012), yet optogenetic stimulation indicated a predominant muscarinic response in MCs. One possibility is that our stimulation protocol induces fast desensitization of nAChRs. However, a similar hyperpolarization of MOB MCs by optogenetic stimulation of HDB

neurons was recently reported (Ma and Luo, 2012). Yet other studies show excitation of MCs in the MOB (Kunze et al., 1991; Zhan et al., 2013; Rothermel et al., 2014). At this time, the reason for these discrepancies remains unknown. One possibility is that the location used for the optical stimulation (i.e. superficial OB, or OB vs. HDB) or actions on multiple targets may have contributed to these differences (Devore et al., 2014). For example, the distribution of cholinergic fibers in the GC layer and the muscarinic effects in GCs reported here and elsewhere (Pressler et al., 2007; Smith and Araneda, 2010) suggest *in vivo* optogenetic stimulation will be affected by the degree GCs are stimulated (see below).

Modulation of gain is a chief mechanism for proper integration and processing of sensory signals, relying on a synaptic network that conducts scaling and thresholding functions (McKenna et al., 1988; Metherate et al., 1988; Pinto et al., 2013). Interestingly, endogenous release of ACh had a different effect on the input/output relationship of MCs in the AOB and MOB, showing a net effect on gain in MCs of the MOB, but not in the AOB. Stimulation of superficial layers of the MOB indicated that ACh increases the threshold for sensory input by exciting MCs (Rothermel et al., 2014). Furthermore, in the MOB ACh has been shown to modulate external tufted and periglomerular cells (Pignatelli and Belluzzi, 2008; D'Souza et al., 2013; Liu et al., 2015). These cells are part of the glomerular network involved in processing incoming odor signals (Shao et al., 2009; Gire et al., 2012). However, it is noteworthy that when the HDB is directly activated, which should achieve a widespread activation of cholinergic fibers, the effect on MOB MCs becomes inhibitory (Ma and Luo, 2012; Rothermel et al., 2014).

Thus, it is possible that while the overall effect of ACh is inhibitory in MOB MCs, excitation, most likely nicotinic (D'Souza and Vijayaraghavan, 2012), at the level of the superficial glomerular circuit could modulate MC gain. Intriguingly, cholinergic fibers and other cholinergic markers appeared excluded from the AOBGL of the AOB, suggesting that ACh could have a lesser role in regulating sensory input at this level. Although we cannot rule out the possibility that ACh could access the GL through volume transmission (Sarter et al., 2009), it is possible, that the lack of innervation on the GL underlies differences in processing. For example, chemosensory representation in the GL of the MOB shows tunotopy, while in the AOB the representation is based on the phenotypic identity of social odors (Ma et al., 2012; Hammen et al., 2014). In addition, in the AOB information from several subclasses of receptor types is integrated into a single MC at the level of the GL (Wagner et al., 2006). Therefore, MCs in the AOB are poised to integrate sensory information from widespread odor sources, while its counterparts in the MOB may serve a more analytical role (Dulac and Wagner, 2006).

Detection and processing of semiochemicals by the VNS is fundamental for several social interactions, predominantly sexual and aggressive behaviors (Halpern and Martinez-Marcos, 2003; Brennan and Zufall, 2006). Not surprisingly, neuromodulation plays a critical role in behaviors that require signaling through the VNS (Brennan and Keverne, 1997; Brennan and Kendrick, 2006). Here, silencing the activity of HDB cholinergic neurons disrupted odor discrimination, while transiently enhancing the activity of these neurons produced a dramatic improvement in the natural discrimination of odors. Previous pharmacological studies reached a similar

conclusion (Mandairon et al., 2006), indicating that the chemogenetic approach, which replicates *in vivo* modifications of synaptic activity and physiological release of ACh, provides a reliable platform to assess the role of cholinergic modulation on VNS function. Using this approach, we found that silencing HDB cholinergic neurons impaired the ability of the defeated mouse to recognize the aggressor's odor and disrupted the investigation of female odors by males. Previous studies have shown the cues necessary for eliciting these behaviors are mediated by the VNS (Chamero et al., 2007; Haga et al., 2010; Haga-Yamanaka et al., 2014). Together, these results indicate that reducing cholinergic tone has deleterious effects on odor-triggered behaviors that rely on VNS signaling. Interestingly, habituation to social odors was reduced by non-selective pharmacological manipulation of the cholinergic system (Winslow and Camacho, 1995); however, our selective chemogenetic silencing of the HDB had no effect in habituation to odors. Our experiments do not rule out the participation of other brain regions targeted by HDB cholinergic neurons, such as the piriform and entorhinal cortices (Zaborsky et al., 2012). However, we found that chemogenetic inhibition of HDB neurons did not impair "recognition memory" (Bevins and Besheer, 2006). Previous studies have shown that this paradigm is affected by damage of forebrain cholinergic neurons (Kornecook et al., 1999; Paban et al., 2005). On the other hand, recent studies suggest the MOB and VNS play complementary roles in processing social odors and therefore the contribution of cholinergic to projections in the MOS could also contribute to the observed effects (Mucignat-Caretta et al., 2012; Korzan et al., 2013; Baum and Cherry, 2014). Nevertheless, our data supports a cholinergic neuromodulatory role for social

behaviors that signal through the VNS; further studies should elucidate the specific contributions of the MOS and VNS in social odor investigations.

In sum, cholinergic modulation in the OB has an important role in the olfactory system; it facilitates odor discrimination and investigation of socially relevant semiochemicals. Despite the conserved nature of the neural circuits that process these sensory cues in the MOB and AOB, cholinergic modulation of these circuits exhibit a marked difference, anatomically and physiologically. It is noteworthy that noradrenaline, another neuromodulator that regulates OB circuits, also shows significant differences in the cellular actions in these circuits (Nai et al., 2009; Zimnik et al., 2013). Thus, these neuromodulatory differences highlight the specialized function of these two parallel pathways in regard to stimulus composition and the behavioral output they trigger. In addition, our results highlight the emerging view on the function of neuromodulation; neural circuits, in the presence of multiple neuromodulators, can produce the same output using several different mechanisms (Marder, 2012). Future studies will examine whether the neuromodulation of upstream components in these pathways also exhibit differential regulation by the cholinergic system.

Chapter 5: Concluding Remarks and Future Experiments

State dependent cholinergic modulation of brain circuits is critical for several high level cognitive functions, including attention and memory. In the present work, we provided new evidence that cholinergic modulation differentially regulates two parallel circuits that process chemosensory information, the accessory and main olfactory bulb. These circuits consist of a remarkable similar synaptic arrangement and neuronal types, yet cholinergic regulation of these circuits produced striking opposite effects in output and intrinsic neurons. While our results demonstrated an important role for cholinergic modulation in odor discrimination and social behaviors, they also raise several exciting new questions regarding how ACh modulation occurs at the cellular and network level and how this modulation contributes to the behaviors these circuits mediate. Here I describe some of the research venues laid down by my work and that remain to be explored.

In the present study, the functional role of ACh was first assessed at a cellular level with patch clamp physiology and a pharmacological approach to establish the basic principles by which ACh regulates excitability in the OB neurons. Throughout the brain, mAChR's modify the physiological state of a wide array of neuronal types, regulating K+ conductances underlying resting state such as the M-current, and/or Ca2+ dependent K+ currents (Hasselmo and Sarter, 2011). In addition to well-accepted physiological mechanisms, several brain circuits exhibit an additional mAChR mediated excitatory mechanism involving the activation of members of the transient receptor potential (TRP) channel family and whose recruitment prolongs neuronal activation, enhancing circuit function (Egorov et al.,

2002). A central theme in the present work is the convergence of neuromodulator-mediated excitatory mechanisms onto GCs, in particular in the AOB. Activation of M1-mAChR combined with calcium influx using a current stimulus that simulates excitatory inputs activates a calcium-sensitive nonselective cationic current I_{CAN} that causes depolarization and leads to further Ca^{2+} influx, most likely via a TRPC channel described in other brain regions (Yan et al., 2009). A similar stimulus evoked sADP is observed in GC's following activation of α_{1A}-ARs. This was the first description of this effect for NA in the OB. Interestingly, in the AOB we showed that activation of mGluR1 also elicited a similar mechanism. As expected, activation of these receptors in GCs leads to an increase in GABA release and inhibition of MCs (Smith et al, 2009; Zimnik et al 2013). Both M1-mAChRs and α_{1A}-ARs GPCR's couple to the Gq signal transduction pathway, activating Phospholipase C (PLC). Activation of this cascade produces diacyl glycerol (DAG) and inositol 1,4,5-trisphosphate (IP3) which can trigger Ca2+ release from intracellular stores and activate protein kinase C (PKC) (Figure 5.1). PKC is a critical kinase involved in memory acquisition and synaptic maintenance in addition to the many other signal processing functions (Sun and Alsko, 2014). In the visual cortex, mAChR and AR activation can lead to long-term depression of synapses (Kirkwood et al., 1999). One plasticity mechanism, spike timing dependent plasticity (STDP), provides a differential plasticity mechanism depending on receptor subtype specific activation (Pawlak et al., 2010). Intriguingly, while AOB and MOB GCs display a conserved M1-mAChR mediated excitatory mechanism that involves activation of a sADPs, in the MOB ACh also activates M2-mAChRs in GCs. Thus in the MOB the cellular effects rely on two different signal transduction pathways (M1-Gq vs. M2-Gi). Interestingly, activation of α_2-ARs on GCs, which also couple through Gi-GPCRs,

has been shown to inhibit GCs (Nai et al., 2009, 2010). During STDP, specific signal transduction pathways are necessary and sufficient for this form of plasticity, G_q for LTD and G_i for LTP, and therefore the MOB and AOB could be relying on different mechanisms for promoting plasticity at the synapses following activation by the cholinergic and noradrenergic systems. Furthermore, this plasticity may depend on the exact point in time of activation of neuromodulator-receptors relative to pre- and postsynaptic spiking, which will depend largely on receptor location and neuromodulatory afferent release properties.

Additional experiments to determine the cellular machinery activated by the cholinergic and noradrenergic systems and their role in shaping OB plasticity are needed. For example, to test whether activation of the cellular machinery underlying the observed differential effects contributes to changes in output in the circuit, we could express genetically engineered Opto-XRs in OB GCs. These genetically modified GPCRs enable optical activation of intracellular signaling (Gq, Gi, Gs), bypassing the need of endogenous ligands (Airan et al., 2009). We can hypothesize that independent of neuromodulatory activation, we can elicit similar physiological activation profiles in GCs with the Opto-XRs, including an sADP and cellular effects. Additional approaches to dissect the molecular machinery of the AOB and MOB differential activation of GCs could utilize shRNA or RNAi to knock down channels (e.g TRPC, GIRK) or interacting proteins (e.g PKC isozymes, MAP Kinases) involved in plasticity mechanisms. Additionally, Opto-XRs could assess, on a exact temporal scale, the role of precisely timed signaling cascades necessary for generating STDP and if the sADP has any function in enhancing this form of plasticity.

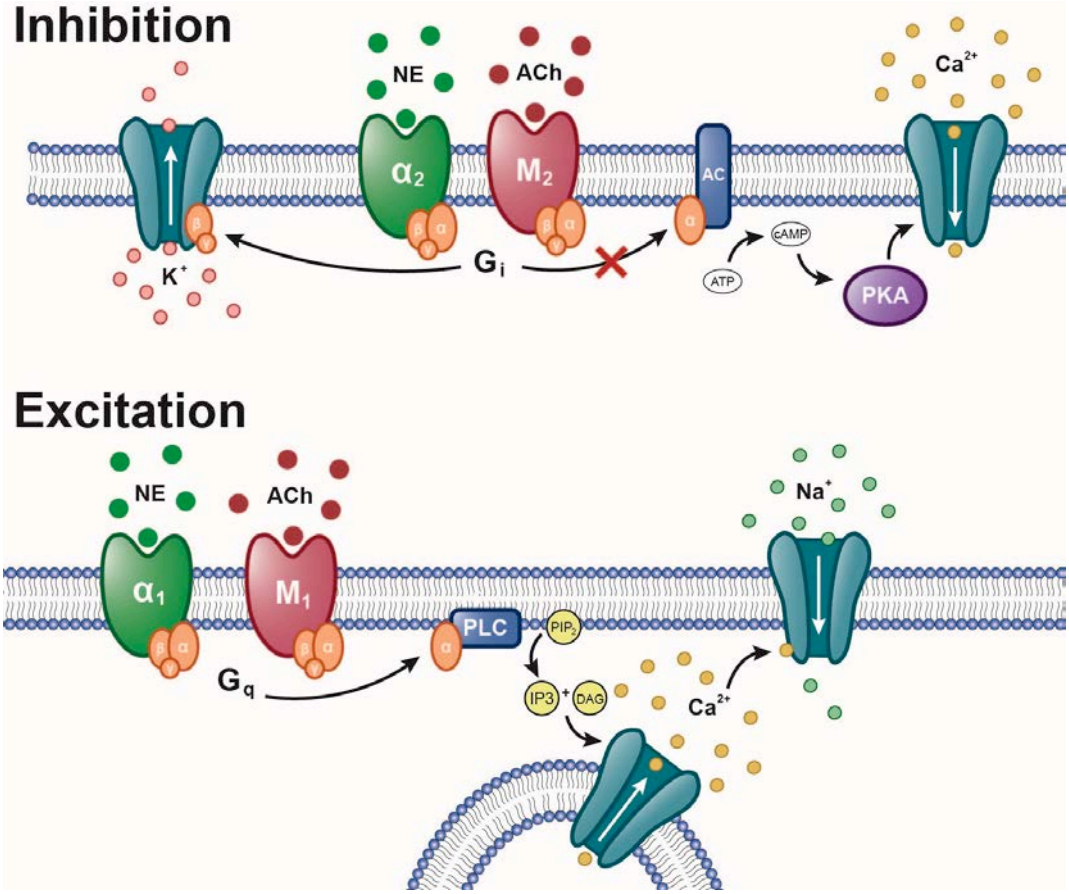

Figure 5.1 Cholinergic and Noradrenergic signal transduction

A. Activation of α_2-AR or M2 mAChRs results in the dissociation of Gi from the G protein complex and its association with the enzyme adenyl cyclase (AC). This causes the inactivation of AC, resulting in a decrease of cAMP produced from ATP, leading to a decrease of intracellular cAMP. Protein Kinase A cannot be activated by cAMP, thereby reducing phosphorylation mediated by PKA. **B**. Activation of α_{1A}-AR or M1 mAChRs results in the dissociation of Gq from the G protein complex and its association with the enzyme phospholipase C (PLC). PLC cleaves the phospholipid phosphatidylinositol 4,5-bisphosphate (PIP2) into diacyl glycerol (DAG) and inositol 1,4,5-trisphosphate (IP3). DAG remains bound to the membrane, and IP3 is released as a soluble structure into the cytosol. IP3 then diffuses through the cytosol to bind to IP3 receptors, particularly calcium channels in the smooth endoplasmic reticulum (ER). This causes the cytosolic concentration of calcium to increase, causing a cascade of intracellular changes and activity.

Local ACh releasing ChAT interneurons can shape neuronal output in brain circuits (von Engelhardt et al., 2007). Recently, a small population of local cholinergic interneurons has been identified in the MOB, primarily in the GL; however, a functional role has yet to be ascribed for these neurons (Krosnowski et al., 2012). Importantly, these ChAT positive neurons do not appear to be present in the AOB (unpublished) and may contribute an added layer of processing differences between the AOB and MOB. In our experiments, we stereotaxiclly targeted DREADD expression to HDB cholinergic neurons, sparing the local ChAT interneurons in the OB. Thus, our *in vivo* studies focused exclusively on extrinsic cholinergic input to the OB during discrimination and behavioral tasks. However, in our *in vitro* optogenetic experiments, using the ChAT-ChR2 mice, expression of ChR2 occurred in all ChAT neurons, therefore these results reflect the total intrinsic and extrinsic cholinergic effects on MC output. Consequently, several questions arise regarding the function of these ChAT neurons, and the balance of intrinsic vs. extrinsic cholinergic input in the OB circuits. Future experiments should target these ChAT neurons using either optogenetic or chemogenetic tools to examine their role in behaviors mediated by both the MOS and VNS. If these ChAT neurons reside primarily in the GL, we could hypothesize a role in enhancing odor threshold detection. Moreover, it is not known if these ChAT interneurons are born in the SVZ and migrate to the OB and whether they exhibit adult neurogenesis. If adult neurogenesis of these ChAT neurons exists it would expand the repertoire of cell types incorporated in the adult OB circuit, as most of the neurons described so far are GABAergic. In this case we could isolate this intrinsic cholinergic modulation by using targeted virus injection of DREADDs into the SVZ of ChAT-Cre mice to assess how their

activation/inhibition can modify odor discrimination *in vivo* in the behaving animal. Likewise, ChR expression in ChAT interneurons, which are primarily located in the GL, could revel an important cholinergic contribution to processing in the glomerular circuit.

Decreasing adult neurogenesis causes a decrease in inhibition onto MCs and disrupts odor associated behaviors, supporting the idea that newly born GCs play an important role in olfactory processing (Breton-Provencher et al., 2009; Lepousez et al., 2013). Cholinergic enrichment has been shown to have a strong positive correlation with adult neurogenesis and cell survival of GCs (Cooper-Kuhn et al., 2004; Mechawar et al., 2004; Kaneko et al., 2006; Whitman and Greer, 2007). Thus, an interesting hypothesis put forward by these observations is that the cholinergic system facilitates the integration of adult born GCs into the AOB and MOB circuitry. For example, ACh could facilitate a form of long-term plasticity that is present in newly born GCs, but absent in mature GCs (Nissant et al., 2009). A potential substrate for this mechanism is I_{CAN}, which is elicited by activation of M1 AChRs both in the MOB and AOB. Cholinergic modulation of the I_{CAN} may contribute to adjusting neural dynamics for active memory maintenance, pacemaking, and spatial navigation (Yoshida et al., 2012; Yamada-Hanff and Bean, 2013). If acquisition of cholinergic I_{CAN} responses is coincident with the final stages of neuronal maturation in the OB, it could suggest a potential conserved role for ACh in GC survival and/or integration. However, it is also possible that the differential mAChRs profile displayed by MOB and AOB newly born GC neurons (i.e. M2- vs. M1-mAChR) could modulate synaptic plasticity at dendrodendritic synapse in one region but not the other. Thus, in future experiments we could test the contribution of these mAChRs to plasticity in the

MOB. For example, we may observe changes in the amplitude of EPSCs or changes in dendritic spine structure, suggesting changes in post or presynaptic sites in the GCs after activation of these receptors. To test this possibility, using chemogenetics, we could make AOB GCs to behave more like MOB GCs (hyperpolarizing) for a chronic period (1 week), and assess how this affects synaptogenesis in the AOB. Additionally, we could use use a chemogenetic approach to chronically enhance/inhibit ACh release from ChAT fibers and assess the role of cholinergic tone in shaping synaptic properties in the OB.

	AOB		MOB	
	MC	GC	MC	GC
mAChR	M1	M1	M2	M2
Δ Vm	▲	▲	▼	▼
Mech	?	TRPC	GIRK	GIRK
sADP	N	Y	N	Y

Table 5.1 Summary of pharmacological and physiological profile of responses to mAChR activation in OB GC and MCs. Selective antagonists and mAChR -/- knock out mice demonstrate M1- and M2-mAChR mediated effects in the AOB and MOB, respectively. Delta Vm (ΔVm) represents the effect on resting membrane potential (Vm), é depolarizing, ê hyperpolarizing. Hypothesized cellular mechanism of activation (Mech); Transient Receptor Potential Channel (TRPC), G-protein Inward Rectifying K^+ Channel (GIRK). Presence (Y) or absence (N) of slow afterdepolarizing potential (sADP) in OB cell types.

While several studies using systemic pharmacology have demonstrated the role of muscarinic antagonism on cognition and formation of new memories, presumed by blocking postsynaptic sites, it is important to consider that these antagonists can also act to inhibit release from presynaptic terminals binding M2-mAChRs, which are present in both on cholinergic and GABAergic axon terminals (Herzog et al., 2003; Hasselmo and Sarter, 2011). Our *in vitro* results suggest a direct M2-mAChR mediated inhibitory conductance activated on MCs and GCs in the MOB.

However, it remains possibility there is also a presynaptic mechanism acting concurrently, particularly on GABAergic afferents, during the *in vivo* behavior experiments. Furthermore, our lab has completed experiments to demonstrate that GABAergic evoked IPSCs in GCs can be inhibited via a presynaptic mechanisms with mAChR agonists (unpublished).

An exciting recent area in neurobiology research is the study of corelease of neurotransmitters and neuropeptides from neurons, and their dual contributions to circuit output (Hnasko and Edwards, 2012). In future studies of ACh in the OB, determining whether cholinergic neurons corelease neurotransmitters in the OB will represent an important challenge. Recently, corelease of GABA and ACh was described in cortically projecting cholinergic neurons residing in the basal forebrain neurons (Saunders et al., 2015), and in thalamocortical experiments where cholinergic activation of nAChRs potentiates glutamatergic-evoked currents (Gil et al., 1997). Importantly, our cholinergic effects persist in the presence of GABA and iGluR blockers, but we cannot rule out the possibility the activation of small excitatory or inhibitory currents. One possible experiment would be to conduct a dose response of the cholinergic effect in both the presence and absence of blockers of GABAR and iGluR. A shift in the dose response (EC50) for the cholinergic activation could suggest a corelease mechanism acting on these cells with degree of impact depending on saturation of cholinergic activation.

While the cellular effect of muscarinic activation AOB and MOB neurons appears to be in opposition, it is worth noting that our results, as well as others, have demonstrated a reliable nAChR mediated depolarization on MCs. This nAChR

activation, shown to be α4β2 in AOB and MOB, occurs on the primary dendritic terminals of MCs. Further, if we target puff ACh onto MC somas we do not observe a depolarization, as you see when targeting ACh to GL layer. Intriguingly, as nAChRs are located primarily in the GL, it would be interesting to determine whether OSN iGluR evoked potentials onto MC dendrites are modulated in the MOB and AOB by nAChRs. Our studies indicate that ChAT fibers are absent in the AOB GL, therefore nAChR modulation of the glutamatergic synapse could be an important difference between the two circuits. In this case we expect that evoked glutamate currents in MCs evoked by a electrical stimulation of the olfactory nerve layer will be enhanced in the presence of cholinergic agonists. Additionally, we could test if glutamatergic input arising from the PC, which has been shown to demonstrate plasticity onto GC, could be modulated in the presence of ACh release.

Examining local interactions within the HDB, particularly with GABAergic neurons, remains an important aim for future experiments. In the HDB, cholinergic neurons reside alongside a much larger population of GABAergic neurons, suggesting potential interactions between these nuclei. To this end, we have conducted experiments to demonstrate that HDB GABAergic neurons can be activated by cholinergic agonists, and conversely, HDB cholinergic neurons are sensitive to GABAergic activation. HDB GABAergic neurons also send axons to the OB and we have recently shown that they provide a robust mechanism for disinhibition in the OB (Nunez-Parra et al., 2013) and that a presynaptic mAChR mediated inhibition of these GABAergic afferents exists (unpublished). Therefore, it is likely that interactions of these systems, both locally in the HDB and via long-range feedback loops, play a role in shaping OB transformations. Interactions between

neuromodulatory systems is an attractive future direction. Namely the exploration of dopamine neurons located in the OB, as we know modulation of striatal cholinergic tone by phasic dopaminergic input adapts two neurotransmitter systems for the detection and selection of relevant stimuli (Wieland et al., 2014). Additional possible experiment would be to selectively cross ChAT-ChR2 x GAD2-Cre mice and selectively target the GABAergic neurons with DREADDs. Enabling the precise control of one population with light (ChAT) and the other with chemogenetics (GABAergic). This would represent an important step in studying these two neurotransmitters system and maintaining bidirectional control in-vivo in the behaving mouse.

While ~70% of HDB cholinergic neurons send axons to the OB, these cholinergic neurons also send a small numer axons to other brain regions. Anatomical studies have shown HDB neurons also project to other olfactory areas, including the PC and AON (Woolf et al, 1986; Markopoulos et al, 2012). Therefore, modulation by ACh through local and long-range connections, across neural circuits via multisynaptic mechanisms remains an important consideration when assessing cholinergic modulation of olfactory behaviors. For example, release of ACh in the parietal cortex can be mediated by stimulation of mAChRs in prefrontal cortex (PFC), most likely via indirect axonal projections to the basal forebrain and/or cortical loops (Nelson et al., 2005). Thus the PC, which receives dense input from the MOB, could play a role in odor aversion and attraction through associative olfactory learning and PC outputs to higher order brain regions, including the ventral striatum and amygdala; where odor valence can be assigned through neuromodulation of learning (Rosenkranz and Grace, 2002; Setlow et al., 2003). We also do not know whether HDB ChAT neurons that project axons to

the AOB are the same population that project axons to the MOB. Or similarly, if a ChAT neuron projecting to the OB also sends axons to a cortical area. Using molecular techniques, such as the rabies virus mediated trans-synaptic tracers, we could determine where HDB neurons project and what type of neurons they make synaptic contacts with. Additionally, it would be interesting to test if a coarse spatial map in HDB neurons axonal targeting exists in the OB (e.g., ChAT nuclei on the more dorsal region of the HDB project to more internal OB layers). This could be accomplished with localized OB injections of retrograde neuronal tracers at different wavelengths to monitor the origin of the axonal fibers. A spatial map of axon fibers would suggest the possibility that subsets of cholinergic neurons could be selectively activated to attend to certain stimuli and therefore modulate different parts of the OB.

Unlike in the MOB, where sensory neurons expressing the same odorant receptor converge onto a single glomerulus, VNO sensory neurons project to multiple glomeruli in the AOB (Larriva-Sahd, 2008). Interestingly, the human OB shows a high ratio of glomeruli to the number of olfactory receptors, predicting a high degree of integration of signals at the GL level (Maresh et al., 2008). Therefore, when comparing the integration of signals in the AOB and MOB to human OB function, the rodent AOB may be a more suitable model to study neuromodulators and odor processing. In humans, olfactory is one of the earliest symptoms associated with neurodegenerative disorders, most strongly observed in AD patients. In a recent anecdotal finding, olfactory disfunction correlated with likelihood of dying within a 5-years period in an old group (Pinto et al., 2014). Thus, olfactory testing may represent an important differential diagnosis of several neurodegenerative diseases (Hawkes et al., 1999; Alves et al., 2014). While

cholinergic loss is attributed with AD and dementia, the topic still remains controversial, as treatment with nonselective mAChR agonists in healthy individuals does not reproduce the symptoms (Hasselmo and Sarter, 2011). M1-mAChR (and α1-AR) activates PKC and defective PKC signaling cascades in neurons is one of the earliest abnormalities in the brains of patients suffering from Alzheimer's disease. Therefore additional studies oriented at understanding how signal transduction triggered by neuromodulatory inputs is operating in the AOB vs. MOB could provide us important information regarding cell death in these neurodegenerative diseases.

Microdialysis studies measuring ACh release have consistently shown increased ACh release during attention tasks. Neuronal oscillations in theta (4-14Hz) and gamma (30-80Hz) are important for certain behaviors, and cholinergic activation can modulate these oscillations (Fisahn et al., 1998; Nagode et al., 2014). Amongst different sensory modalities, ACh generally acts to enhance sensory processing, for example, increasing neuronal thresholding in cat auditory cortex (McKenna et al., 1988), improving cell responsiveness somatosensory cortex (Mentherate et al 1988), and improving sensory gain in visual cortex (Disney et al., 2007). Interestingly, cholinergic input plays a critical role in cross-modal signal detection that requires attention to visual and auditory conditioned stimuli (Turchi and Sarter, 1997). Noting ACh's importance across systems, additional cross-modal studies, such as an auditory/visual pre-pulse before an olfactory task while modulating HDB neurons could be completed to assess the role of the cholinergic system and multisensory interactions.

The activation of nAChR and mAChRs on MCs raises several additional questions regarding the role timing plays for nAChR and mAChR activation in OB sensory transformations. nAChR display faster activation and quicker desensitization comparably to mAChRs, but mAChR's coupling to signaling cascade provides long term and amplified activation properties. Several studies indicate that cholinergic release is diffuse, occurring on a time scale of several seconds to minutes (Descarries, et al). This model has lead to the view that activation of postsynaptic targets by ACh occurs by volume transmission instead of a classic "wired circuit" (Sarter et al, 2009). Indeed, this is one of the reasons we opted for studies using DREADD compared to optogenetic activation of HDB neurons, for our in-vivo studies. However, for our *in vitro* studies, the fast activation kinetics of optogenetic probes does allow for precise temporal response profiling in neural circuits. As the ChAT fiber innervation pattern in the GL appeared different in the AOB and MOB, we attempted focal laser activation of ACh release in specific compartments in the OB (i.e. GL, GCL). Unfortunately, these experiments yielded no discernable effects on MCs, suggesting slow kinetics of ACh release in the OB and the necessity for extended light stimulations (data not shown). Moreover, this protocol of stimulation did not reveal significant nicotinic responses in MCs. Future experiment and modeling should address the kinetics of nAChR and mAChR activation by considering volume transmission of ACh and receptor AChR locations.

To discuss how ACh modifies olfactory processing in the MOS and VNS, first we must consider the anatomical and functional differences, which contribute to their inherent odor coding strategies. As previously described (Page 4), odor signals from peripheral OSNs converge onto MOB output neurons and display column-like flow of odor information, with an emphasis on MTC signal saliency to

neighboring MTCs (decreased integration). Conversely, the lack of convergence in the VNS signals onto AOB output neurons causes widespread MTC activation and predicts a lacks of precise single MTC signal saliency relative to neighboring MTCs. We explored these differences further in the experiments shown in Figure 4.3, where we studied the input/output (I/O) relationship in MTCs across a range of input intensities.

We found an important difference in the responses of MTCs in the presence of ACh. While in the AOB, there was an additive shift in the threshold for MTC action potential firing, in the MOB, we found a multiplicative scaling of sensitivity. This differential effect of ACh on the I/O response of MTCs posits several intriguing questions as to how ACh participates in odor processing in AOB and MOB. One possibility is that in the MOB ACh may suppress weak MC activity more strongly compared to larger input intensities and this mechanism of modulation could shape MTC neuronal gain in the MOB and play an important role in odor-guided behaviors including odor discrimination and detection. In contrast, in the AOB, fine odor discriminations could prove less vital, but more important to ensure animals detect all relevant odors present, in a usually complex odor blend. Thus, in the AOB, we find the depolarization of output neurons in the presence of ACh may provide a thresholding solution for increasing MTC output across all sensory information arriving from the VNO, with less of a focus on improving signal saliency. Further, this additive modulation of threshold in the AOB may help to filter out slow variations in background activity without compromising sensitivity of incoming odor signals. Importantly, in both the AOB and MOB, we observe a stimulus-elicited sADP, which enhances inhibition from GCs -> MTCs. This mechanism of temporally precise and prolonged inhibition sharpens MTC responses and inhibits the lateral network of

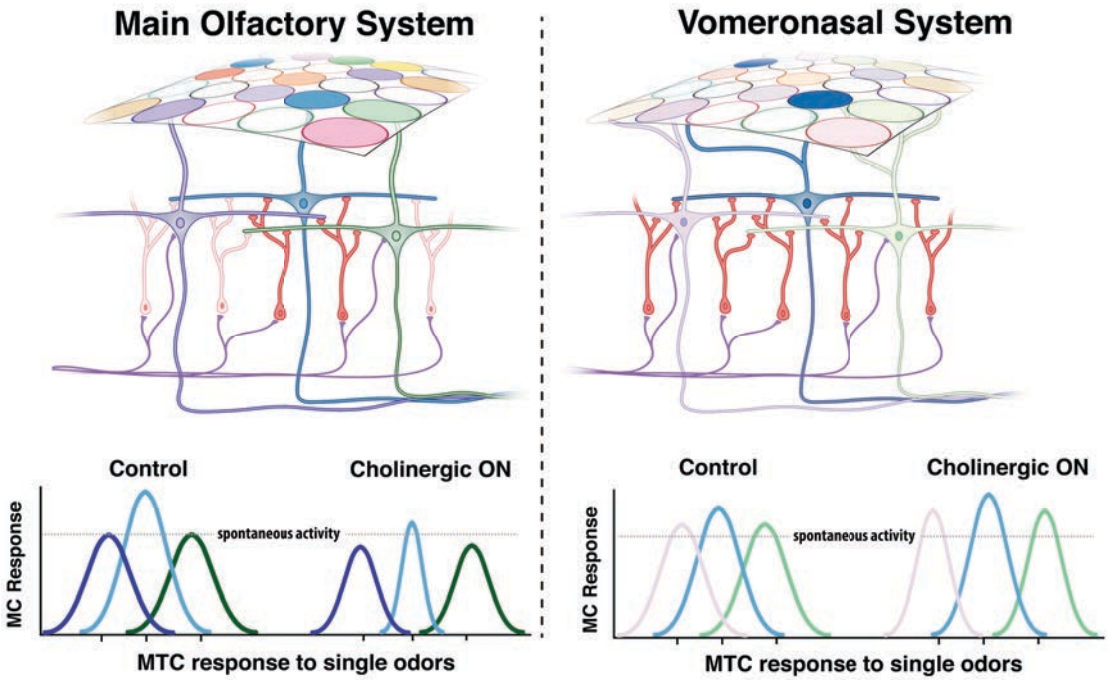

Figure 5.2 Comparison of the effect of acetylcholine on olfactory signal processing in the MOS and VNS. *Top*, in both systems, MTCs project to glomeruli in which sensory signals from OSNs expressing the same odor receptor converge, here shown as circles of different colors. In addition, in both systems, MTCs are inhibited by GCs (shown in red). GCs and MTs cells undergo top-down regulation by several afferent systems including cholinergic (purple fibers). However, in the MOB MTCs connect only to one glomerulus while in the AOB MTCs project to multiple glomeruli. Furthermore, MTCs in the MOB and AOB respond differentially to ACh activation; depolarization in the AOB and hyperpolarization and MOB. *Left, bottom,* in the MOS, odor evoked excitation of MTCs in both "Control" and during ACh release (Cholinergic ON). During ACh activation, the strongly activated MTC (blue) and the weakly activated MTCs (purple, green) show a decrease in response amplitude comparably to control. During concurrent ACh activation and Ca^{+} entry (stimulus), we hypothesize a sharpening of MTC responses (x-axis width decreases), via a sADP mediated enhancement of GCs inhibition. GC neuronal activity is coded in opacity (darker red = more depolarized). *Right, bottom,* in the VNS odor activation of MTCs elicits broad activation of several MTCs. Odor activation during ACh release (Cholinergic ON) increases the threshold for firing in MTCs and an enhancement in MTC responses comparably to control. During ACh and Ca^{+} entry (stimulus) in the VNS, we observe a cellular depolarization of GCs and a sADP. mAChR enhancement of GCs firing sharpens MTC responses and improves signal saliency via inhibition of lateral MTCs.

MTCs. Thus, while the ACh cellular effects are opposing, the ACh activated sADP could represent an important conserved target between olfactory systems for supporting odor processing of behaviors detected by these two systems.

In conclusion, while the AOB and MOB appear remarkably similar in premise, several layers of differences exist, including how neuromodulation activates these circuits to modify OB odor transformations. Numerous lingering questions remain,

including 1. How and why do neurogenic neurons (GCs) arriving from the same population of progenitors cells in the SVZ develop grossly different physiological responses to the same neurotransmitter? 2. What is unique about the release pattern of ACh in the OB (*en passage,* global nonspecific release), compared to "wired" afferent release, that enables ACh such a robust neuromodulatory control? 3. Why use three neurotransmitters (NA, ACh, Glu) to act on three different metabotropic receptors to achieve the same goal, activating the sADP? 4. Considering mAChRs are having opposing effects from cellular activation in AOB vs. MOB, how can decreased cholinergic input have the same effect on the behavioral output (decreased olfactory abilities)? 5. Is different molecular machinery (e.g kinases, channels) necessary and sufficient to meet the unique signal processing demands of the AOB and MOB?

APPENDIX A

Title: Properties of developing $GABA_A$ receptors in cerebellar molecular layer interneurons: Studies with GABA uncaging

Abstract

The distribution of $GABA_A$ receptors ($GABA_A$Rs) on neuronal membranes, as well as their biophysical properties, are key elements in the function of inhibition in neural circuits. Even minor changes in the spatial distribution of these receptors, in their number or in their biophysical properties can influence processes such as synaptic efficacy and signal integration. In fact, changes in the distribution and properties of neuronal receptors are characteristic of several highly relevant physiological processes, such as synaptic maturation and long-term potentiation. This work aims to characterize the distribution and biophysical properties of $GABA_A$Rs in the dendritic domain of molecular layer interneurons (MLI's) of the cerebellar cortex during development. We achieve this using a combination of electrophysiological, optical, and immunohistochemical methods. Activation of $GABA_A$Rs is accomplished by photolysis of GABA from the caged compound DPNI-GABA at different locations of the dendritic domain of the neurons, while in the voltage-clamp. We then determine the exact distribution of the receptors and their relationship to synaptic structures using immunohistochemistry. We conclude that α1-sububit containing $GABA_A$Rs display refined clustering at synaptic structures in mature MLIs dendrites, while exhibiting a more homogenous distribution pattern in young MLIs. Evoked inhibitory postsynaptic currents (IPSCs) on mature MLI dendrites displayed increased sensitivity to a selective modulator of α1-$GABA_A$ subunits, compared to young MLIs, suggesting a higher α1 component in $GABA_A$Rs of mature MLIs. These findings suggest the existence of a developmental maturation process for GABAergic inhibition on MLIs that increases inhibitory tone with age, most likely via α1-$GABA_A$ refinement and activation.

LIST OF ABBREVIATIONS

α1-GABA$_A$ GABA class-A receptors containing α1 subunit
BC Basket Cell
CF climbing fibers
DPNI-GABA nitroindoline-caged GABA
eIPSC Laser evoked inhibitory post synaptic current
GABA γ-aminobutyric acid
GABA$_A$R γ-aminobutyric acid class A receptors
GC Granule Cell
GCL Granule Cell Layer
IN interneurons
IPSC inhibitory post-synaptic current
Mature >PN-30
MF mossy fibers
mIPSC miniature inhibitory post-synaptic current
ML Molecular Layer
MLI molecular layer interneurons
PF Parallel Fibers
PN days post-natal
PC Purkinje cells
PCL Purkinje cell Layer
RT rise-time (10-90%)
sIPSC spontaneous Inhibitory post-synaptic current
SC Stellate Cells
Young PN-8 to 12

Introduction

Predicting and qualifying neuronal inhibition throughout the nervous system has been a persistent theme in neurobiology research for the last half-century. Various forms of neuronal inhibition, across several brain regions, are routinely quantified and mechanistic hypotheses tested. Within the mammalian brain, highly heterogeneous populations of neurons, termed interneurons (INs), release the inhibitory neurotransmitter γ-aminobutyric acid (GABA) which binds two main classes of metabotropic and ionotropic receptors (Farrant and Nusser, 2005). Activation of postsynaptic ionotropic GABA receptors ($GABA_AR$) regulates numerous physiological processes, such as the frequency of neuronal oscillations and feed-forward inhibition of principal neurons in most brain regions (Flores and Méndez, 2014). GABA released from INs binds to postsynaptic $GABA_ARs$, which are ligand-gated ion channels permeable to Cl^-. In most neurons of the adult nervous system, the physiological gradient for Cl^- across the neuronal membrane is such that binding of GABA to $GABA_ARs$ generates inhibitory postsynaptic currents (IPSCs). These receptors are heteropentameric channels, grouped in seven classes according to their sequence homology, with 19 candidate subunits (α1–6, β1–3, γ1–3, δ, ε, θ, π, ρ1–3), but generally $GABA_ARs$ are comprised of three subunits. The most common $GABA_ARs$ configuration in the brain consists of α1β2α1β2γ2 subunits (Laurie et al., 1992; Sperk et al., 1997). Importantly, different subunit compositions bestow unique activation kinetics, pharmacological profiles, and conductance properties to each receptor subtype (Kralic et al., 2006). For example, benzodiazepines act in a subunit specific manner on α-$GABA_ARs$, with different α subunits conferring sedative

or anxiolytic effects (Rudolph and Knoflach, 2011). In addition to these different biophysical properties, $GABA_AR$ distribution throughout the various neuronal compartments is a key element in the function of neural circuits (Flores and Méndez, 2014). Within the cerebellum, INs in the granule cell and molecular layers (ML) tightly regulate the output of Purkinje cells (PCs)(Fig A.1). PCs possess abundant inhibitory synapses, receiving GABAergic input from molecular layer interneurons (MLIs), the basket and stellate cells (BC and SC, respectively), as well as neighboring PCs (See Fig A.1 (Eccles, 1967)). BCs and SCs are spatially separated in the ML, with BCs contributing inhibition at the more proximal PC dendritic compartments (inner third of the ML), while SCs synapse at more distal dendritic compartments(outer two thirds of the ML) and axon initial segments (Eccles et al., 1966; Chan-Palay and Palay, 1972). In addition, electrical coupling has been characterized in MLIs, and shown to be a robust activator of inhibitory cells in the ML circuit, particularly in BCs (Sotelo and Llinás, 1972; Chu et al., 2012; Alcami and Marty, 2013). Feed-forward inhibition of PCs via MLIs, which can be activated within 1 ms, has been shown to sharply curtail PC excitation and to increase the precision of the resulting action potentials (Mittmann et al., 2005). Thus, the activation of the MLI network plays a critical role in shaping inhibition, and enabling reduced PC spike generation by asynchronous inputs.

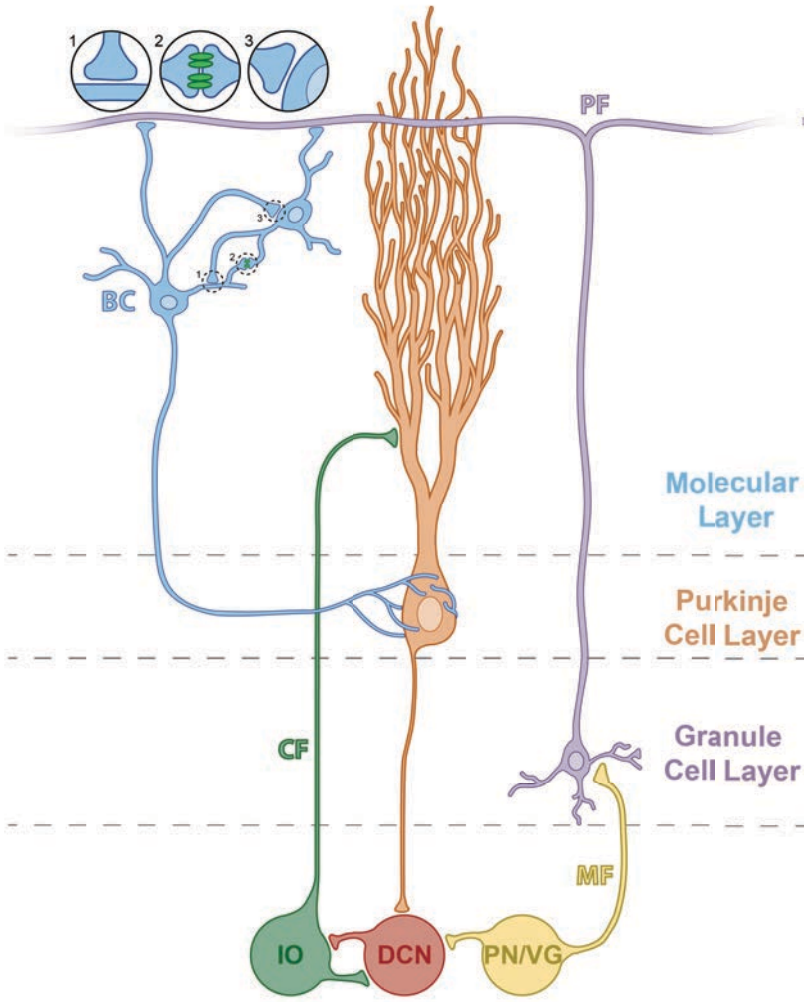

Figure A.1 Diagram of the neuronal circuitry in the cerebellar cortex. Two excitatory pathways provide glutamatergic inputs to the cerebellar cortex: the mossy fibers (MF) pathway and the climbing fibers (CF) pathway. MF originate in the brain stem and spinal cord, making glutamatergic excitatory synapses with dendrites of the granule cells (GC). The GCs relay MF inputs to Purkinje cells (PC) via the parallel fibers (PF), which form excitatory glutamatergic synapses with PC molecular layer dendrites. Purkinje cells, which provide the sole output of the cerebellar cortex, are controlled by feedforward inhibitory inputs from molecular layer interneurons (MLIs), which are divided into two classes: basket cells (BC) and stellate cells. MLIs interact at several levels synaptically (Inset **1,3**) and also display electrical coupling (Insert **2**) via gap junctions between MLIs. GABAA receptor-mediated synaptic transmission at synapses between MLIs and Purkinje cells (MLI-PC) and between MLIs (MLI-MLI) drastically shape the responsiveness of PCs to PF input.

GABAergic synapses on MLIs convey robust inhibitory synaptic currents (Llano and Gerschenfeld, 1993a). Importantly, cerebellar synaptogenesis, including GABAergic synapses, is completed postnatally, with MLIs positioned in the neural circuit by postnatal day 7 (PN-7), differentiated by PN-12, and completely developed past PN-15 (Altman, 1972). Expression of $GABA_A$Rs in the ML is developmentally regulated, with the first receptors observed at ~PN-7 that continue to develop past PN-21 (Viltono et al., 2008). Proper maturation and clustering of $GABA_A$Rs is critical for accurate signal transformations in brain circuits and several molecules underlie this process (Choii and Ko, 2015). One protein commonly localized with GABAergic synapses is gephyrin, an anchoring protein, which has been shown to be important in the maturation and stabilization of $GABA_A$Rs clusters at synapses (Choii and Ko, 2015). Throughout the brain, several studies have shown the localization of specific $GABA_A$Rs subunits to synapses, however, even the α1β2β3γ2 configuration, which is highly enriched in synapses, can be readily found outside the synaptic cleft (Nusser et al., 1998; Farrant and Nusser, 2005). Additionally, subunit selectivity also appears to contribute to different modes of inhibition. For example, $GABA_A$Rs containing γ2 subunit in association with α1, α2 or α3 subunits (α1β2/3γ2, α2β2/3γ2 and α3β2/3γ2) are the predominant receptor subtypes that mediate phasic synaptic inhibition (Farrant and Nusser, 2005), while receptors containing the α6 and δ subunits are involved in tonic subunit activation (Brickley et al., 1996; Farrant and Nusser, 2005). Another important consideration is the differential sensitivity and gating of the various $GABA_A$Rs subunits to endogenous GABA activation. For example, in $GABA_A$Rs containing α, β and γ subunits, the receptor sensitivity is strongly affected by

the type of α subunit present, with EC50 values ranking from lowest to highest; α6<α1<α2<α4<α5<<α3 (Böhme et al., 2004). Activation of these receptors with different affinities at low concentrations of GABA, particularly high affinity receptors, represents an important component for activation of tonic inhibition, as well as sensitivity to ambient GABA in extrasynaptic spaces (Farrant and Nusser, 2005). Interestingly, this form of inhibition, particularly tonic activation of inhibition in the ventral tegmental area, has been shown to be developmentally regulated, suggesting that subunit specific expression in maturing neurons could underlie this process (Ye et al., 2004). Furthermore, it has been shown that the GABAergic system is important contributor to establishing neuronal connectivity during neurodevelopment (Wang and Kriegstein, 2008).

MLI dendrites are large in diameter and exhibit GABAergic IPSCs that display limited effects of dendritic filtering when recorded at the soma (Llano and Gerschenfeld, 1993b). Thus, the MLIs provide a stable model for studying kinetics of single photon DPNI-GABA uncaging evoked IPSCs (eIPSC) along the MLI dendritic domains, in both synaptic and extrasynaptic regions. In the present work, we analyzed the development of functional GABAergic synapses on MLIs in the cerebellar cortex in the young (PN-8 to PN-12) and adult (~PN-30) mice. Our findings indicate a robust refinement of postsynaptic $GABA_A$Rs with presynaptic synapses, labeled with vesicular GABA transporter (VGAT), as the animal matures. In addition, localized activation of MLI dendrites reveals striking differences in the properties of GABA evoked inhibition; younger animals had smaller IPSC amplitude, and longer rise time (RT, 10 - 90%) and longer decay (Decay, t = 1/e). Last, the evoked IPSC

magnitude is not only determined by channel conductance and receptor number, but also by the channel open times, which are highly dependent on $GABA_A$Rs subunit composition. For this reason, we utilized an allosteric modulator specific to α1-$GABA_A$Rs, zolpidem (100 nM), to assess α1-containing $GABA_A$Rs in the young and adult in synaptic and extrasynaptic areas of MLI dendrites. eIPSCs on mature MLI dendrites displayed increased sensitivity to a α1-$GABA_A$ modulation, compared to young MLIs, suggesting a larger α1 component in the mature MLIs inhibition. These findings suggest the existence of a developmental maturation of GABAergic synapses in MLIs and that α1-$GABA_A$ synaptic refinement and activation could underlie this process.

Methods

Slice preparation

Male and female C57BL/6 mice (PN-12 to PN-36) were anesthetized with isoflurane and euthanized. The cerebellum was quickly removed and placed in oxygenated ice-cold sucrose ACSF of the following composition (in mM); 75 sucrose, 27 $NaHCO_3$, 1.25 NaH_2PO_4, 2.5 KCl, 1 $CaCl_2$ and 6 $MgCl_2$. Parasagittal sections of the cerebellar vermis were sliced using a Leica VT1200s vibratome. The slices were then placed in normal ACSF (see below) and left to recuperate for 60 min at 34°C, and then at room temperature for at

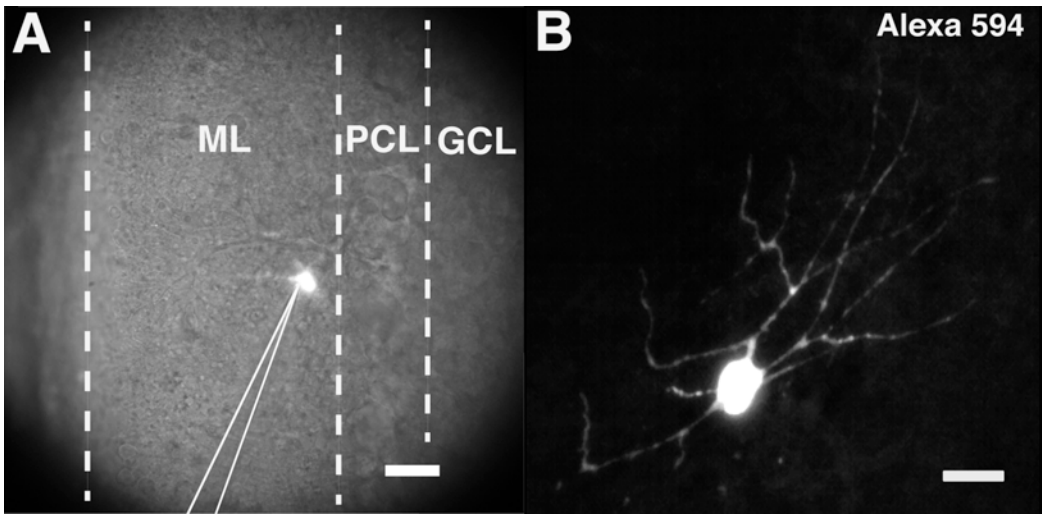

Figure A.2 In vitro brain slice preparation of the Cerebellum. A. Simultaneous bright field image of a cerebellar slice and a fluorescently labeled basket cell loaded with Alexa Fluor 594 dye (5μM) in the recording pipette. The distinct cerebellar layers are indicated by dotted lines; calibration bar is 25 μm. **B.** Confocal image of a previously recorded BC labeled with Alexa Fluor 594 dye, the calibration bar is 10 μm. Molecular Layer (ML); Purkinje cell Layer (PCL); Granule Cell Layer (GCL).

least 30 min before use. In older animals (PN > 30), 1 mM kynurenic acid was added to the slicing solution to prevent neuronal excitoxcitity. The slices were kept on normal ACSF of the following composition (in mM): 122 NaCl, 26 $NaHCO_3$, 1.25 NaH_2PO_4, 25 glucose, 2.5 KCl, 2 $CaCl_2$ and 1 $MgCl_2$,

continuously oxygenated (95% O_2 and 5% CO_2). Electrophysiological experiments were performed in a HEPES buffered extracellular solution containing (in mM): 135 NaCl, 4 KCl, 2 $NaHCO_3$, 25 Glucose, 2 $CaCl_2$ and 1 $MgCl_2$, 0.5 TTX, 10 HEPES to a pH 7.4 with 1M NaOH and 310 ± 5 mOsm/KgH_2O.

Electrophysiological recordings

The slices were placed in a submerged recording chamber mounted on a fixed-stage upright Olympus microscope. The recording chamber was continuously perfused with ACSF (~2 mL/min). Whole-cell patch-clamp recordings were performed on MLI, basket and stellate cells, visualized using a water-immersion 60x objective. Cells were recorded in voltage clamp mode using a dual EPC10 amplifier. For data analysis we used the Igor Pro and Neuromatic softwares. Recording electrodes had a final resistance of 3-7 MΩ when filled with an intracellular solution containing (in mM); 125 KCl, 1 EGTA, 10 HEPES, 4.6 MgCl2, 0.6 CaCl2, 4 Na_2ATP, 0.4 NaGTP (300 ± 10 mOsm; pH 7.3). To visualize the morphology of the recorded cell and conduct post-recording immunochemistry, the fluorescent dye Alexa 594 (20 µM) was included in the pipette. Photolysis was performed as previously described in (Trigo et al., 2009) with laser input from OBIS 405 nm LX (Coherent, USA) focused through the microscope objective (see figure A.3). Standard immunohistochemical protocols were followed for post-hoc detection of GABA-A receptors, using primary antibodies against the α1-GABA subunit (Gift from Fritschy JM, (Benke et al., 1991)) and the anti-vesicular GABA transporter (VGAT, Synaptic System). A LSM510 confocal microscope was utilized and offline image analysis was performed using the ImageJ software. Correlation

analysis of two fluorescence wavelengths was completed using a Pearson correlation coefficient ImageJ plugin, whereby the linear correlation (dependence) between two variables, i.e VGAT and GABA, is presented on a range from +1 to −1, where 1 is total positive correlation, 0 no correlation, and −1 is total negative correlation.

Results

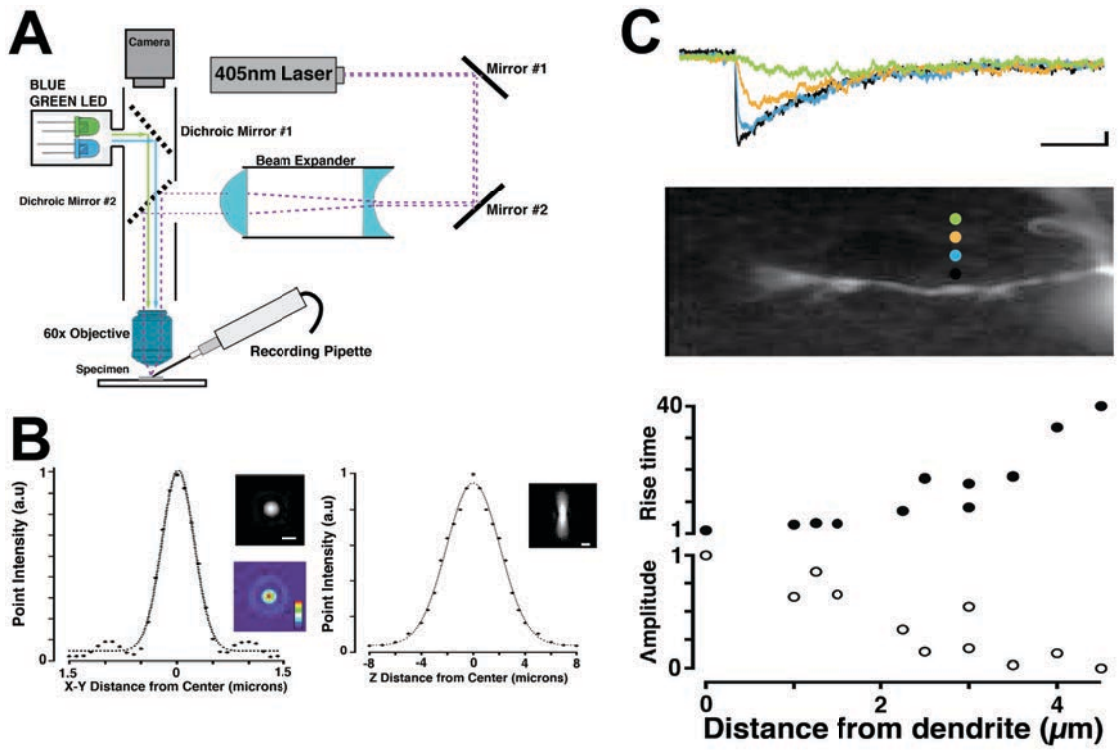

Figure A.3. Design and Calibration of the GABA Uncaging Setup
A. Experimental setup used for the GABA uncaging experiments. To visualize the recorded cell using fluorescent dyes we used LED excitation at 594 nm. Photolysis of DNPI-GABA is achieved using a 405 nm laser. The beam expander contained plano-concave (f=–25mm) and plano-convex (f=250mm) lenses to backfill the entire 60x objective. **B.** Lateral and axial resolution of the laser spot. Left, the x-y profile of light intensity is plotted and fitted with a Gaussian function (1/e^2 = 0.93 μm) at the objective's focal point. Right, top insert, reflected image of laser dot in the x-y plane, scale bar 1 μm. Bottom insert, pseudocolor intensity profile for laser dot; red indicates high intensity. Right. z-profile of light intensity fitted to a Gaussian function (1/e^2 = 8.1 μm). Right, top insert, image of laser in z plane, white indicates the highest intensity point; calibration bar 1 μm. **C.** Neuronal responses to DPNI-GABA photolysis in the lateral plane: *Top,* color coded representative current traces recorded from soma of MLI (middle panel) while laterally stepping away from original dendritic uncaging point (x=0). Scale bar is 20 pA and 60 ms. *Middle,* fluorescence image of a MLI dendrite from the experiment shown above in panel A. The black dot closest to the dendrite is the starting point (x=0); scale bar is 2 μm. *Bottom*, plot showing the normalized amplitude (open circles) and normalized rise time (closed circles) as a function of lateral displacement (x-y plane, in μm) from the dendrite (n = 3).

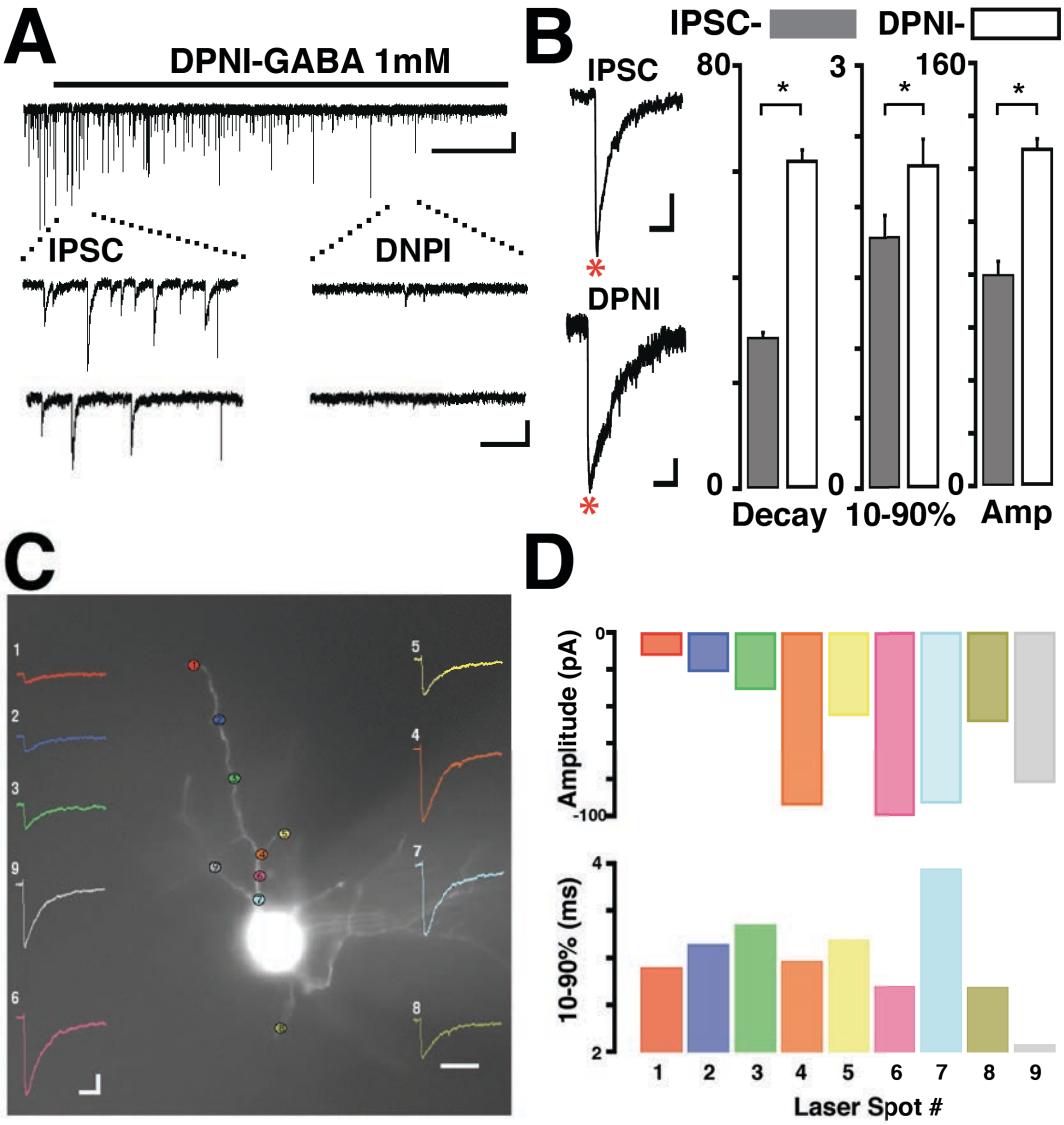

Figure A.4 Properties of GABA evoked responses with DPNI-GABA photolysis

A. Voltage clamp recording of miniature inhibitory postsynaptic currents (mIPSCs) from the MLI pictured below (Fig1c). Bath application of DPNI-GABA (1 mM) decreases the frequency and amplitude of mIPSCs. *Bottom,* expanded traces of laser evoked IPSCs (eIPSCs). *Top* calibration bar is 50 pA and 5 s. *Bottom* calibration bar is 50 pA and 0.2 s. **B.** *Left Panels*, representative IPSC in control conditions (*top trace*) and laser-evoked eIPSCs (eIPSC) (*bottom trace*); red asterisk indicates time of photolysis. Calibration bar is 20 pA and 20 s. *Right*, summary bar graphs comparing the kinetics of spontaneous IPSCs (sIPSCs) and photolysis-evoked currents. **C.** MLI filled with Alexa 594 (20 µM). Traces 1-9 show laser-evoked currents with DPNI-GABA (1 mM) at different locations in the neuron, specified by color traces and numbered dots, (average of 10 traces per spot). Left calibration bar is 50 ms and 20 pA; the right calibration bar is 10 µm. **D.** Summary bar graphs depict the rise times and amplitudes of the eIPSCs throughout the several locations shown in panel C (using the same color and number codes).

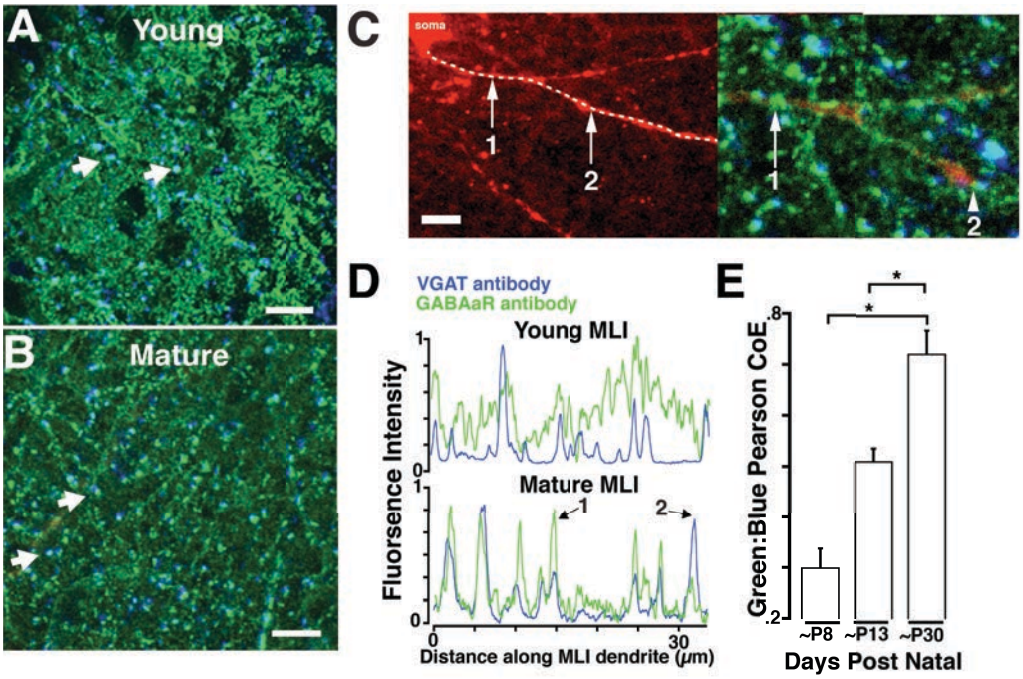

Figure A.5 Age dependent immunohistochemical staining of pre- and postsynaptic GABAergic markers. A. Confocal images of the ML (left edge correspond to the boundary of the PC layer) in young and **(B)** mature cerebellar cortex. Images show the superimposition of the vesicular GABA transporter (VGAT, Blue) and the GABA-α1 receptor subunit (Green) immunostaining. Colocalization of antibody staining (Cyan) indicates the prescence of GABAergic synapses (white arrows show representative synapses) Scale bar is 25 μM. **C.** *Left*, Confocal image of mature MLI soma and dendrite loaded with Alexa-Flour 594 (Red). White dotted line indicates ROI for fluorescence line intensity analysis shown in **(Fig 5D)**. Calibration bar is 10 μm. *Right,* confocal image showing the superimposition in the same dendrite of the Alexa 594 dye (Red), and the VGAT (Blue) and $GABA_A$-α1 receptor subunit immunostaining (Green) **D**. Top trace, intensity profile of green and blue fluorescence through the length of the dendrite in the young. Bottom trace, intensity profile of green and blue fluorescence through the length of the dendrite marked by dotted line in Fig 5C. **E**. Bar graph, colocalization analysis of VGAT and $GABA_A$-α1, presented as pearson correlation coefficient.

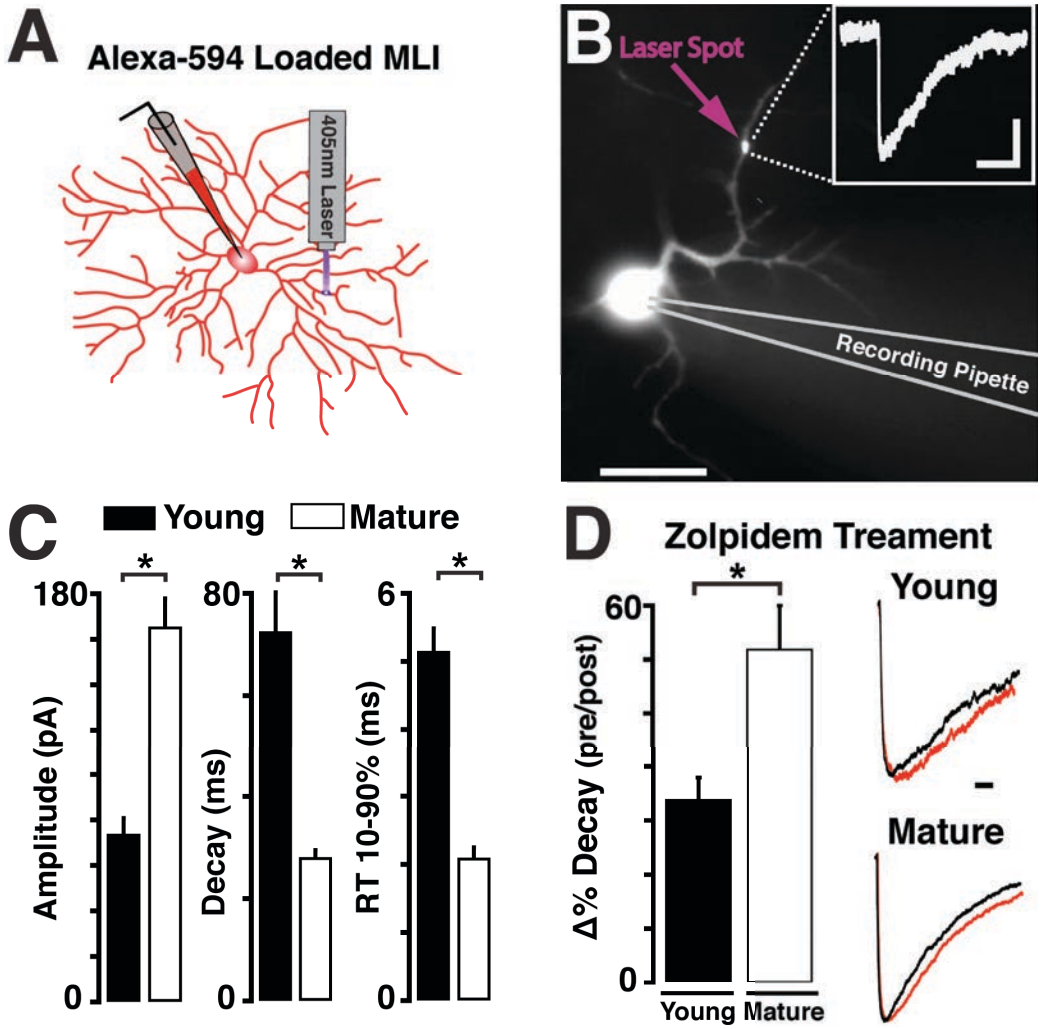

Figure A.6 eIPSCs on MLIs from young and mature ages show differential IPSC kinetics and sensitivity to zolpidem

A. Diagram showing the experimental design used for the recordings; MLI were loaded with Alexa-594 and targeted with single photon photolysis of GABA. **B.** Epifluorescence image of a BC loaded with Alexa-594, the inset shows a representative voltage-clamp trace of the eIPSC at the spot indicated by purple arrow. The calibration bar is 20 pA and 20 ms. Bottom left, calibration bar is 10 µm. **C.** Summary of the properties of the eIPSC in the young and mature MLIs. **D.** Summary of the eIPSC decay kinetics in mature and young MLIs as the percent change from pre- to post-zolpidem treatment. *Right*, eIPSC at the same synaptic location on mature and young MLIs before (black traces) and after treatment with zolpidem (red traces).

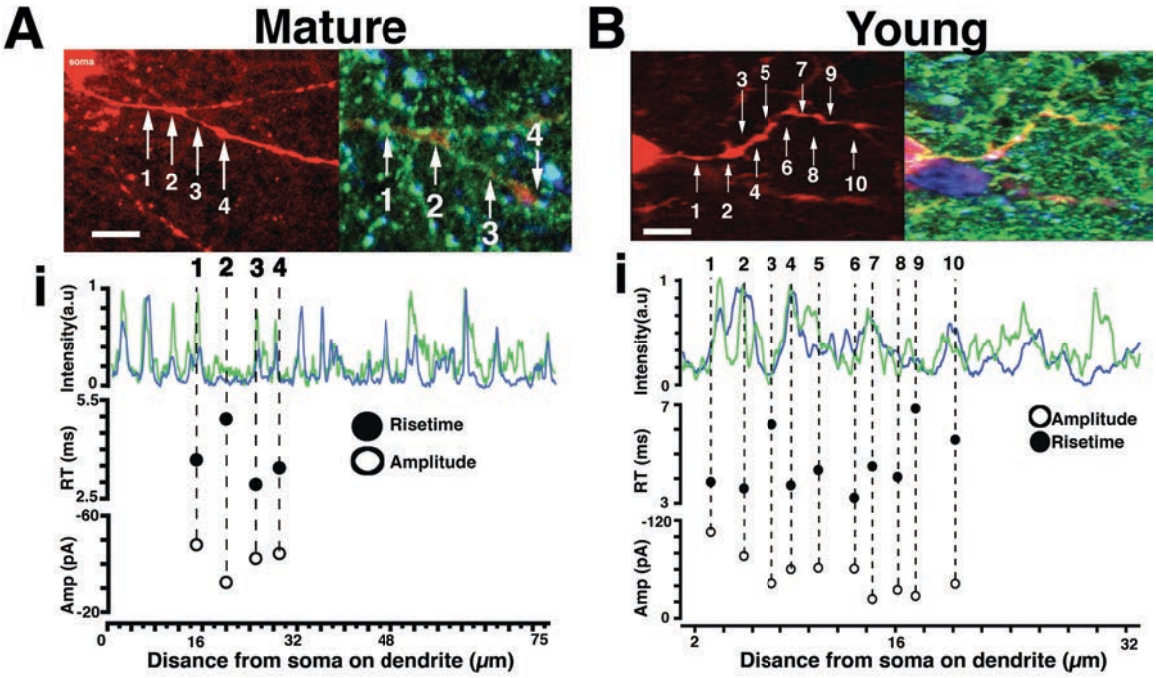

Figure A.7 Electrophysiological and immunohistochemical analysis of MLIs at young and mature ages. **A.** *Left*, confocal image of mature MLI loaded with Alexa-Flour 594 (Red). *Right*, merged confocal image of pre- and post-synaptic markers: Alexa 594 (Red), GABAA-α1subunit (Green), and VGAT (Blue). Calibration bar is 10 μm. Arrows 1-4 show locations of GABA uncaging. **Ai,** *Top*, Intensity profile of GABAA-α1 (Green) and VGAT (Blue) fluorescence signal through the length of the dendritic domain. *Middle,* rise time (RT) calculated as 10 to 90% of the amplitude of eIPSCs at locations indicated (1-4). *Bottom*, amplitude (Amp) of eIPSCs at locations indicated (1-4). **B.** *Left*, Confocal image of mature MLI loaded with Alexa-Fluor 594 (Red). *Right*, merged confocal image of the Alexa 594 dye (Red) and the pre- and post-synaptic markers:, $GABA_A$-α1 (Green), VGAT (Blue). Calibration bar is 10 μm. Arrows 1-10 show the locations of GABA uncaging. **Bi,** *Top*, Intensity profile of $GABA_A$-α1 (Green) and VGAT fluorescence signal (Blue) through the length of the dendritic domain. *Middle,* RT, of the eIPSCs at locations indicated above (1-10). *Bottom*, Amp of eIPSCs at the indicated locations (1-10).

Discussion

Modifications to MLI's electrical properties can shape PC responses and strongly affect the output of the cerebellar cortex (Chu et al., 2012). The present work reveals a developmental shift in GABAergic activation on MLIs that is likely mediated by changes in $GABA_AR$ localization and subunit composition. On MLIs, postsynaptic clustering of $GABA_ARs$ with presynaptic markers drastically increases with the age, and α1-$GABA_AR$'s show decreased expression in extrasynaptic areas in comparison to synaptic areas. In addition, targeted GABA activation of MLI dendrites indicates differences in kinetics of evoked GABA currents in young vs. mature MLIs. Thus, the eIPSCs recorded in younger animals on average have smaller amplitude, but prolonged rise time and decay, suggesting that different $GABA_AR$ subunit composition most likely underlies these different kinetics. Also, targeted $GABA_AR$ activation in synaptic and extrasynaptic domains revealed eIPSCs with markedly different kinetics; synaptic eIPSCs have faster RT and larger amplitudes, in both young and mature mice. Additionally, kinetics of eIPSCs is modulated differentially by application of zolpidem in the young vs. mature, lending further support that throughout development the MLIs rely on different $GABA_AR$ subunits.

Immunohistochemical analysis of pre- and postsynaptic markers of GABAergic synapses showed little correlation on MLIs at young ages, as α1-$GABA_ARs$ appear more homogenously distributed along MLI dendritic domains. Conversely, in MLIs at mature ages, the presynaptic and postsynaptic markers reveled a positive correlation, as $GABA_ARs$ appeared to cluster significantly with presynaptic structures and show low fluorescence signal in extrasynaptic

regions. This localization likely relies on post-synaptic gephyrin clustering within GABAergic synapses, which is developmentally regulated and provides the required subcellular anchoring to stabilize receptors within the synapse (Craig et al., 1996; Choii and Ko, 2015). Our data shows that presynaptic markers establish before the maturation of the $GABA_A$ synapse, which suggests the presynaptic release machinery may be important during GABAergic synaptogenesis. The size of presynaptic and postsynaptic markers increases with age on MLIs, which has several functional implications, such as increase in size of the active zone and total number of receptors capable of being activated.

Our results have shown that the eIPSCs evoked at synapses are larger and exhibit faster kinetics compared to currents elicited extrasynaptically. However, while the eIPSCs elicited in extrasynaptic areas are smaller and slower on average, they do produce substantial GABA currents in both young and mature MLIs. Importantly when we compare the amplitude of synaptic and extrasynaptic eIPSCs, in young MLIs, the eIPSCs in extrasynaptic areas appear more similar to synaptically targeted eIPSCs. Within extrasynaptic domains, high-affinity $GABA_A$Rs, likely containing the δ, or only α and β subunits, detect low concentrations of ambient GABA (Nusser et al., 1998; Thomas et al., 2005). These extrasynaptic receptors mediate tonic inhibition and show slower rise times compared to IPSCs elsewhere (For Review Farrant and Nusser; 2005). These studies fit well with our results, as rise-times in extrasynaptic spaces show significantly slower activation times in both young and mature MLIs. Nevertheless, as GABAergic activation is an important contributor to establishing neuronal connectivity, these functional

extrasynaptic $GABA_AR$ receptors could play an important role in shaping this process (Wang and Kriegstein, 2008).

Several questions remain regarding the functional role of $GABA_ARs$ throughout development, particularly how subunit specific activation contributes to circuit output at different developmental stages. Our results indicate that modulation of the α1-$GABA_ARs$ is capable of prolonging eIPSCs in both young and mature MLIs, but it does it to a much larger degree in mature MLIs. Our antibody studies reveled basal levels of extrasynaptic α1-$GABA_ARs$ receptors in young MLIs and photolysis experiments show that $GABA_AR$ are functional, suggesting a role for extrasynaptic $GABA_AR$ activation on the physiology of the circuit, particularly in the young MLIs. These analysis could be improved by splitting the zolpidem treated eIPSCs into synaptic vs. extrasynaptic data sets, demonstrating functional contributions of α1-$GABA_ARs$ to extra- vs. synaptic synapses.

In addition, $GABA_AR$ plasticity mechanisms at these developmental time points remains to be studied. Several mechanisms of $GABA_AR$ plasticity has been proposed, including changes in the phosphorylation state of gephyrin clusters, which can alter cluster size and density, leading to changes in GABAergic synaptic transmission (Tyagarajan et al., 2011). Furthermore, the developmental changes of IPSC kinetics also does not depend entirely on subunit composition (Koksma et al., 2005; Peden et al., 2008). As such, post-translational changes in $GABA_AR$ gating, subcellular protein interactions, and recycling of receptors may play an important role in modulating MLIs GABA activation at different developmental points. To this extent, we conducted

preliminary experiments of $GABA_AR$ dynamics using the small inhibitory peptide dynamin in the recording pipette, which reduces $GABA_AR$ internalization. These experiments showed no effect on plasticity of eIPSCs over an extended duration (~30 min) in the adult MLIs, both synaptic and extrasynaptic (data not shown). Additional experiments to evaluate $GABA_AR$ plasticity in the young MLIs should be completed, both within and at extrasynaptic sites.

References

Airan RD, Thompson KR, Fenno LE, Bernstein H, Deisseroth K (2009) Temporally precise in vivo control of intracellular signalling. Nature 458:1025–1029 Available at: http://www.ncbi.nlm.nih.gov/pubmed/19295515

Albuquerque EX, Pereira EFR, Alkondon M, Rogers SW (2009) Mammalian Nicotinic Acetylcholine Receptors: From Structure to Function. Physiol Rev 89:73–120 Available at: <Go to ISI>://WOS:000262247600003.

Alves J, Petrosyan A, Magalhães R (2014) Olfactory dysfunction in dementia. World J Clin cases 2:661–667 Available at: http://www.pubmedcentral.nih.gov/articlerender.fcgi?artid=4233420&tool=pmcentrez&rendertype=abstract

Araneda RC, Kini AD, Firestein S (2000) The molecular receptive range of an odorant receptor. Nat Neurosci 3:1248–1255 Available at: http://www.ncbi.nlm.nih.gov/pubmed/11100145

Araneda RC, Peterlin Z, Zhang X, Chesler A, Firestein S (2004) A pharmacological profile of the aldehyde receptor repertoire in rat olfactory epithelium. J Physiol 555:743–756 Available at: http://www.pubmedcentral.nih.gov/articlerender.fcgi?artid=1664868&tool=pmcentrez&rendertype=abstract

Arevian AC, Kapoor V, Urban NN (2008) Activity-dependent gating of lateral inhibition in the mouse olfactory bulb. Nat Neurosci 11:80–87 Available at: http://www.pubmedcentral.nih.gov/articlerender.fcgi?artid=2720685&tool=pmcentrez&rendertype=abstract.

Armbruster BN, Li X, Pausch MH, Herlitze S, Roth BL (2007) Evolving the lock to fit the key to create a family of G protein-coupled receptors potently activated by an inert ligand. Proc Natl Acad Sci U S A 104:5163–5168 Available at: http://www.ncbi.nlm.nih.gov/pubmed/17360345

Balu R, Pressler RT, Strowbridge BW (2007) Multiple modes of synaptic excitation of olfactory bulb granule cells. J Neurosci 27:5621–5632 Available at: http://www.ncbi.nlm.nih.gov/pubmed/17522307.

Baum MJ, Cherry JA (2014) Processing by the main olfactory system of chemosignals that facilitate mammalian reproduction. Horm Behav Available at: http://www.ncbi.nlm.nih.gov/pubmed/24929017.

Bevins RA, Besheer J (2006) Object recognition in rats and mice: a one-trial non-matching-to-sample learning task to study "recognition memory". Nat Protoc 1:1306–1311 Available at: http://www.ncbi.nlm.nih.gov/pubmed/17406415

Bloom FE, Costa E, Salmoiraghi GC (1964) Analysis Of Individual Rabbit Olfactory Bulb Neuron Responses To Microelectrophoresis Of Acetylcholine Norepinephrine + Serotonin Synergists + Antagonists. J Pharmacol Exp Ther 146:16 – & Available at: http://www.ncbi.nlm.nih.gov/pubmed/14221220.

Boyd AM, Kato HK, Komiyama T, Isaacson JS (2015) Broadcasting of cortical activity to the olfactory bulb. Cell Rep 10:1032–1039 Available at: http://www.ncbi.nlm.nih.gov/pubmed/25704808

Brennan P, Keverne EB (2015) Biological complexity and adaptability of simple mammalian olfactory memory systems. Neurosci Biobehav Rev 50:29–40 Available at: http://www.ncbi.nlm.nih.gov/pubmed/25451762

Brennan PA (2009) VOMERONASAL PROCESSING AND PHEROMONAL LEARNING IN MICE. J Physiol Sci 59:32 Available at: <Go to ISI>://WOS:000271023100112.

Brennan PA, Kendrick KM (2006) Mammalian social odours: attraction and individual recognition. Philos Trans R Soc Lond B Biol Sci 361:2061–2078 Available at: http://www.ncbi.nlm.nih.gov/pubmed/17118924

Brennan PA, Keverne EB (1997) Neural mechanisms of mammalian olfactory learning. Prog Neurobiol 51:457–481 Available at: http://www.ncbi.nlm.nih.gov/pubmed/9106902.

Brennan PA, Peele P (2003) Towards an understanding of the pregnancy-blocking urinary chemosignals of mice. Biochem Soc Trans 31:152–155 Available at: http://www.ncbi.nlm.nih.gov/entrez/query.fcgi?cmd=Retrieve&db=PubMed&dopt=Citation&list_uids=12546674.

Brennan PA, Schellinck HM, de la Riva C, Kendrick KM, Keverne EB (1998) Changes in neurotransmitter release in the main olfactory bulb following an olfactory conditioning procedure in mice. Neuroscience 87:583–590 Available at: http://www.ncbi.nlm.nih.gov/entrez/query.fcgi?cmd=Retrieve&db=PubMed&dopt=Citation&list_uids=9758225.

Brennan PA, Zufall F (2006) Pheromonal communication in vertebrates. Nature 444:308–315 Available at: http://www.ncbi.nlm.nih.gov/pubmed/17108955

Breton-Provencher V, Lemasson M, Peralta III MR, Saghatelyan A (2009) Interneurons Produced in Adulthood Are Required for the Normal Functioning of the Olfactory Bulb Network and for the Execution of Selected Olfactory Behaviors. J Neurosci 29:15245–15257 Available at: <Go to ISI>://WOS:000272361700025.

Buck L, Axel R (1991) A Novel Multigene Family May Encode Odorant Receptors - A Molecular-Basis For Odor Recognition. Cell 65:175–187 Available at: <Go to ISI>://A1991FF77300019.

Buckley NJ, Bonner TI, Brann MR (1988) LOCALIZATION OF A FAMILY OF MUSCARINIC RECEPTOR MESSENGER-RNAS IN RAT-BRAIN. J Neurosci 8:4646–4652 Available at: <Go to ISI>://WOS:A1988R501300023.

Carey RM, Sherwood WE, Shipley MT, Borisyuk A, Wachowiak M (2015) Role of intraglomerular circuits in shaping temporally structured responses to naturalistic inhalation-driven sensory input to the olfactory bulb. J Neurophysiol 113:3112–3129 Available at: http://www.ncbi.nlm.nih.gov/pubmed/25717156

Castillo PE, Carleton A, Vincent JD, Lledo PM (1999) Multiple and opposing roles of cholinergic transmission in the main olfactory bulb. J Neurosci 19:9180–9191 Available at: http://www.ncbi.nlm.nih.gov/pubmed/10531421.

Chamero P, Marton TF, Logan DW, Flanagan K, Cruz JR, Saghatelian A, Cravatt BF, Stowers L (2007) Identification of protein pheromones that promote aggressive behaviour. Nature 450:899–902 Available at: http://www.ncbi.nlm.nih.gov/pubmed/18064011

Chance FS, Abbott LF, Reyes AD (2002) Gain modulation from background synaptic input. Neuron 35:773–782 Available at: http://www.ncbi.nlm.nih.gov/pubmed/12194875.

Chapuis J, Wilson DA (2013) Cholinergic modulation of olfactory pattern separation. Neurosci Lett 545:50–53 Available at: http://www.ncbi.nlm.nih.gov/pubmed/23624024.

Chaudhury D, Escanilla O, Linster C (2009) Bulbar acetylcholine enhances neural and perceptual odor discrimination. J Neurosci 29:52–60 Available at: http://www.ncbi.nlm.nih.gov/pubmed/19129384.

Clancy AN, Coquelin A, Macrides F, Gorski RA, Noble EP (1984) Sexual behavior and aggression in male mice: involvement of the vomeronasal system. J Neurosci 4:2222–2229 Available at: http://www.ncbi.nlm.nih.gov/pubmed/6541245

Cleland TA, Linster C (2005) Computation in the olfactory system. Chem Senses 30:801–813 Available at: <Go to ISI>://WOS:000233415400009.

Constanti A, Bagetta G, Libri V (1993) PERSISTENT MUSCARINIC EXCITATION IN GUINEA-PIG OLFACTORY CORTEX NEURONS - INVOLVEMENT OF A SLOW POSTSTIMULUS AFTER DEPOLARIZING CURRENT. Neuroscience 56:887–904 Available at: <Go to ISI>://WOS:A1993MB76600009.

Cooper-Kuhn CM, Winkler J, Kuhn HG (2004) Decreased neurogenesis after cholinergic forebrain lesion in the adult rat. J Neurosci Res 77:155–165 Available at: http://www.ncbi.nlm.nih.gov/entrez/query.fcgi?cmd=Retrieve&db=PubMed&dopt=Citation&list_uids=15211583.

Cury KM, Uchida N (2010) Robust Odor Coding via Inhalation-Coupled Transient Activity in the Mammalian Olfactory Bulb. Neuron 68:570–585 Available at: <Go to ISI>://WOS:000284255800022.

D'Souza RD, Parsa P V, Vijayaraghavan S (2013) Nicotinic receptors modulate olfactory bulb external tufted cells via an excitation-dependent inhibitory mechanism. J Neurophysiol 110:1544–1553 Available at: http://www.ncbi.nlm.nih.gov/pubmed/23843430

D'Souza RD, Vijayaraghavan S (2012) Nicotinic receptor-mediated filtering of mitral cell responses to olfactory nerve inputs involves the alpha3beta4 subtype. J Neurosci 32:3261–3266 Available at: http://www.ncbi.nlm.nih.gov/pubmed/22378897.

D'Souza RD, Vijayaraghavan S (2014) Paying attention to smell: cholinergic signaling in the olfactory bulb. Front Synaptic Neurosci 6:21 Available at: http://www.ncbi.nlm.nih.gov/pubmed/25309421

Davison IG, Ehlers MD (2011) Neural Circuit Mechanisms for Pattern Detection and Feature Combination in Olfactory Cortex. Neuron 70:82–94 Available at: http://www.ncbi.nlm.nih.gov/pubmed/21482358.

Davison IG, Katz LC (2007) Sparse and selective odor coding by mitral/tufted neurons in the main olfactory bulb. J Neurosci 27:2091–2101 Available at: <Go to ISI>://WOS:000244381400029.

De Olmos J, Hardy H, Heimer L (1978) The afferent connections of the main and the accessory olfactory bulb formations in the rat: an experimental HRP-study. J Comp Neurol 181:213–244 Available at: http://www.ncbi.nlm.nih.gov/pubmed/690266

Descarries L, Gisiger V, Steriade M (1997) Diffuse transmission by acetylcholine in the CNS. Prog Neurobiol 53:603–625 Available at: http://www.ncbi.nlm.nih.gov/pubmed/9421837

Devore S, de Almeida L, Linster C (2014) Distinct roles of bulbar muscarinic and nicotinic receptors in olfactory discrimination learning. J Neurosci 34:11244–11260 Available at: http://www.ncbi.nlm.nih.gov/pubmed/25143606.

Devore S, Linster C (2012) Noradrenergic and cholinergic modulation of olfactory bulb sensory processing. Front Behav Neurosci 6 Available at: <Go to ISI>://WOS:000308428400001.

Dhawale AK, Hagiwara A, Bhalla US, Murthy VN, Albeanu DF (2010) Non-redundant odor coding by sister mitral cells revealed by light addressable glomeruli in the mouse. Nat Neurosci 13:1404–U183 Available at: <Go to ISI>://WOS:000283658200022.

Dietz SB, Murthy VN (2005) Contrasting short-term plasticity at two sides of the mitral-granule reciprocal synapse in the mammalian olfactory bulb. J Physiol 569:475–488 Available at: http://www.pubmedcentral.nih.gov/articlerender.fcgi?artid=1464232&tool=pmcentrez&rendertype=abstract

Disney AA, Aoki C, Hawken MJ (2007) Gain modulation by nicotine in macaque V1. Neuron 56:701–713 Available at: <Go to ISI>://WOS:000251306600012.

Do Monte FHM, Canteras NS, Fernandes D, Assreuy J, Carobrez AP (2008) New perspectives on beta-adrenergic mediation of innate and learned fear responses to predator odor. J Neurosci 28:13296–13302 Available at: http://www.ncbi.nlm.nih.gov/pubmed/19052221

Doty RL, Bagla R, Kim N (1999) Physostigmine enhances performance on an odor mixture discrimination test. Physiol Behav 65:801–804 Available at: http://www.ncbi.nlm.nih.gov/pubmed/10073483.

Doucette W, Gire DH, Whitesell J, Carmean V, Lucero MT, Restrepo D (2011) Associative cortex features in the first olfactory brain relay station. Neuron 69:1176–1187 Available at: http://www.ncbi.nlm.nih.gov/pubmed/21435561.

Dulac C, Wagner S (2006) Genetic analysis of brain circuits underlying pheromone signaling. Annu Rev Genet 40:449–467 Available at: http://www.ncbi.nlm.nih.gov/pubmed/16953793.

Durand M, Coronas V, Jourdan F, Quirion R (1998) Developmental and aging aspects of the cholinergic innervation of the olfactory bulb. Int J Dev Neurosci 16:777–785 Available at: http://www.ncbi.nlm.nih.gov/pubmed/10198824

Egorov A V, Hamam BN, Fransen E, Hasselmo ME, Alonso AA (2002) Graded persistent activity in entorhinal cortex neurons. Nature 420:173–178 Available at: <Go to ISI>://WOS:000179200900045.

Egorov A V, Unsicker K, von Bohlen und Halbach O (2006) Muscarinic control of graded persistent activity in lateral amygdala neurons. Eur J Neurosci 24:3183–3194 Available at: <Go to ISI>://WOS:000243361700022.

Elaagouby A, Gervais R (1992) ACH-INDUCED LONG-LASTING ENHANCEMENT IN EXCITABILITY OF THE OLFACTORY-BULB. Neuroreport 3:10–12 Available at: <Go to ISI>://WOS:A1992HC65900002.

Elaagouby A, Ravel N, Gervais R (1991) Cholinergic Modulation Of Excitability In The Rat Olfactory-Bulb - Effect Of Local Application Of Cholinergic Agents On Evoked Field Potentials. Neuroscience 45:653–662 Available at: <Go to ISI>://A1991GR44900013.

Ennis M, Hamilton K, Hayar A (2007) Neurochemistry of the Main Olfactory System. In: Handbook of Neurochemistry and Molecular Neurobiology, pp 137–204. Springer US. Available at: http://link.springer.com/referenceworkentry/10.1007%2F978-0-387-30374-1_6?LI=true.

Fan S, Luo M (2009) The organization of feedback projections in a pathway important for processing pheromonal signals. Neuroscience 161:489–500 Available at: http://www.sciencedirect.com/science/article/pii/S0306452209004928

Fisahn A, Pike FG, Buhl EH, Paulsen O (1998) Cholinergic induction of network oscillations at 40 Hz in the hippocampus in vitro. Nature 394:186–189 Available at: <Go to ISI>://000074705900055.

Fletcher ML, Chen WR (2010) Neural correlates of olfactory learning: Critical role of centrifugal neuromodulation. Learn Mem 17:561–570 Available at: <Go to ISI>://000283716500002.

Fournier GN, Semba K, Rasmusson DD (2004) Modality- and region-specific acetylcholine release in the rat neocortex. Neuroscience 126:257–262 Available at: http://www.ncbi.nlm.nih.gov/pubmed/15207343.

Freeman WJ, Schneider W (1982) Changes in spatial patterns of rabbit olfactory EEG with conditioning to odors. Psychophysiology 19:44–56 Available at: http://www.ncbi.nlm.nih.gov/pubmed/7058239

Fucile S (2004) Ca2+ permeability of nicotinic acetylcholine receptors. Cell Calcium 35:1–8 Available at: http://www.sciencedirect.com/science/article/pii/S0143416003001854

Galan RF, Ermentrout GB, Urban NN (2008) Optimal time scale for spike-time reliability: theory, simulations, and experiments. J Neurophysiol 99:277–283 Available at: http://www.ncbi.nlm.nih.gov/pubmed/17928562.

Gao Y, Strowbridge BW (2009) Long-term plasticity of excitatory inputs to granule cells in the rat olfactory bulb. Nat Neurosci 12:731–733 Available at: <Go to ISI>://WOS:000266380900016.

Gautam D, Heard TS, Cui Y, Miller G, Bloodworth L, Wess J (2004) Cholinergic stimulation of salivary secretion studied with M1 and M3 muscarinic receptor single- and double-knockout mice. Mol Pharmacol 66:260–267 Available at: http://www.ncbi.nlm.nih.gov/pubmed/15266016.

Gelperin A, Ghatpande A (2009) Neural basis of olfactory perception. Ann N Y Acad Sci 1170:277–285 Available at: http://www.ncbi.nlm.nih.gov/pubmed/19686148.

Ghatpande AS, Sivaraaman K, Vijayaraghavan S (2006) Store calcium mediates cholinergic effects on mIPSCs in the rat main olfactory bulb. J Neurophysiol 95:1345–1355 Available at: http://www.ncbi.nlm.nih.gov/pubmed/16319214.

Ghosh S, Larson SD, Hefzi H, Marnoy Z, Cutforth T, Dokka K, Baldwin KK (2011) Sensory maps in the olfactory cortex defined by long-range viral tracing of single neurons. Nature 472:217–220 Available at: http://dx.doi.org/10.1038/nature09945

Gil Z, Connors BW, Amitai Y (1997) Differential regulation of neocortical synapses by neuromodulators and activity. Neuron 19:679–686 Available at: http://www.ncbi.nlm.nih.gov/pubmed/9331357

Gire DH, Franks KM, Zak JD, Tanaka KF, Whitesell JD, Mulligan AA, Hen R, Schoppa NE (2012) Mitral cells in the olfactory bulb are mainly excited through a multistep signaling path. J Neurosci 32:2964–2975 Available at: http://www.ncbi.nlm.nih.gov/pubmed/22378870.

Gire DH, Restrepo D, Sejnowski TJ, Greer C, De Carlos JA, Lopez-Mascaraque L (2013) Temporal processing in the olfactory system: can we see a smell? Neuron 78:416–432 Available at: http://www.ncbi.nlm.nih.gov/pubmed/23664611

Goard M, Dan Y (2009) Basal forebrain activation enhances cortical coding of natural scenes. Nat Neurosci 12:1444–1449 Available at: http://www.ncbi.nlm.nih.gov/pubmed/19801988.

Gotti C, Moretti M, Gaimarri A, Zanardi A, Clementi F, Zoli M (2007) Heterogeneity and complexity of native brain nicotinic receptors. Biochem Pharmacol 74:1102–1111 Available at: <Go to ISI>://WOS:000250188900003.

Gotti C, Zoli M, Clementi F (2006) Brain nicotinic acetylcholine receptors: native subtypes and their relevance. Trends Pharmacol Sci 27:482–491 Available at: <Go to ISI>://WOS:000240611100006.

Haberly LB (1985) Neuronal circuitry in olfactory cortex: anatomy and functional implications. Chem Senses 10:219–238 Available at: http://chemse.oxfordjournals.org/content/10/2/219.abstract

Haberly LB (2001) Parallel-distributed processing in olfactory cortex: new insights from morphological and physiological analysis of neuronal circuitry. Chem Senses 26:551–576 Available at: http://www.ncbi.nlm.nih.gov/pubmed/11418502

Haddad R, Lanjuin A, Madisen L, Zeng H, Murthy VN, Uchida N (2013) Olfactory cortical neurons read out a relative time code in the olfactory bulb. Nat Neurosci 16:949–957 Available at: http://www.ncbi.nlm.nih.gov/pubmed/23685720.

Haga S, Hattori T, Sato T, Sato K, Matsuda S, Kobayakawa R, Sakano H, Yoshihara Y, Kikusui T, Touhara K (2010) The male mouse pheromone ESP1 enhances female sexual receptive behaviour through a specific vomeronasal receptor. Nature 466:118–122 Available at: http://www.ncbi.nlm.nih.gov/pubmed/20596023

Haga-Yamanaka S, Ma L, He J, Qiu Q, Lavis LD, Looger LL, Yu CR (2014) Integrated action of pheromone signals in promoting courtship behavior in male mice. Elife 3:e03025 Available at: http://www.ncbi.nlm.nih.gov/pubmed/25073926 [

Haj-Dahmane S, Andrade R (1999) Muscarinic receptors regulate two different calcium-dependent non-selective cation currents in rat prefrontal cortex. Eur J Neurosci 11:1973–1980 Available at: <Go to ISI>://WOS:000080720600015.

HajDahmane S, Andrade R (1996) Muscarinic activation of a voltage-dependent cation nonselective current in rat association cortex. J Neurosci 16:3848–3861 Available at: <Go to ISI>://WOS:A1996UP38300007.

Halasz N, Shepherd GM (1983) Neurochemistry of the vertebrate olfactory bulb. Neuroscience 10:579–619 Available at: http://www.ncbi.nlm.nih.gov/entrez/query.fcgi?cmd=Retrieve&db=PubMed&dopt=Citation&list_uids=6196683.

Halpern M, Martinez-Marcos A (2003) Structure and function of the vomeronasal system: an update. Prog Neurobiol 70:245–318 Available at: http://www.ncbi.nlm.nih.gov/entrez/query.fcgi?cmd=Retrieve&db=PubMed&dopt=Citation&list_uids=12951145.

Hammen GF, Turaga D, Holy TE, Meeks JP (2014) Functional organization of glomerular maps in the mouse accessory olfactory bulb. Nat Neurosci 17:953–961 Available at: http://www.ncbi.nlm.nih.gov/pubmed/24880215.

Hardy A, Palouzier-Paulignan B, Duchamp A, Royet J-P, Duchamp-Viret P (2005) 5-Hydroxytryptamine action in the rat olfactory bulb: in vitro electrophysiological patch-clamp recordings of juxtaglomerular and mitral cells. Neuroscience 131:717–731 Available at: http://www.sciencedirect.com/science/article/pii/S0306452204010188

Hasselmo ME, Sarter M (2011) Modes and Models of Forebrain Cholinergic Neuromodulation of Cognition. Neuropsychopharmacology 36:52–73 Available at: <Go to ISI>://WOS:000284877300004.

Hawkes CH, Shephard BC, Daniel SE (1999) Is Parkinson's disease a primary olfactory disorder? QJM 92:473–480 Available at: http://www.ncbi.nlm.nih.gov/pubmed/10627864

Hellier JL, Arevalo NL, Smith L, Xiong K-N, Restrepo D (2012) alpha 7-Nicotinic Acetylcholine Receptor: Role in Early Odor Learning Preference in Mice. PLoS One 7 Available at: www.ncbi.nlm.nih.gov/pubmed/22514723.

Hendrickson RC, Krauthamer S, Essenberg JM, Holy TE (2008) Inhibition Shapes Sex Selectivity in the Mouse Accessory Olfactory Bulb. J Neurosci 28:12523–12534 Available at: <Go to ISI>://WOS:000261191000037.

Herzog CD, Nowak KA, Sarter M, Bruno JP (2003) Microdialysis without acetylcholinesterase inhibition reveals an age-related attenuation in stimulated cortical acetylcholine release. Neurobiol Aging 24:861–863 Available at: http://www.ncbi.nlm.nih.gov/pubmed/12927768

Hill JA, Zoli M, Bourgeois JP, Changeux JP (1993) IMMUNOCYTOCHEMICAL LOCALIZATION OF A NEURONAL NICOTINIC RECEPTOR - THE BETA-2-SUBUNIT. J Neurosci 13:1551–1568 Available at: <Go to ISI>://WOS:A1993KV71100020.

Hnasko TS, Edwards RH (2012) Neurotransmitter Corelease: Mechanism and Physiological Role. Annu Rev Physiol 74:225–243 Available at: http://www.pubmedcentral.nih.gov/articlerender.fcgi?artid=4090038&tool=pmcentrez&rendertype=abstract

Hogg RC, Raggenbass M, Bertrand D (2003) Nicotinic acetylcholine receptors: from structure to brain function. Rev Physiol Biochem Pharmacol Vol 147 2003 147:1–46 Available at: <Go to ISI>://WOS:000185285700001.

Huo Y, Fang Q, Shi Y-L, Zhang Y-H, Zhang J-X (2014) Chronic exposure to a predator or its scent does not inhibit male-male competition in male mice lacking brain serotonin. Front Behav Neurosci 8:116 Available at: http://www.pubmedcentral.nih.gov/articlerender.fcgi?artid=3986541&tool=pmcentrez&rendertype=abstract

Ichikawa T, Hirata Y (1986) Organization of choline acetyltransferase-containing structures in the forebrain of the rat. J Neurosci 6:281–292 Available at: http://www.ncbi.nlm.nih.gov/pubmed/3944622

Igarashi KM, Ieki N, An M, Yamaguchi Y, Nagayama S, Kobayakawa K, Kobayakawa R, Tanifuji M, Sakano H, Chen WR, Mori K (2012) Parallel mitral and tufted cell pathways route distinct odor information to different targets in the olfactory cortex. J Neurosci 32:7970–7985 Available at: http://www.pubmedcentral.nih.gov/articlerender.fcgi?artid=3636718&tool=pmcentrez&rendertype=abstract

Illig KR, Haberly LB (2003) Odor-evoked activity is spatially distributed in piriform cortex. J Comp Neurol 457:361–373 Available at: http://www.ncbi.nlm.nih.gov/pubmed/12561076

Imai T, Sakano H, Vosshall LB (2010) Topographic mapping--the olfactory system. Cold Spring Harb Perspect Biol 2:a001776 Available at: http://www.pubmedcentral.nih.gov/articlerender.fcgi?artid=2908763&tool=pmcentrez&rendertype=abstract

Isaacson JS, Strowbridge BW (1998) Olfactory reciprocal synapses: dendritic signaling in the CNS. Neuron 20:749–761 Available at: http://www.ncbi.nlm.nih.gov/entrez/query.fcgi?cmd=Retrieve&db=PubMed&dopt=Citation&list_uids=9581766.

Jia C, Halpern M (1996) Subclasses of vomeronasal receptor neurons: differential expression of G proteins (Giα2 and Goα) and segregated projections to the accessory olfactory bulb. Brain Res 719:117–128 Available at: http://www.sciencedirect.com/science/article/pii/0006899396001102

Kaneko N, Okano H, Sawamoto K (2006) Role of the cholinergic system in regulating survival of newborn neurons in the adult mouse dentate gyrus and olfactory bulb. Genes Cells 11:1145–1159 Available at: http://www.ncbi.nlm.nih.gov/entrez/query.fcgi?cmd=Retrieve&db=PubMed&dopt=Citation&list_uids=16999735.

Kasa P, Hlavati I, Dobo E, Wolff A, Joo F, Wolff JR (1995) Synaptic and non-synaptic cholinergic innervation of the various types of neurons in the main olfactory bulb of adult rat: immunocytochemistry of choline acetyltransferase. Neuroscience 67:667–677 Available at: http://www.ncbi.nlm.nih.gov/entrez/query.fcgi?cmd=Retrieve&db=PubMed&dopt=Citation&list_uids=7675193.

Kaupp UB (2010) Olfactory signalling in vertebrates and insects: differences and commonalities. Nat Rev Neurosci 11:188–200 Available at: http://dx.doi.org/10.1038/nrn2789

Kay LM, Laurent G (1999) Odor- and context-dependent modulation of mitral cell activity in behaving rats. Nat Neurosci 2:1003–1009 Available at: <Go to ISI>://WOS:000083883300018.

Kay LM, Sherman SM (2007) An argument for an olfactory thalamus. Trends Neurosci 30:47–53 Available at: http://www.ncbi.nlm.nih.gov/pubmed/17161473.

Kay LM, Stopfer M (2006) Information processing in the olfactory systems of insects and vertebrates. Semin Cell Dev Biol 17:433–442 Available at: http://www.sciencedirect.com/science/article/pii/S1084952106000437

Keiger CJH, Walker JC (2000) Individual variation in the expression profiles of nicotinic receptors in the olfactory bulb and trigeminal ganglion and identification of alpha 2, alpha 6, alpha 9, and beta 3 transcripts. Biochem Pharmacol 59:233–240 Available at: <Go to ISI>://WOS:000084267300003.

Keller M, Baum MJ, Brock O, Brennan PA, Bakker J (2009) The main and the accessory olfactory systems interact in the control of mate recognition and sexual behavior. Behav Brain Res 200:268–276 Available at: http://www.ncbi.nlm.nih.gov/pubmed/19374011.

Keller M, Douhard Q, Baum MJ, Bakker J (2006) Destruction of the main olfactory epithelium reduces female sexual behavior and olfactory investigation in female mice. Chem Senses 31:315–323 Available at: http://www.pubmedcentral.nih.gov/articlerender.fcgi?artid=2263131&tool=pmcentrez&rendertype=abstract

Kilgard MP, Merzenich MM (1998) Cortical map reorganization enabled by nucleus basalis activity. Science (80-) 279:1714–1718 Available at: <Go to ISI>://000072490000054.

Kimchi T, Xu J, Dulac C (2007) A functional circuit underlying male sexual behaviour in the female mouse brain. Nature 448:1009–1014 Available at: http://dx.doi.org/10.1038/nature06089

Kirkwood A, Rozas C, Kirkwood J, Perez F, Bear MF (1999) Modulation of long-term synaptic depression in visual cortex by acetylcholine and norepinephrine. J Neurosci 19:1599–1609 Available at: http://www.ncbi.nlm.nih.gov/pubmed/10024347

Kiselycznyk CL, Zhang S, Linster C (2006) Role of centrifugal projections to the olfactory bulb in olfactory processing. Learn Mem 13:575–579 Available at: http://learnmem.cshlp.org/content/13/5/575.long

Koolhaas JM, Coppens CM, de Boer SF, Buwalda B, Meerlo P, Timmermans PJ (2013) The resident-intruder paradigm: a standardized test for aggression, violence and social stress. J Vis Exp:e4367 Available at: http://www.ncbi.nlm.nih.gov/pubmed/23852258.

Kornecook TJ, Kippin TE, Pinel JP (1999) Basal forebrain damage and object-recognition in rats. Behav Brain Res 98:67–76 Available at: http://www.ncbi.nlm.nih.gov/pubmed/10210523

Korzan WJ, Freamat M, Johnson AG, Cherry JA, Baum MJ (2013) Either main or accessory olfactory system signaling can mediate the rewarding effects of estrous female chemosignals in sexually naive male mice. Behav Neurosci 127:755–762 Available at: http://www.ncbi.nlm.nih.gov/pubmed/23978150.

Krnjevic K, Pumain R, Renaud L (1971) MECHANISM OF EXCITATION BY ACETYLCHOLINE IN CEREBRAL CORTEX. J Physiol 215:247 – & Available at: <Go to ISI>://WOS:A1971J478500014.

Krosnowski K, Ashby S, Sathyanesan A, Luo W, Ogura T, Lin W (2012) Diverse populations of intrinsic cholinergic interneurons in the mouse olfactory bulb. Neuroscience 213:161–178 Available at: http://www.ncbi.nlm.nih.gov/pubmed/22525133.

Kunze WAA, Shafton AD, Kemm RE, McKenzie JS (1991) Effect Of Stimulating The Nucleus Of The Horizontal Limb Of The Diagonal Band On Single Unit-Activity In The Olfactory-Bulb. Neuroscience 40:21–27 Available at: http://www.ncbi.nlm.nih.gov/pubmed/2052151.

Lanzafame AA, Christopoulos A, Mitchelson F (2003) Cellular signaling mechanisms for muscarinic acetylcholine receptors. Receptors Channels 9:241–260 Available at: <Go to ISI>://WOS:000186344300004.

Larriva-Sahd J (2008) The accessory olfactory bulb in the adult rat: a cytological study of its cell types, neuropil, neuronal modules, and interactions with the main olfactory system. J Comp Neurol 510:309–350 Available at: http://www.ncbi.nlm.nih.gov/pubmed/18634021.

Le Jeune H, Aubert I, Jourdan F, Quirion R (1995) Comparative laminar distribution of various autoradiographic cholinergic markers in adult rat main olfactory bulb. J Chem Neuroanat 9:99–112 Available at: http://www.ncbi.nlm.nih.gov/pubmed/8561953.

Le Jeune H, Aubert I, Jourdan F, Quirion R, LeJeune H, Aubert I, Jourdan F, Quirion R (1996) Developmental profiles of various cholinergic markers in the rat main olfactory bulb using quantitative autoradiography. J Comp Neurol 373:433–450 Available at: http://www.ncbi.nlm.nih.gov/pubmed/8889937.

Lee MG, Hassani OK, Alonso A, Jones BE (2005) Cholinergic basal forebrain neurons burst with theta during waking and paradoxical sleep. J Neurosci 25:4365–4369 Available at: http://www.ncbi.nlm.nih.gov/pubmed/15858062

Lepousez G, Lledo P-M (2013) Odor discrimination requires proper olfactory fast oscillations in awake mice. Neuron 80:1010–1024 Available at: http://www.sciencedirect.com/science/article/pii/S0896627313006491

Lepousez G, Valley MT, Lledo PM (2013) The impact of adult neurogenesis on olfactory bulb circuits and computations. Annu Rev Physiol 75:339–363 Available at: http://www.ncbi.nlm.nih.gov/pubmed/23190074.

Lévy F, Gervais R, Kindermann U, Orgeur P, Piketty V (1990) Importance of beta-noradrenergic receptors in the olfactory bulb of sheep for recognition of lambs. Behav Neurosci 104:464–469 Available at: http://www.ncbi.nlm.nih.gov/pubmed/2162183

Leypold BG, Yu CR, Leinders-Zufall T, Kim MM, Zufall F, Axel R (2002) Altered sexual and social behaviors in trp2 mutant mice. Proc Natl Acad Sci U S A 99:6376–6381 Available at: http://www.pubmedcentral.nih.gov/articlerender.fcgi?artid=122956&tool=pmcentrez&rendertype=abstract

Li G, Cleland TA (2013) A two-layer biophysical model of cholinergic neuromodulation in olfactory bulb. J Neurosci 33:3037–3058 Available at: <Go to ISI>://WOS:000314887200028.

Libri V, Constanti A, Calaminici M, Nistico G (1994) A COMPARISON OF THE MUSCARINIC RESPONSE AND MORPHOLOGICAL PROPERTIES OF IDENTIFIED CELLS IN THE GUINEA-PIG OLFACTORY CORTEX IN-VITRO. Neuroscience 59:331–347 Available at: <Go to ISI>://WOS:A1994NC41400009.

Licht G, Meredith M (1987) Convergence of main and accessory olfactory pathways onto single neurons in the hamster amygdala. Exp brain Res 69:7–18 Available at: http://www.ncbi.nlm.nih.gov/pubmed/3325300

Linster C, Cleland TA (2002) Cholinergic modulation of sensory representations in the olfactory bulb. Neural Netw 15:709–717 Available at: http://www.ncbi.nlm.nih.gov/pubmed/12371521.

Linster C, Fontanini A (2014) Functional neuromodulation of chemosensation in vertebrates. Curr Opin Neurobiol 29C:82–87 Available at: http://www.ncbi.nlm.nih.gov/pubmed/24971592.

Linster C, Garcia PA, Hasselmo ME, Baxter MG (2001) Selective loss of cholinergic neurons projecting to the olfactory system increases perceptual generalization between similar, but not dissimilar, odorants. Behav Neurosci 115:826–833 Available at: <Go to ISI>://000170911600008.

Liu S, Aungst JL, Puche AC, Shipley MT (2012) Serotonin modulates the population activity profile of olfactory bulb external tufted cells. J Neurophysiol 107:473–483 Available at: http://jn.physiology.org/content/107/1/473.long

Liu S, Shao Z, Puche A, Wachowiak M, Rothermel M, Shipley MT (2015) Muscarinic receptors modulate dendrodendritic inhibitory synapses to sculpt glomerular output. J Neurosci 35:5680–5692 Available at: http://www.ncbi.nlm.nih.gov/pubmed/25855181

Lucas-Meunier E, Monier C, Amar M, Baux G, Fregnac Y, Fossier P (2009) Involvement of Nicotinic and Muscarinic Receptors in the Endogenous Cholinergic Modulation of the Balance between Excitation and Inhibition in the Young Rat Visual Cortex. Cereb Cortex 19:2411–2427 Available at: <Go to ISI>://WOS:000269957900019.

Luetje CW, Patrick J (1991) BOTH ALPHA- AND BETA-SUBUNITS CONTRIBUTE TO THE AGONIST SENSITIVITY OF NEURONAL NICOTINIC ACETYLCHOLINE-RECEPTORS. J Neurosci 11:837–845 Available at: <Go to ISI>://WOS:A1991FB93900025.

Luo M, Fee MS, Katz LC (2003) Encoding pheromonal signals in the accessory olfactory bulb of behaving mice. Science 299:1196–1201 Available at: http://www.ncbi.nlm.nih.gov/pubmed/12595684

Ma L, Qiu Q, Gradwohl S, Scott A, Yu EQ, Alexander R, Wiegraebe W, Yu CR (2012) Distributed representation of chemical features and tunotopic organization of glomeruli in the mouse olfactory bulb. Proc Natl Acad Sci U S A 109:5481–5486 Available at: http://www.ncbi.nlm.nih.gov/pubmed/22431605

Ma M, Luo M (2012) Optogenetic Activation of Basal Forebrain Cholinergic Neurons Modulates Neuronal Excitability and Sensory Responses in the Main Olfactory Bulb. J Neurosci 32:10105–10116 Available at: http://www.ncbi.nlm.nih.gov/pubmed/22836246.

Macrides F, Davis BJ, Youngs WM, Nadi NS, Margolis FL (1981) Cholinergic and catecholaminergic afferents to the olfactory bulb in the hamster: a neuroanatomical, biochemical, and histochemical investigation. J Comp Neurol 203:495–514 Available at: http://www.ncbi.nlm.nih.gov/entrez/query.fcgi?cmd=Retrieve&db=PubMed&dopt=Citation&list_uids=6274923.

Mandairon N, Ferretti CJ, Stack CM, Rubin DB, Cleland TA, Linster C (2006) Cholinergic modulation in the olfactory bulb influences spontaneous olfactory discrimination in adult rats. Eur J Neurosci 24:3234–3244 Available at: <Go to ISI>://000243361700027.

Mandiyan VS, Coats JK, Shah NM (2005) Deficits in sexual and aggressive behaviors in Cnga2 mutant mice. Nat Neurosci 8:1660–1662 Available at: http://dx.doi.org/10.1038/nn1589

Manns ID, Alonso A, Jones BE (2000) Discharge Properties of Juxtacellularly Labeled and Immunohistochemically Identified Cholinergic Basal Forebrain Neurons Recorded in Association with the Electroencephalogram in Anesthetized Rats. J Neurosci 20:1505–1518 Available at: http://www.jneurosci.org/content/20/4/1505.long

Marder E (2012) Neuromodulation of neuronal circuits: back to the future. Neuron 76:1–11 Available at: http://www.ncbi.nlm.nih.gov/pubmed/23040802.

Maresh A, Rodriguez Gil D, Whitman MC, Greer CA (2008) Principles of glomerular organization in the human olfactory bulb--implications for odor processing. PLoS One 3:e2640 Available at: http://www.pubmedcentral.nih.gov/articlerender.fcgi?artid=2440537&tool=pmcentrez&rendertype=abstract

Margrie TW, Schaefer AT (2003) Theta oscillation coupled spike latencies yield computational vigour in a mammalian sensory system. J Physiol 546:363–374 Available at: http://www.pubmedcentral.nih.gov/articlerender.fcgi?artid=2342519&tool=pmcentrez&rendertype=abstract

Marguet SL, Harris KD (2011) State-dependent representation of amplitude-modulated noise stimuli in rat auditory cortex. J Neurosci 31:6414–6420 Available at: http://www.ncbi.nlm.nih.gov/pubmed/21525282.

Markopoulos F, Rokni D, Gire DH, Murthy VN (2012) Functional Properties of Cortical Feedback Projections to the Olfactory Bulb. Neuron 76:1175–1188 Available at: <Go to ISI>://WOS:000313154800014.

Maruniak JA, Wysocki CJ, Taylor JA (1986) Mediation of male mouse urine marking and aggression by the vomeronasal organ. Physiol Behav 37:655–657 Available at: http://www.sciencedirect.com/science/article/pii/0031938486903008

Matsuoka M, Kaba H, Moriya K, Yoshida-Matsuoka J, Costanzo RM, Norita M, Ichikawa M (2004) Remodeling of reciprocal synapses associated with persistence of long-term memory. Eur J Neurosci 19:1668–1672 Available at: http://www.ncbi.nlm.nih.gov/pubmed/15066163

McKenna TM, Ashe JH, Hui GK, Weinberger NM (1988) Muscarinic agonists modulate spontaneous and evoked unit discharge in auditory cortex of cat. Synapse 2:54–68 Available at: http://www.ncbi.nlm.nih.gov/pubmed/3420531

McLean JH, Shipley MT (1987) Serotonergic afferents to the rat olfactory bulb: I. Origins and laminar specificity of serotonergic inputs in the adult rat. J Neurosci 7:3016–3028 Available at: http://www.ncbi.nlm.nih.gov/pubmed/2822862

McLean JH, Shipley MT, Nickell WT, Aston-Jones G, Reyher CK (1989) Chemoanatomical organization of the noradrenergic input from locus coeruleus to the olfactory bulb of the adult rat. J Comp Neurol 285:339–349 Available at: http://www.ncbi.nlm.nih.gov/entrez/query.fcgi?cmd=Retrieve&db=PubMed&dopt=Citation&list_uids=2547851.

McNamara AM, Magidson PD, Linster C, Wilson DA, Cleland TA (2008) Distinct neural mechanisms mediate olfactory memory formation at different timescales. Learn Mem 15:117–125 Available at: http://www.pubmedcentral.nih.gov/articlerender.fcgi?artid=2275653&tool=pmcentrez&rendertype=abstract

Mechawar N, Saghatelyan A, Grailhe R, Scoriels L, Gheusi G, Gabellec MM, Lledo PM, Changeux JP (2004) Nicotinic receptors regulate the survival of newborn neurons in

the adult olfactory bulb. Proc Natl Acad Sci U S A 101:9822–9826 Available at: http://www.ncbi.nlm.nih.gov/entrez/query.fcgi?cmd=Retrieve&db=PubMed&dopt=Citation&list_uids=15210938.

Metherate R, Tremblay N, Dykes RW (1988) The effects of acetylcholine on response properties of cat somatosensory cortical neurons. J Neurophysiol 59:1231–1252 Available at: http://www.ncbi.nlm.nih.gov/pubmed/2897434

Miyamichi K, Serizawa S, Kimura HM, Sakano H (2005) Continuous and overlapping expression domains of odorant receptor genes in the olfactory epithelium determine the dorsal/ventral positioning of glomeruli in the olfactory bulb. J Neurosci 25:3586–3592 Available at: http://www.jneurosci.org/content/25/14/3586.long

Mohedano-Moriano A, Pro-Sistiaga P, Ubeda-Bañón I, Crespo C, Insausti R, Martinez-Marcos A (2007) Segregated pathways to the vomeronasal amygdala: differential projections from the anterior and posterior divisions of the accessory olfactory bulb. Eur J Neurosci 25:2065–2080 Available at: http://www.ncbi.nlm.nih.gov/pubmed/17419754

Mohedano-Moriano A, Pro-Sistiaga P, Ubeda-Bañon I, de la Rosa-Prieto C, Saiz-Sanchez D, Martinez-Marcos A (2008) V1R and V2R segregated vomeronasal pathways to the hypothalamus. Neuroreport 19:1623–1626 Available at: http://www.ncbi.nlm.nih.gov/pubmed/18845942

Mombaerts P, Wang F, Dulac C, Chao SK, Nemes A, Mendelsohn M, Edmondson J, Axel R (1996) Visualizing an olfactory sensory map. Cell 87:675–686 Available at: http://www.ncbi.nlm.nih.gov/entrez/query.fcgi?cmd=Retrieve&db=PubMed&dopt=Citation&list_uids=8929536.

Mori K, Nagao H, Yoshihara Y (1999) The olfactory bulb: Coding and processing of odor molecule information. Science (80-) 286:711–715 Available at: <Go to ISI>://000083303200040.

Mori K, Sakano H (2011) How is the olfactory map formed and interpreted in the mammalian brain? Annu Rev Neurosci 34:467–499 Available at: http://www.annualreviews.org/doi/full/10.1146/annurev-neuro-112210-112917?url_ver=Z39.88-2003&rfr_id=ori:rid:crossref.org&rfr_dat=cr_pub%3dpubmed

Mori K, Takagi SF (1978) An intracellular study of dendrodendritic inhibitory synapses on mitral cells in the rabbit olfactory bulb. J Physiol 279:569–588 Available at: http://www.pubmedcentral.nih.gov/articlerender.fcgi?artid=1282633&tool=pmcentrez&rendertype=abstract

Mouret A, Lepousez G, Gras J, Gabellec MM, Lledo PM (2009a) Turnover of newborn olfactory bulb neurons optimizes olfaction. J Neurosci 29:12302–12314 Available at: http://www.ncbi.nlm.nih.gov/entrez/query.fcgi?cmd=Retrieve&db=PubMed&dopt=Citation&list_uids=19793989.

Mouret A, Murray K, Lledo PM (2009b) Centrifugal drive onto local inhibitory interneurons of the olfactory bulb. Ann N Y Acad Sci 1170:239–254 Available at: http://www.ncbi.nlm.nih.gov/entrez/query.fcgi?cmd=Retrieve&db=PubMed&dopt=Citation&list_uids=19686142.

Mucignat-Caretta C, Redaelli M, Caretta A (2012) One nose, one brain: contribution of the main and accessory olfactory system to chemosensation. Front Neuroanat 6:46 Available at: http://www.ncbi.nlm.nih.gov/pubmed/23162438

Nagode DA, Tang AH, Yang K, Alger BE (2014) Optogenetic identification of an intrinsic cholinergically driven inhibitory oscillator sensitive to cannabinoids and opioids in hippocampal CA1. J Physiol 592:103–123 Available at: http://www.ncbi.nlm.nih.gov/pubmed/24190932.

Nai Q, Dong H-W, Hayar A, Linster C, Ennis M (2009) Noradrenergic Regulation of GABAergic Inhibition of Main Olfactory Bulb Mitral Cells Varies as a Function of Concentration and Receptor Subtype. J Neurophysiol 101:2472–2484 Available at: http://www.ncbi.nlm.nih.gov/pubmed/19279145.

Nai Q, Dong HW, Linster C, Ennis M (2010) Activation of alpha1 and alpha2 noradrenergic receptors exert opposing effects on excitability of main olfactory bulb granule cells. Neuroscience 169:882–892 Available at: http://www.ncbi.nlm.nih.gov/pubmed/20466037.

Nelson CL, Sarter M, Bruno JP (2005) Prefrontal cortical modulation of acetylcholine release in posterior parietal cortex. Neuroscience 132:347–359 Available at: http://www.ncbi.nlm.nih.gov/pubmed/15802188

Nickell WT, Shipley MT (1988) Neurophysiology of magnocellular forebrain inputs to the olfactory bulb in the rat: frequency potentiation of field potentials and inhibition of output neurons. J Neurosci 8:4492–4502 Available at: <Go to ISI>://A1988R501300010.

Niell CM, Stryker MP (2010) Modulation of visual responses by behavioral state in mouse visual cortex. Neuron 65:472–479 Available at: http://www.ncbi.nlm.nih.gov/pubmed/20188652.

Niessing J, Friedrich RW (2010) Olfactory pattern classification by discrete neuronal network states. Nature 465:47–52 Available at: http://dx.doi.org/10.1038/nature08961

Nissant A, Bardy C, Katagiri H, Murray K, Lledo PM (2009) Adult neurogenesis promotes synaptic plasticity in the olfactory bulb. Nat Neurosci 12:728–730 Available at: http://www.ncbi.nlm.nih.gov/entrez/query.fcgi?cmd=Retrieve&db=PubMed&dopt=Citation&list_uids=19412168.

Nunez-Parra A, Maurer RK, Krahe K, Smith RS, Araneda RC (2013) Disruption of centrifugal inhibition to olfactory bulb granule cells impairs olfactory discrimination. Proc Natl Acad Sci U S A 110:14777–14782 Available at: http://www.ncbi.nlm.nih.gov/pubmed/23959889.

Ojima H, Yamasaki T, Kojima H, Akashi A (1988) Cholinergic innervation of the main and the accessory olfactory bulbs of the rat as revealed by a monoclonal antibody against choline acetyltransferase. Anat Embryol 178:481–488 Available at: http://www.ncbi.nlm.nih.gov/entrez/query.fcgi?cmd=Retrieve&db=PubMed&dopt=Citation&list_uids=3223607.

Olsen SR, Wilson RI (2008) Lateral presynaptic inhibition mediates gain control in an olfactory circuit. Nature 452:956–960 Available at: http://dx.doi.org/10.1038/nature06864

Omura M, Mombaerts P (2014) Trpc2-expressing sensory neurons in the main olfactory epithelium of the mouse. Cell Rep 8:583–595 Available at: http://www.ncbi.nlm.nih.gov/pubmed/25001287

Paban V, Chambon C, Jaffard M, Alescio-Lautier B (2005) Behavioral effects of basal forebrain cholinergic lesions in young adult and aging rats. Behav Neurosci 119:933–945 Available at: http://www.ncbi.nlm.nih.gov/pubmed/16187821

Padmanabhan K, Urban NN (2010) Intrinsic biophysical diversity decorrelates neuronal firing while increasing information content. Nat Neurosci 13:1276–1282 Available at: http://www.ncbi.nlm.nih.gov/pubmed/20802489.

Papes F, Logan DW, Stowers L (2010) The vomeronasal organ mediates interspecies defensive behaviors through detection of protein pheromone homologs. Cell 141:692–703 Available at: http://www.pubmedcentral.nih.gov/articlerender.fcgi?artid=2873972&tool=pmcentrez&rendertype=abstract

Parikh V, Sarter M (2008) Cholinergic mediation of attention - Contributions of phasic and tonic increases in prefrontal cholinergic activity. Ann N Y Acad Sci 1129:225–235 Available at: http://www.ncbi.nlm.nih.gov/pubmed/18591483

Pawlak V, Wickens JR, Kirkwood A, Kerr JND (2010) Timing is not Everything: Neuromodulation Opens the STDP Gate. Front Synaptic Neurosci 2:146 Available at: http://www.pubmedcentral.nih.gov/articlerender.fcgi?artid=3059689&tool=pmcentrez&rendertype=abstract

Petersen CC (2014) Cortical control of whisker movement. Annu Rev Neurosci 37:183–203 Available at: http://www.ncbi.nlm.nih.gov/pubmed/24821429.

Petzold GC, Hagiwara A, Murthy VN (2009) Serotonergic modulation of odor input to the mammalian olfactory bulb. Nat Neurosci 12:784–U142 Available at: <Go to ISI>://WOS:000266380900023.

Pfeiffer CA, Johnston RE (1994) Hormonal and behavioral responses of male hamsters to females and female odors: Roles of olfaction, the vomeronasal system, and sexual experience. Physiol Behav 55:129–138 Available at: http://www.sciencedirect.com/science/article/pii/0031938494900205

Pignatelli A, Belluzzi O (2008) Cholinergic modulation of dopaminergic neurons in the mouse olfactory bulb. Chem Senses 33:331–338 Available at: http://www.ncbi.nlm.nih.gov/pubmed/18209017.

Pinto JM, Wroblewski KE, Kern DW, Schumm LP, McClintock MK (2014) Olfactory dysfunction predicts 5-year mortality in older adults. PLoS One 9:e107541 Available at: http://journals.plos.org/plosone/article?id=10.1371/journal.pone.0107541

Pinto L, Goard MJ, Estandian D, Xu M, Kwan AC, Lee SH, Harrison TC, Feng G, Dan Y (2013) Fast modulation of visual perception by basal forebrain cholinergic neurons.

Nat Neurosci 16:1857–1863 Available at: http://www.ncbi.nlm.nih.gov/pubmed/24162654.

Pressler RT, Inoue T, Strowbridge BW (2007) Muscarinic receptor activation modulates granule cell excitability and potentiates inhibition onto mitral cells in the rat olfactory bulb. J Neurosci 27:10969–10981 Available at: http://www.ncbi.nlm.nih.gov/pubmed/17928438.

Price JL, Powell TP (1970a) The synaptology of the granule cells of the olfactory bulb. J Cell Sci 7:91–123 Available at: http://www.ncbi.nlm.nih.gov/entrez/query.fcgi?cmd=Retrieve&db=PubMed&dopt=Citation&list_uids=5476864

Price JL, Powell TP (1970b) An experimental study of the origin and the course of the centrifugal fibres to the olfactory bulb in the rat. J Anat 107:215–237 Available at: http://www.pubmedcentral.nih.gov/articlerender.fcgi?artid=1234020&tool=pmcentrez&rendertype=abstract

Pro-Sistiaga P, Mohedano-Moriano A, Ubeda-Bañon I, del mar Arroyo-Jimenez M, Marcos P, Artacho-Pérula E, Crespo C, Insausti R, Martinez-Marcos A (2007) Convergence of olfactory and vomeronasal projections in the rat basal telencephalon. J Comp Neurol 504:346–362 Available at: http://doi.wiley.com/10.1002/cne.21455

Rall W, Shepherd GM (1968) Theoretical reconstruction of field potentials and dendrodendritic synaptic interactions in olfactory bulb. J Neurophysiol 31:884–915 Available at: http://jn.physiology.org/content/31/6/884.long

Ravel N, Elaagouby A, Gervais R (1994) Scopolamine injection into the olfactory bulb impairs short-term olfactory memory in rats. Behav Neurosci 108:317–324 Available at: http://www.ncbi.nlm.nih.gov/entrez/query.fcgi?cmd=Retrieve&db=PubMed&dopt=Citation&list_uids=8037875.

Ressler KJ, Sullivan SL, Buck LB (1993) A zonal organization of odorant receptor gene expression in the olfactory epithelium. Cell 73:597–609 Available at: http://www.sciencedirect.com/science/article/pii/009286749390145G

Rinberg D, Koulakov A, Gelperin A (2006) Sparse odor coding in awake behaving mice. J Neurosci 26:8857–8865 Available at: <Go to ISI>://000240006200024.

Rodriguez I, Feinstein P, Mombaerts P (1999) Variable patterns of axonal projections of sensory neurons in the mouse vomeronasal system. Cell 97:199–208 Available at: http://www.ncbi.nlm.nih.gov/entrez/query.fcgi?cmd=Retrieve&db=PubMed&dopt=Citation&list_uids=10219241.

Roman FS, Simonetto I, Soumireumourat B (1993) Learning And Memory Of Odor-Reward Association - Selective Impairment Following Horizontal Diagonal Band Lesions. Behav Neurosci 107:72–81 Available at: <Go to ISI>://A1993KN95000006.

Root CM, Denny CA, Hen R, Axel R (2014) The participation of cortical amygdala in innate, odour-driven behaviour. Nature 515:269–273 Available at: http://dx.doi.org/10.1038/nature13897

Rosenkranz JA, Grace AA (2002) Dopamine-mediated modulation of odour-evoked amygdala potentials during pavlovian conditioning. Nature 417:282–287 Available at: http://dx.doi.org/10.1038/417282a

Rossi J, Balthasar N, Olson D, Scott M, Berglund E, Lee CE, Choi MJ, Lauzon D, Lowell BB, Elmquist JK (2011) Melanocortin-4 receptors expressed by cholinergic neurons regulate energy balance and glucose homeostasis. Cell Metab 13:195–204 Available at: <Go to ISI>://WOS:000287431600012

Rothermel M, Carey RM, Puche A, Shipley MT, Wachowiak M (2014) Cholinergic inputs from Basal forebrain add an excitatory bias to odor coding in the olfactory bulb. J Neurosci 34:4654–4664 Available at: http://www.ncbi.nlm.nih.gov/pubmed/24672011.

Royet JP, Souchier C, Jourdan F, Ploye H (1988) Morphometric study of the glomerular population in the mouse olfactory bulb: numerical density and size distribution along the rostrocaudal axis. J Comp Neurol 270:559–568 Available at: http://www.ncbi.nlm.nih.gov/pubmed/3372747

Sachs BD, Rodriguiz RM, Siesser WB, Kenan A, Royer EL, Jacobsen JPR, Wetsel WC, Caron MG (2013) The effects of brain serotonin deficiency on behavioural disinhibition and anxiety-like behaviour following mild early life stress. Int J Neuropsychopharmacol 16:2081–2094 Available at: http://www.pubmedcentral.nih.gov/articlerender.fcgi?artid=3931011&tool=pmcentrez&rendertype=abstract

Salazar I, Brennan PA (2001) Retrograde labelling of mitral/tufted cells in the mouse accessory olfactory bulb following local injections of the lipophillic tracer DiI into the vomeronasal amygdala. Brain Res 896:198–203 Available at: http://www.sciencedirect.com/science/article/pii/S0006899301022259

Salazar I, Sanchez-Quinteiro P, Cifuentes JM, De Troconiz PF (2006) General organization of the perinatal and adult accessory olfactory bulb in mice. Anat Rec Part a-Discoveries Mol Cell Evol Biol 288A:1009–1025 Available at: <Go to ISI>://WOS:000240295400010.

Salcedo E, Tuan T, Ly X, Lopez R, Barbica C, Restrepo D, Vijayaraghavan S (2011) Activity-Dependent Changes in Cholinergic Innervation of the Mouse Olfactory Bulb. PLoS One 6 Available at: http://www.ncbi.nlm.nih.gov/pubmed/22053179.

Sarter M, Parikh V, Howe WM (2009) Phasic acetylcholine release and the volume transmission hypothesis: time to move on. Nat Rev Neurosci 10:383–390 Available at: http://www.ncbi.nlm.nih.gov/pubmed/19377503.

Saunders A, Granger AJ, Sabatini BL (2015) Corelease of acetylcholine and GABA from cholinergic forebrain neurons. Elife 4 Available at: http://www.pubmedcentral.nih.gov/articlerender.fcgi?artid=4371381&tool=pmcentrez&rendertype=abstract

Scalia F, Winans SS (1975) The differential projections of the olfactory bulb and accessory olfactory bulb in mammals. J Comp Neurol 161:31–55 Available at: http://www.ncbi.nlm.nih.gov/pubmed/1133226.

Schaal B, Coureaud G, Langlois D, Giniès C, Sémon E, Perrier G (2003) Chemical and behavioural characterization of the rabbit mammary pheromone. Nature 424:68–72 Available at: http://dx.doi.org/10.1038/nature01739

Schmidt LJ, Strowbridge BW (2014) Modulation of olfactory bulb network activity by serotonin: synchronous inhibition of mitral cells mediated by spatially localized GABAergic microcircuits. Learn Mem 21:406–416 Available at: http://www.ncbi.nlm.nih.gov/pubmed/25031366

Schoppa NE, Urban NN (2003) Dendritic processing within olfactory bulb circuits. Trends Neurosci 26:501–506 Available at: http://www.ncbi.nlm.nih.gov/entrez/query.fcgi?cmd=Retrieve&db=PubMed&dopt=Citation&list_uids=12948662.

Schwindt PC, Spain WJ, Foehring RC, Chubb MC, Crill WE (1988) SLOW CONDUCTANCES IN NEURONS FROM CAT SENSORIMOTOR CORTEX INVITRO AND THEIR ROLE IN SLOW EXCITABILITY CHANGES. J Neurophysiol 59:450–467 Available at: <Go to ISI>://WOS:A1988M213900011.

Setlow B, Schoenbaum G, Gallagher M (2003) Neural Encoding in Ventral Striatum during Olfactory Discrimination Learning. Neuron 38:625–636 Available at: http://www.sciencedirect.com/science/article/pii/S0896627303002642

Shao Z, Puche AC, Kiyokage E, Szabo G, Shipley MT (2009) Two GABAergic Intraglomerular Circuits Differentially Regulate Tonic and Phasic Presynaptic Inhibition of Olfactory Nerve Terminals. J Neurophysiol 101:1988–2001 Available at: http://www.ncbi.nlm.nih.gov/pubmed/19225171.

Shepherd GM, Chen WR, Willhite D, Migliore M, Greer CA (2007) The olfactory granule cell: From classical enigma to central role in olfactory processing. Brain Res Rev 55:373–382 Available at: http://www.ncbi.nlm.nih.gov/pubmed/17434592.

Shepherd GM, Greer CA (1998) Olfactory Bulb. In: The synaptic organization of the brain, 4th ed. (Shepherd GM, ed), pp 159–204. Oxford University Press.

Shipley MT, Adamek GD (1984) THE CONNECTIONS OF THE MOUSE OLFACTORY-BULB - A STUDY USING ORTHOGRADE AND RETROGRADE TRANSPORT OF WHEAT-GERM-AGGLUTININ CONJUGATED TO HORSERADISH-PEROXIDASE. Brain Res Bull 12:669–688 Available at: <Go to ISI>://WOS:A1984TE96200009.

Shpak G, Zylbertal A, Wagner S (2014) Transient and sustained afterdepolarizations in accessory olfactory bulb mitral cells are mediated by distinct mechanisms that are differentially regulated by neuromodulators. Front Cell Neurosci 8:432 Available at: http://www.pubmedcentral.nih.gov/articlerender.fcgi?artid=4294165&tool=pmcentrez&rendertype=abstract

Shusterman R, Smear MC, Koulakov AA, Rinberg D (2011) Precise olfactory responses tile the sniff cycle. Nat Neurosci 14:1039–U136 Available at: http://www.ncbi.nlm.nih.gov/pubmed/21765422.

Smear M, Shusterman R, O'Connor R, Bozza T, Rinberg D (2011) Perception of sniff phase in mouse olfaction. Nature 479:397–400 Available at: http://www.ncbi.nlm.nih.gov/pubmed/21993623.

Smith RS, Araneda RC (2010) Cholinergic Modulation of Neuronal Excitability in the Accessory Olfactory Bulb. J Neurophysiol 104:2963–2974 Available at: http://www.ncbi.nlm.nih.gov/pubmed/20861438.

Smith RS, Weitz CJ, Araneda RC (2009) Excitatory Actions of Noradrenaline and Metabotropic Glutamate Receptor Activation in Granule Cells of the Accessory Olfactory Bulb. J Neurophysiol 102:1103–1114 Available at: http://www.ncbi.nlm.nih.gov/pubmed/19474170.

Sosulski DL, Bloom ML, Cutforth T, Axel R, Datta SR (2011) Distinct representations of olfactory information in different cortical centres. Nature 472:213–216 Available at: http://www.pubmedcentral.nih.gov/articlerender.fcgi?artid=3354569&tool=pmcentrez&rendertype=abstract

Spencer DG, Horvath E, Traber J (1986) DIRECT AUTORADIOGRAPHIC DETERMINATION OF M1-MUSCARINIC AND M2-MUSCARINIC ACETYLCHOLINE-RECEPTOR DISTRIBUTION IN THE RAT-BRAIN - RELATION TO CHOLINERGIC NUCLEI AND PROJECTIONS. Brain Res 380:59–68 Available at: <Go to ISI>://WOS:A1986D649700008.

Spors H, Grinvald A (2002) Spatio-temporal dynamics of odor representations in the mammalian olfactory bulb. Neuron 34:301–315 Available at: http://www.sciencedirect.com/science/article/pii/S089662730200644X

Staples LG, McGregor IS, Apfelbach R, Hunt GE (2008) Cat odor, but not trimethylthiazoline (fox odor), activates accessory olfactory and defense-related brain regions in rats. Neuroscience 151:937–947 Available at: http://www.sciencedirect.com/science/article/pii/S0306452207015473

Sternson SM, Roth BL (2014) Chemogenetic tools to interrogate brain functions. Annu Rev Neurosci 37:387–407 Available at: http://www.ncbi.nlm.nih.gov/pubmed/25002280.

Stettler DD, Axel R (2009) Representations of odor in the piriform cortex. Neuron 63:854–864 Available at: http://www.sciencedirect.com/science/article/pii/S0896627309006849

Stowers L, Cameron P, Keller JA (2013) Ominous odors: olfactory control of instinctive fear and aggression in mice. Curr Opin Neurobiol 23:339–345 Available at: http://www.ncbi.nlm.nih.gov/pubmed/23415829.

Stowers L, Holy TE, Meister M, Dulac C, Koentges G (2002) Loss of sex discrimination and male-male aggression in mice deficient for TRP2. Science 295:1493–1500 Available at: http://www.sciencemag.org/content/295/5559/1493.long

Takahashi Y, Kaba H (2010) Muscarinic receptor type 1 (M1) stimulation, probably through KCNQ/Kv7 channel closure, increases spontaneous GABA release at the dendrodendritic synapse in the mouse accessory olfactory bulb. Brain Res 1339:26–40 Available at: <Go to ISI>://000279041000004.

Takahashi YK, Kurosaki M, Hirono S, Mori K (2004) Topographic representation of odorant molecular features in the rat olfactory bulb. J Neurophysiol 92:2413–2427 Available at: http://jn.physiology.org/content/92/4/2413.long

Thiele A (2013) Muscarinic signaling in the brain. Annu Rev Neurosci 36:271–294 Available at: http://www.annualreviews.org/doi/full/10.1146/annurev-neuro-062012-170433

Tirindelli R, Dibattista M, Pifferi S, Menini A (2009) From pheromones to behavior. Physiol Rev 89:921–956 Available at: http://www.ncbi.nlm.nih.gov/entrez/query.fcgi?cmd=Retrieve&db=PubMed&dopt=Citation&list_uids=19584317.

Tremblay N, Warren RA, Dykes RW (1990) Electrophysiological studies of acetylcholine and the role of the basal forebrain in the somatosensory cortex of the cat. II. Cortical neurons excited by somatic stimuli. J Neurophysiol 64:1212–1222 Available at: http://jn.physiology.org/content/64/4/1212.long

Tsuno Y, Kashiwadani H, Mori K (2008) Behavioral state regulation of dendrodendritic synaptic inhibition in the olfactory bulb. J Neurosci 28:9227–9238 Available at: http://www.ncbi.nlm.nih.gov/pubmed/18784303.

Turchi J, Sarter M (1997) Cortical acetylcholine and processing capacity: effects of cortical cholinergic deafferentation on crossmodal divided attention in rats. Brain Res Cogn Brain Res 6:147–158 Available at: http://www.ncbi.nlm.nih.gov/pubmed/9450608

Uchida N, Takahashi YK, Tanifuji M, Mori K (2000) Odor maps in the mammalian olfactory bulb: domain organization and odorant structural features. Nat Neurosci 3:1035–1043 Available at: <Go to ISI>://000167177500022.

Von BAUMGARTEN, GREEN JD, MANCIA M (1962) Recurrent inhibition in the olfactory bulb. II. Effects of antidromic stimulation of commissural fibers. J Neurophysiol 25:489–500 Available at: http://www.ncbi.nlm.nih.gov/pubmed/13865954

Von Campenhausen H, Mori K (2000) Convergence of segregated pheromonal pathways from the accessory olfactory bulb to the cortex in the mouse. Eur J Neurosci 12:33–46 Available at: http://doi.wiley.com/10.1046/j.1460-9568.2000.00879.x

Von Engelhardt J, Eliava M, Meyer AH, Rozov A, Monyer H (2007) Functional characterization of intrinsic cholinergic interneurons in the cortex. J Neurosci 27:5633–5642 Available at: http://www.jneurosci.org/content/27/21/5633.long

Wagner S, Gresser AL, Torello AT, Dulac C (2006) A multireceptor genetic approach uncovers an ordered integration of VNO sensory inputs in the accessory olfactory bulb. Neuron 50:697–709 Available at: http://www.ncbi.nlm.nih.gov/pubmed/16731509.

Wenk H, Bigl V, Meyer U (1980) Cholinergic projections from magnocellular nuclei of the basal forebrain to cortical areas in rats. Brain Res 2:295–316 Available at: http://www.ncbi.nlm.nih.gov/pubmed/7470857

Wess J, Eglen RM, Gautam D (2007) Muscarinic acetylcholine receptors: mutant mice provide new insights for drug development. Nat Rev Drug Discov 6:721–733 Available at: http://www.ncbi.nlm.nih.gov/pubmed/17762886.

Whiteaker P, Wilking JA, Brown RWB, Brennan RJ, Collins AC, Lindstrom JM, Boulter J (2009) Pharmacological and immunochemical characterization of alpha 2*nicotinic

acetylcholine receptors (nAChRs) in mouse brain. Acta Pharmacol Sin 30:795–804 Available at: <Go to ISI>://WOS:000266916900016.

Whitman MC, Greer CA (2007) Adult-generated neurons exhibit diverse developmental fates. Dev Neurobiol 67:1079–1093 Available at: <Go to ISI>://WOS:000247769000007.

Wieland S, Du D, Oswald MJ, Parlato R, Köhr G, Kelsch W (2014) Phasic dopaminergic activity exerts fast control of cholinergic interneuron firing via sequential NMDA, D2, and D1 receptor activation. J Neurosci 34:11549–11559 Available at: http://www.ncbi.nlm.nih.gov/pubmed/25164653

Wilson DA (1995) NMDA receptors mediate expression of one form of functional plasticity induced by olfactory deprivation. Brain Res 677:238–242 Available at: http://www.sciencedirect.com/science/article/pii/000689939500151F

Wilson DA, Fletcher ML, Sullivan RM (2004) Acetylcholine and olfactory perceptual learning. Learn Mem 11:28–34 Available at: http://www.ncbi.nlm.nih.gov/pubmed/14747514.

Winslow JT, Camacho F (1995) Cholinergic modulation of a decrement in social investigation following repeated contacts between mice. Psychopharmacology (Berl) 121:164–172 Available at: http://www.ncbi.nlm.nih.gov/pubmed/8545521.

Woolf NJ, Hernit MC, Butcher LL (1986) Cholinergic and non-cholinergic projections from the rat basal forebrain revealed by combined choline acetyltransferase and Phaseolus vulgaris leucoagglutinin immunohistochemistry. Neurosci Lett 66:281–286 Available at: http://www.sciencedirect.com/science/article/pii/0304394086900327

Yamada-Hanff J, Bean BP (2013) Persistent sodium current drives conditional pacemaking in CA1 pyramidal neurons under muscarinic stimulation. J Neurosci 33:15011–15021 Available at: http://www.pubmedcentral.nih.gov/articlerender.fcgi?artid=3776055&tool=pmcentrez&rendertype=abstract

Yan H-D, Villalobos C, Andrade R (2009) TRPC Channels Mediate a Muscarinic Receptor-Induced Afterdepolarization in Cerebral Cortex. J Neurosci 29:10038–10046 Available at: http://www.pubmedcentral.nih.gov/articlerender.fcgi?artid=2747319&tool=pmcentrez&rendertype=abstract

Yoshida M, Knauer B, Jochems A (2012) Cholinergic modulation of the CAN current may adjust neural dynamics for active memory maintenance, spatial navigation and time-compressed replay. Front Neural Circuits 6:10 Available at: http://www.pubmedcentral.nih.gov/articlerender.fcgi?artid=3304506&tool=pmcentrez&rendertype=abstract

Zaborszky L, Carlsen J, Brashear HR, Heimer L (1986) Cholinergic and GABAergic afferents to the olfactory bulb in the rat with special emphasis on the projection neurons in the nucleus of the horizontal limb of the diagonal band. J Comp Neurol 243:488–509 Available at: http://www.ncbi.nlm.nih.gov/pubmed/3512629.

Zaborszkyy L, van den Pol A, Gyengesi E (2012) The Basal Forebrain Cholinergic Projection System in Mice. Mouse Nerv Syst:684–718 Available at: <Go to ISI>://WOS:000320856100029.

Zhan X, Yin P, Heinbockel T (2013) The basal forebrain modulates spontaneous activity of principal cells in the main olfactory bulb of anesthetized mice. Front Neural Circuits 7 Available at: http://www.ncbi.nlm.nih.gov/pubmed/24065892.

Zhang X, Firestein S (2002) The olfactory receptor gene superfamily of the mouse. Nat Neurosci 5:124–133 Available at: http://www.ncbi.nlm.nih.gov/pubmed/11802173

Zhao S, Ting JT, Atallah HE, Qiu L, Tan J, Gloss B, Augustine GJ, Deisseroth K, Luo M, Graybiel AM, Feng G (2011) Cell type-specific channelrhodopsin-2 transgenic mice for optogenetic dissection of neural circuitry function. Nat Methods 8:745–752 Available at: <Go to ISI>://000294439100011

Zimnik NC, Treadway T, Smith RS, Araneda RC (2013) alpha(1A)-Adrenergic regulation of inhibition in the olfactory bulb. J Physiol 591:1631–1643 Available at: http://www.ncbi.nlm.nih.gov/pubmed/23266935.

Cerebellar References

Alcami P, Marty A (2013) Estimating functional connectivity in an electrically coupled interneuron network. Proc Natl Acad Sci U S A 110:E4798–E4807 Available at: http://www.pubmedcentral.nih.gov/856846

Altman J (1972) Postnatal development of the cerebellar cortex in the rat. I. The external germinal layer and the transitional molecular layer. J Comp Neurol 145:353–397 Available at: http://www.ncbi.nlm.nih.gov/pubmed/4113154

Benke D, Cicin-Sain A, Mertens S, Mohler H (1991) Immunochemical identification of the alpha 1- and alpha 3-subunits of the GABAA-receptor in rat brain. J Recept Res 11:407–424 Available at: http://www.ncbi.nlm.nih.gov/pubmed/1653345

Böhme I, Rabe H, Lüddens H (2004) Four amino acids in the alpha subunits determine the gamma-aminobutyric acid sensitivities of GABAA receptor subtypes. J Biol Chem 279:35193–35200 Available at: http://www.jbc.org/content/279/34/35193.long

Brickley SG, Cull-Candy SG, Farrant M (1996) Development of a tonic form of synaptic inhibition in rat cerebellar granule cells resulting from persistent activation of GABAA receptors. J Physiol 497 (Pt 3:753–759 Available at: http://www.pubmedcentral.nih.gov/1160971

Chan-Palay V, Palay SL (1972) The stellate cells of the rat's cerebellar cortex. Z Anat Entwicklungsgesch 136:224–248 Available at: http://www.ncbi.nlm.nih.gov/pubmed/5042759

Choii G, Ko J (2015) Gephyrin: a central GABAergic synapse organizer. Exp Mol Med 47:e158 Available at: http://www.ncbi.nlm.nih.gov/pubmed/25882190

Chu C-P, Bing Y-H, Liu H, Qiu D-L (2012) Roles of molecular layer interneurons in sensory information processing in mouse cerebellar cortex Crus II in vivo. PLoS One 7:e37031 Available at: http://www.pubmedcentral.nih.gov/3356402

Craig AM, Banker G, Chang W, McGrath ME, Serpinskaya AS (1996) Clustering of gephyrin at GABAergic but not glutamatergic synapses in cultured rat hippocampal neurons. J Neurosci 16:3166–3177 Available at: http://www.ncbi.nlm.nih.gov/pubmed/8627355

Eccles JC (1967) Circuits in the cerebellar control of movement. Proc Natl Acad Sci U S A 58:336–343 Available at: http://www.pubmedcentral.nih.gov/335638

Eccles JC, Llinás R, Sasaki K (1966) The inhibitory interneurones within the cerebellar cortex. Exp brain Res 1:1–16 Available at: http://www.ncbi.nlm.nih.gov/pubmed/5910941

Farrant M, Nusser Z (2005) Variations on an inhibitory theme: phasic and tonic activation of GABA(A) receptors. Nat Rev Neurosci 6:215–229 Available at: http://dx.doi.org/10.1038/nrn1625

Flores CE, Méndez P (2014) Shaping inhibition: activity dependent structural plasticity of GABAergic synapses. Front Cell Neurosci 8:327 Available at: http://www.pubmedcentral.nih.gov/4209871

Koksma J-J, Fritschy J-M, Mack V, Van Kesteren RE, Brussaard AB (2005) Differential GABAA receptor clustering determines GABA synapse plasticity in rat oxytocin neurons around parturition and the onset of lactation. Mol Cell Neurosci 28:128–140 Available at: http://www.ncbi.nlm.nih.gov/pubmed/15607948

Kralic JE, Sidler C, Parpan F, Homanics GE, Morrow AL, Fritschy J-M (2006) Compensatory alteration of inhibitory synaptic circuits in cerebellum and thalamus of gamma-aminobutyric acid type A receptor alpha1 subunit knockout mice. J Comp Neurol 495:408–421 Available at: http://www.ncbi.nlm.nih.gov/pubmed/16485284

Laurie DJ, Wisden W, Seeburg PH (1992) The distribution of thirteen GABAA receptor subunit mRNAs in the rat brain. III. Embryonic and postnatal development. J Neurosci 12:4151–4172.

Llano I, Gerschenfeld HM (1993a) Inhibitory synaptic currents in stellate cells of rat cerebellar slices. J Physiol 468:177–200 Available at: http://www.ncbi.nlm.nih.gov/ 7504726.

Llano I, Gerschenfeld HM (1993b) Inhibitory synaptic currents in stellate cells of rat cerebellar slices. J Physiol 468:177–200 Available at: http://doi.wiley.com/10.1113/jphysiol.1993.sp019766

Mittmann W, Koch U, Häusser M (2005) Feed-forward inhibition shapes the spike output of cerebellar Purkinje cells. J Physiol 563:369–378 Available at: http://www.pubmedcentral.nih.gov/1665592

Nusser Z, Sieghart W, Somogyi P (1998) Segregation of Different GABAA Receptors to Synaptic and Extrasynaptic Membranes of Cerebellar Granule Cells. J Neurosci 18:1693–1703 Available at: http://www.jneurosci.org/content/18/5/1693.long

Peden DR, Petitjean CM, Herd MB, Durakoglugil MS, Rosahl TW, Wafford K, Homanics GE, Belelli D, Fritschy J-M, Lambert JJ (2008) Developmental maturation of synaptic and extrasynaptic GABAA receptors in mouse thalamic ventrobasal neurones. J Physiol 586:965–987 Available at: http://www.pubmedcentral.nih.gov/2375643

Rudolph U, Knoflach F (2011) Beyond classical benzodiazepines: novel therapeutic potential of GABAA receptor subtypes. Nat Rev Drug Discov 10:685–697 Available at: http://www.pubmedcentral.nih.gov/ 3375401

Sotelo C, Llinás R (1972) Specialized membrane junctions between neurons in the vertebrate cerebellar cortex. J Cell Biol 53:271–289 Available at: http://www.pubmedcentral.nih.gov/2108717

Sperk G, Schwarzer C, Tsunashima K, Fuchs K, Sieghart W (1997) GABAA receptor subunits in the rat hippocampus I: Immunocytochemical distribution of 13 subunits. Neuroscience 80:987–1000 Available at: http://www.sciencedirect.com/science/article/pii/S0306452297001462

Thomas P, Mortensen M, Hosie AM, Smart TG (2005) Dynamic mobility of functional GABAA receptors at inhibitory synapses. Nat Neurosci 8:889–897 Available at: http://www.ncbi.nlm.nih.gov/pubmed/15951809.

Trigo FF, Corrie JET, Ogden D (2009) Laser photolysis of caged compounds at 405 nm: photochemical advantages, localisation, phototoxicity and methods for calibration. J Neurosci Methods 180:9–21 Available at: http://www.ncbi.nlm.nih.gov/pubmed/19427524

Tyagarajan SK, Ghosh H, Harvey K, Fritschy J-M (2011) Collybistin splice variants differentially interact with gephyrin and Cdc42 to regulate gephyrin clustering at GABAergic synapses. J Cell Sci 124:2786–2796 Available at: http://www.pubmedcentral.nih.gov/3148131

Viltono L, Patrizi A, Fritschy JM, Sassoe-Pognetto M (2008) Synaptogenesis in the cerebellar cortex: differential regulation of gephyrin and GABAA receptors at somatic and dendritic synapses of Purkinje cells. J Comp Neurol 508:579–591 Available at: http://www.ncbi.nlm.nih.gov/pubmed/18366064.

Wang DD, Kriegstein AR (2008) GABA regulates excitatory synapse formation in the neocortex via NMDA receptor activation. J Neurosci 28:5547–5558 Available at: http://www.pubmedcentral.nih.gov/2684685

Ye J-H, Wang F, Krnjevic K, Wang W, Xiong Z-G, Zhang J (2004) Presynaptic glycine receptors on GABAergic terminals facilitate discharge of dopaminergic neurons in ventral tegmental area. J Neurosci 24:8961–8974 Available at: http://www.ncbi.nlm.nih.gov/pubmed/15483115